OPTOGENETIC DISSECTION OF SEPTOHIPPOCAMPAL NEURAL CIRCUITRY FOR THE TREATMENT OF EPILEPSY

A Thesis
Presented to
The Academic Faculty

by

Nealen G. Laxpati

In Partial Fulfillment
Of the Requirements for the Degree
Doctor of Philosophy in Biomedical Engineering

Georgia Institute of Technology and Emory University School of Medicine

May 2015

OPTOGENETIC DISSECTION OF SEPTOHIPPOCAMPAL NEURAL CIRCUITRY FOR THE TREATMENT OF EPILEPSY

Approved by:

Dr. Robert E. Gross, Advisor
Department of Neurosurgery
Emory University School of Medicine
Department of Biomedical Engineering
Georgia Institute of Technology

Dr. Kerry J. Ressler
Department of Psychiatry and Behavioral
Sciences
Emory University School of Medicine
Department of Neuroscience
Emory University

Professor Garrett B. Stanley
Department of Biomedical Engineering
Georgia Institute of Technology

Professor Joseph R. Manns
Department of Psychology
Emory University

Professor Dieter Jaeger
Department of Biomedical Engineering
Georgia Institute of Technology
Department of Biology
Emory University

Date Approved: July 16, 2014

To my family and friends

ACKNOWLEDGEMENTS

TABLE OF CONTENTS

LIST OF TABLES

LIST OF FIGURES

SUMMARY

Over 50 million people worldwide suffer from epilepsy. Of these, nearly a third will be refractory to medical therapy, and many will be poor candidates for surgical resection. Thus there is a need for novel targets and therapies, the former of which will require a greater understanding of neural networks involved in epilepsy, and the latter of which demands the development of novel therapeutic techniques. Seizures are less frequent during periods where theta − a 3-12Hz oscillatory rhythm in the hippocampal local field potential − is present. Theta is thought to originate in the medial septum, a basal forebrain structure that projects to the site of origin for the most common form of intractable epilepsy, the hippocampus. As has been demonstrated with pharmacologic and electrical stimulation, theta generation via the medial septum is consequently an ideal target for intervention. However, of the three neuron populations within the medial septum − cholinergic, GABAergic, and glutamatergic − it is unclear which is responsible for theta, or indeed if a single population is driving the oscillation. Optogenetics, a novel technique that enables activation and inhibition of genetically-defined neurons on a millisecond time-scale, provides the means to functionally dissect this septohippocampal axis and leverage the results for seizure therapy. In this thesis, I detail the current state of deep brain stimulation for epilepsy, and describe our motivation for targeting the medial septum and the importance of the hippocampal theta rhythm. I describe new technologies, software, and adaptations to our electrophysiology platform, NeuroRighter, to enable concurrent optogenetic neuromodulation and electrophysiology in awake and behaving animals, and demonstrate how these technologies and techniques can be used in several experimental approaches. I next use this system to show that both the GABAergic and

glutamatergic neurons of the medial septum can drive and pace hippocampal oscillatory rhythms, but only the glutamatergic neurons are necessary to maintain phase relationships between successive theta cycles. I also demonstrate that activating and inhibiting the cholinergic neurons of the medial septum does not alter hippocampal local field potential activity, but does alter single-unit firing rates. These results shed light on the function of the medial septum in generating and modulating theta, and provide clear targets for optogenetic modulation of epilepsy.

CHAPTER I

INTRODUCTION

1.1 AN UNMET NEED

1.1.1 The current state of epilepsy therapy

A large proportion of patients with temporal lobe epilepsy are unable to achieve seizure freedom with pharmacologic medical therapy (Kwan and Sperling 2009; Kwan et al. 2011). Those who fail to respond to two antiepileptic drugs only possess a 5-10% chance of responding to a new drug therapy (Kwan and Sperling 2009). Surgery, only sometimes an option, is not always effective (Wiebe et al. 2001) and can generate new morbidities such as memory deficits (Helmstaedter et al. 2008; Helmstaedter et al. 2011). Thus, there is a defined need for novel, function-preserving therapeutic strategies. Electrical stimulation of the brain has been shown to reduce seizure frequency, but only a small proportion of patients become seizure free (Boon et al. 2009; Fisher et al. 2010), regardless of anatomical target. These results are potentially the result of several factors.

1.1.2 Empirically-derived clinical targets and stimulation parameters

The targets and parameters used in deep brain stimulation (DBS) of a variety of neurologic disorders have largely been determined observationally and empirically (Hunka et al. 2005). Indeed, parameters used at a particular anatomical target have often gone unchanged for decades, despite their lack of success (CHAPTER II, Table 1). In large part, the clinical targets and stimulation parameters chosen for a new trial are based

on limited case-control studies, and are not necessarily grounded in mechanistic concepts. Thus, it is unclear to what extent the poor results of clinical trials of deep brain stimulation for epilepsy therapy are in part due to the chosen stimuli (McIntyre and Grill 2002). A more rational approach is to leverage our existing knowledge of hippocampal neural activity and epilepsy to guide targeting, stimulation choices, and therapeutic approaches.

1.1.3 The hippocampus is a large and complex structure

Successful amygdalohippocampectomy involves resecting a large hippocampal volume to remove epileptic foci (Helmstaedter et al. 2008). However, the volume of neural tissue directly modulated by electrical stimulation is much smaller than this (McIntyre et al. 2006). Direct hippocampal single-electrode electrical stimulation may fail to alleviate seizures because it is unable to sufficiently impact the entire epileptic foci. Stimulation of an upstream target that projects to a large hippocampal volume is a rational alternative approach which has some demonstrated success (Fisher et al. 2010).

1.1.4 Cell-type non-specificity of electrical stimulation.

Electrical stimulation affects all neural tissue within the voltage gradient established around an electrode, including both excitatory and inhibitory neurons, axons, and dendrites (Ranck 1975; Histed et al. 2009), not to mention glial cells and even blood vessels. The impact of electrical stimulation on a laminar structure like the hippocampus, and the neuron subpopulations that will be recruited by electrical stimulation, is highly dependent on the electrode location relative to these structures. This is problematic, as the physiologic rhythms of the hippocampus – such as theta, gamma, and ripple oscillations –

are thought to be generated from complex interactions between interneurons and pyramidal cells (Freund and Buzsáki 1996; Buzsáki 2002; Klausberger et al. 2003; Gloveli et al. 2005). Interactions between inhibitory and excitatory neurons could thus play a prominent role in generating the pathologic oscillations of epileptic activity (Ziburkus et al. 2006). Altering these dynamics through excitation/inhibition of specific neuronal subpopulations in the network would prove useful not only in deciphering their role in producing normal oscillatory activity, but furthermore in understanding and preventing the generation and propagation of seizures.

1.2. THETA REPRESENTS A SEIZURE-RESISTANT FUNCTIONAL STATE

The theta rhythm is a 3-12 Hz oscillation of hippocampal local field potential (LFP) – observed during active awake behavior and random-eye-movement (REM) sleep – that plays a role in several behaviors, such as memory and navigation (Bland and Colom 1993; Buzsáki 2002; Patel et al. 2012; Buzsaki and Moser 2013). A large body of evidence indicates that in epileptic models, however, theta activity is disturbed (Arabadzisz et al. 2005; Colom 2006; Dugladze et al. 2007; García-Hernández et al. 2010; Kitchigina et al. 2013). In the tetanus toxin model of epilepsy used by our group (Rolston et al. 2010) we have observed significant reductions in theta power as compared to normal controls.

However, during periods of prominent theta power epileptic seizures are less frequent (Colom 2006). Seizures in epileptic patients occurred less frequently during REM sleep (Montplaisir et al. 1987). Furthermore, induction of hippocampal theta activity demonstrably reduces and arrests epileptic activity in several animal and seizure models (Miller et al. 1994; Colom et al. 2006; Kitchigina and Butuzova 2009). Miller et

al. showed that microinjections of the muscarinic agonist carbachol into the medial septum – a procedure known to generate hippocampal theta oscillations (Monmaur and Breton 1991) – arrested pentylenetetrazol (PTZ) induced behavioral seizures and EEG spiking (Miller et al. 1994). Carbachol-injected animals demonstrated a significant reduction in seizure duration (6.8 s) as compared to controls (26.8 s). In an additional four rats, the authors successfully electrically stimulated the medial septum with 100 μA 4-8 Hz electrical stimulation to produce a similar antiseizure effect (Miller et al. 1994).

This work supporting theta as an antiepileptic intervention was further substantiated by Colom et al. in the pilocarpine model of chronic epilepsy (Colom et al. 2006). The authors showed that the hippocampal theta rhythm was also reduced in this model of epilepsy, and that its restoration – either observed spontaneously, induced by sensory stimulation (tail pinch), or by carbachol administration – reduced the frequency of hippocampal epileptic discharges to 7-14% of their peak in all cases. The authors thus proposed that due to these disparate methods of induction, the primary modulator of this antiepileptic effect was the theta oscillatory functional state, and not the method used to induce it.

1.3. THE MEDIAL SEPTUM IS AN ATTRACTIVE FOCAL TARGET FOR DISTRIBUTED HIPPOCAMPAL OSCILLATORY CONTROL

The medial septum, the fimbria/fornix, and the hippocampus comprise one continuous anatomical structure – the septohippocampal axis (Colom 2006). Substantial evidence implicates the medial septum-diagonal band complex (MSDB) in the generation and maintenance of the theta rhythm in the hippocampus, and indeed the medial septum is the hypothesized pacemaker for this 3-12 Hz oscillatory rhythm (Stewart and Fox 1990; Tóth

et al. 1997; Buzsáki 2002; Colom et al. 2006; Kitchigina et al. 2013). Colom et al.

hypothesized that this septohippocampal network plays an important role in maintaining

hippocampal activity and oscillations within non-pathologic regimes, preventing the

occurrence of abnormally excited states (Colom 2006; Colom et al. 2006; Colom and

Garrido-Sanabria 2007; García-Hernández et al. 2010). Induction of theta via

pharmacologic and electrical methods has often acted through the medial septum (Miller

et al. 1994; Kitchigina and Butuzova 2009), and it is also an attractive target for epilepsy

neuromodulation due to its distributed projections to the hippocampus. It provides a

single target location that projects bilaterally to both hippocampi, potentially impacting

seizure foci regardless of location or distribution (Figure 1).
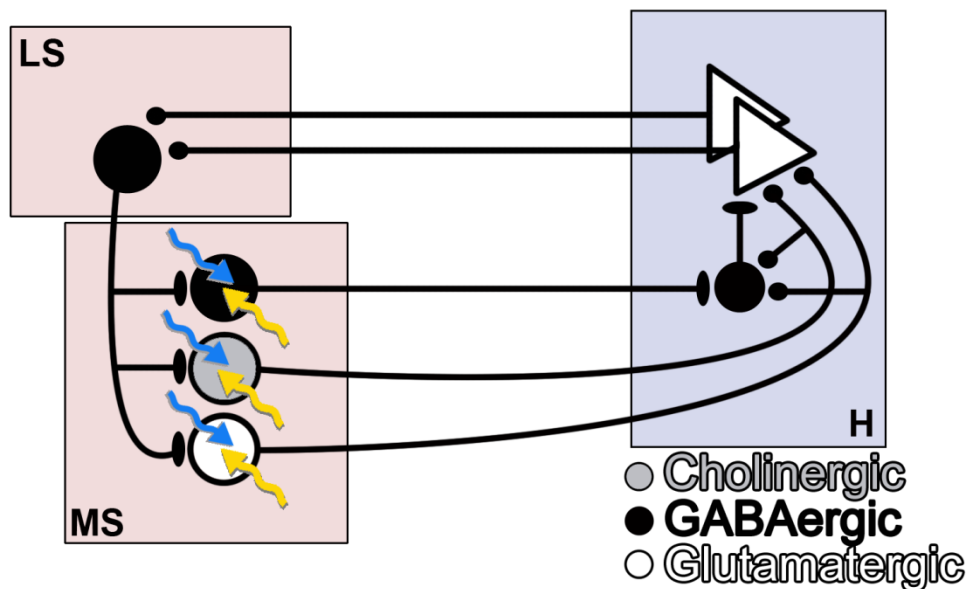
Figure 1: The septohippocampal network and targets for optogenetic neuromodulation
Schematic representation of the major cholinergic **(gray)**, GABAergic **(black)**, and glutamatergic **(white)** connections in the septohippocampal network between the hippocampus **(H)**, medial septum **(MS)**, and lateral septum **(LS)**. Also represented are targets for optogenetic excitation **(blue arrows)** and inhibition **(yellow arrows)**. Note that this schematic does not fully represent the local connectivity within these nuclei.

Three genetically-distinct neuron subpopulations have been identified within the MSDB – GABAergic, glutamatergic, and cholinergic neurons – all of which project to the hippocampus and may play a role in modulating hippocampal activity and theta oscillations (Figure 1) (Freund and Antal 1988; Sotty et al. 2003; Yoder and Pang 2005; Huh et al. 2010; Bell et al. 2013). In order to evaluate the role of each of these populations in modulating hippocampal theta – and in turn determining an optimum target for arresting seizure activity – we need to employ a spatially, temporally, and genetically selective method for excitation and inhibition in awake and behaving animals.

1.4. OPTOGENETIC NEUROMODULATION

Optogenetics is a powerful approach for neuromodulation that enables selective activation or inhibition of genetically-defined neuron subpopulations *in vivo* at the millisecond time scale (Yizhar et al. 2011). Optogenetics thus provides a powerful means to elucidate the specific cellular mechanisms underlying MSDB regulation of hippocampal theta oscillations. Optogenetics provides the cell-type specificity of pharmacologic techniques while retaining the temporal specificity of electrical stimulation. This enables time-sensitive manipulation of the neural code (Stanley 2013) in genetically-defined neuron subpopulations to an impressive and heretofore unprecedented degree, enabling exquisite insight into neural network function (Gradinaru et al. 2009; Liu et al. 2012; Bell et al. 2013).

Optogenetics involves a set of techniques to introduce and manipulate microbial light-sensitive ion channels and pumps (LSICs) in genetically-specified cell populations. LSICs enable the passage of ions across a cell membrane – either down the electrochemical gradient or pumped against it – altering the membrane potential of the

cell. In neurons, excitation (channelrhodopsin-2 and its peers) can be used to bring the cell to threshold, while hyperpolarization (halorhodopsin, archaerhodopsin) can inhibit cell firing. As many LSICs have been designed to respond to light on a millisecond timescale (Yizhar et al. 2011; Tchumatchenko et al. 2013), complex and temporally-sensitive stimulation patterns can be provided to particular subpopulations within a complex neural circuit.

One of the most successful channels is channelrhodopsin-2 (ChR2), which enables cation entry in response to light stimulation (Boyden et al. 2005). Continued manipulation and discovery have rapidly expanded the available repertoire of optogenetic channels (Gradinaru et al. 2010; Gunaydin et al. 2010; Diester et al. 2011; Witten et al. 2011; Yizhar et al. 2011), including inhibitory pumps for effective neural silencing (Gradinaru et al. 2010). Indeed, a vast repertoire of optogenetic tools are being designed to fit numerous experimental needs (Diester et al. 2011; Yizhar et al. 2011; Lin et al. 2013).

Optogenetics takes advantage of gene therapy-based selectivity for targeted channel expression in particular genetically-defined neuron subpopulations within a heterogeneous network (Davidson and Breakefield 2003). The genetic code for a LSIC is coupled to a particular sequence known as a promoter. Different promoters are active in different cell types – such as the choline acetyltransferase (ChAT) promoter in cholinergic neurons. Promoters are regions of DNA which initiate transcription and translation of particular genes specific to a cell's function (Klein et al. 1998; Paterna et al. 2000). By driving expression of our channel with these promoters, we can selectively express the LSIC in specific cell subtypes. Cells whose transcriptional pathways do not

target the promoter will ignore the gene, and thus not express the channel, enabling cell-type specific expression and manipulation.

Viral vectors have consequently become a favored means of introducing genetic constructs into the nervous system *in vivo* for targeted expression (Davidson and Breakefield 2003; Burger et al. 2004; Cockrell and Kafri 2007; Howard et al. 2008; Nathanson et al. 2009; Blits et al. 2010). Different viruses possess different tropisms (Davidson and Breakefield 2003; Burger et al. 2004), that when coupled with promoter-type specificity can more effectively limit gene expression to particularly desired subpopulations. Lentivirus (Cockrell and Kafri 2007) and adeno-associated virus (AAV) (Tenenbaum et al. 2004) have been most commonly used in optogenetic experiments, but a diverse repertoire of viral methods can enable complex and targeted experimentation to be performed (Yizhar et al. 2011).

Increasingly, Cre-Lox recombination systems are being employed to target optogenetic LSICs (Witten et al. 2011; Madisen et al. 2012). Transgenic animals are produced that constitutively express the Cre bacterial enzyme in particular cell-types based on promoter sequence (e.g. ChAT-Cre). This enzyme can selectively excise sequences flanked by LoxP sites, reverse the sequence, and then reintegrate it. As a result, it can take a reversed non-expressing sequence and change it to an expressing one. As the selectivity of this system is determined by transgenic Cre expression, strong ubiquitous promoters with short sequences can be coupled to our introduced gene to produce robust expression selectively in our desired cell population.

Finally, as the name implies, control of light-sensitive ion channels is mediated optically. Activation and inhibition with light possesses a number of advantages over

electrical stimulation. Different LSICs are uniquely sensitive to particular wavelengths of light, enabling simultaneous and independent excitation and inhibition within the same neural network, or even the same neuron (Zhang et al. 2007; Yizhar et al. 2011). Substantial efforts have been made to produce LSICs with unique wavelength responsiveness (Lin et al. 2013), expanding the repertoire of experiments that can be performed, particularly with combinatorial approaches.

Light is also advantageous in that it distributes predictably through nervous system tissue, providing for greater prediction of the volume of tissue manipulated (Aravanis et al. 2007). In addition, optically-induced artifacts are often negligible, particularly when compared to those experienced during electrical stimulation. Electrical stimulation necessitates the use of stimulating voltages many orders of magnitude greater than those being recorded, resulting in large, amplifier-saturating artifacts. Optogenetics, on the other hand, enables simultaneous stimulation and recording to be performed.

1.5. OPTOGENETIC MODULATION OF EPILEPTIC ACTIVITY

The advantages optogenetics holds over electrical and pharmacologic stimulation have provided great insight into nervous system function in normal and pathologic states (Gradinaru et al. 2009; Liu et al. 2012), including epilepsy. The earliest work was performed with optogenetic inhibition in hippocampal slice models of epileptiform activity (Tønnesen et al. 2009). Lentiviral vectors introduced a halorhodopsin chloride pump (NpHR) under the calcium/calmodulin-dependent protein kinase IIα (CaMKIIα) promoter, selectively expressing in principal cells of the hippocampus and cortex. Optogenetic hyperpolarization of these neurons was sufficient to arrest induced

epileptiform activity, providing proof of concept that optogenetic neuromodulation could be an effective therapeutic tool for seizures.

This finding was recapitulated by Wykes et al. in the tetanus toxin motor cortex model of epilepsy (Wykes et al. 2012). Focal injection of tetanus toxin into the motor cortex generates bursts of epileptiform EEG activity and associated clonic movements of the face and forelimbs. The authors tested whether acute inhibition of principal neurons (targeted by a lentivirus encoding CaMKIIα-NpHR2.0) in the induced epileptic focus could attenuate or arrest network excitability. They used a 20-s on/20-s off protocol to provide for NpHR recovery and prevent desensitization and chloride shifting. Inhibition did not visibly affect rat behavior, but did significantly reduce high-frequency power. Furthermore it decreased the frequency of epileptic events.

Krook-Magnuson et al. used a closed-loop approach to directly inhibit pyramidal neurons in the kainate-induced epileptic hippocampus (Krook-Magnuson et al. 2013). Selective expression of halorhodopsin in pyramidal neurons was achieved by crossing CaMKIIα-Cre with Cre-halorhodopsin mouse lines. The authors then designed a novel, tunable closed-loop seizure detection program to randomly inhibit 50% of detected events, thus letting each animal serve as its own control. Inhibition of the pyramidal neurons in this fashion significantly reduced seizure duration (70%), with 57% of seizures arresting with one second of light delivery.

In a second set of experiments, the authors sought to excite the inhibitory interneurons of the hippocampus using the same closed-loop stimulation approach (Krook-Magnuson et al. 2013). Optogenetic stimulation of this population (achieved by crossing PV-Cre mice with mice expressing Cre-dependent ChR2) also significantly

reduced seizure duration (43%). Intriguingly, stimulation of inhibitory neurons contralateral to the kainic acid injection was also able to significantly reduce seizure duration, indicating distributed effects on epileptiform foci were a feasible epilepsy control strategy in the hippocampus. Arresting behavioral seizures proved more difficult, however, with a 29.6% reduction observed. In order to accomplish this level of success, bilateral excitation of inhibitory neurons was necessary, presumably to impact a larger volume of tissue. As the authors discuss, seizures originate outside the focal site, or have diffuse onset. This makes seizure control difficult with focal interventions, particularly in larger nervous systems. There is consequently an advantage to targeting focal regions with large distributions (i.e. bottlenecks), particularly as efforts scale to non-human primates and human patients.

Further support for the effectiveness of indirect neuromodulation of epileptic foci through a distributed network was provided by Paz et al. (Paz et al. 2013). The cortex is intimately connected to the thalamus, and also appears to play a role in the network oscillations underlying epilepsy (Paz et al. 2013). The authors sought to selectively inhibit thalamocortical neurons using eNpHR3.0, and consequently arrest focal cortical seizures in their photothrombotic stroke model. Selective illumination of this population interrupted epileptic activity in the thalamus and cortex, as well as the associated behavioral seizure. This suggests that targeting a central location in a distributed network, such as the medial septum in the septohippocampal axis, may prove more effective in modulating the electrographic and behavioral elements of epilepsy.

My thesis work involves the development of tools for *in vivo* optogenetic neuromodulation of the septohippocampal axis with concurrent electrophysiologic

recording, and the application of these tools to the different subpopulations of the medial septum to examine their role in producing hippocampal theta. The goal of this work is to develop open-source and low cost tools for optogenetic experiments, gain insight into the role of the medial septum in hippocampal theta oscillations, and identify cellular targets for optogenetic neuromodulation of the medial septum for the treatment of epilepsy.

1.6. THESIS ORGANIZATION

The rest of the thesis is as follows:

CHAPTER II: *The Current State of Deep Brain Stimulation for the Treatment of Epilepsy: Circuits, Targets, and Trials*, Dr. Willard Kasoff and I elaborate on the current state of clinical trials and techniques available for deep brain stimulation in the treatment of medically-refractory epilepsy. We discuss the results of clinical trials for several anatomical targets, including the empirical nature by which the targets and stimulation patterns have been run.

CHAPTER III: *Real-time in vivo Optogenetic Neuromodulation and Multielectrode Electrophysiologic Recording with NeuroRighter* discusses the development and performance characteristics of adaptations that my collaborators, Jon P. Newman, Riley Zeller-Townson, and the Potter Lab, and I made to the open-source NeuroRighter electrophysiology platform for *in vivo* behavioral experimentation with optogenetics. I detail two kinds of experiments – proximal stimulation and recording in the hippocampus and distal stimulation of the medial septum and recording in the hippocampus, and present some methods for analyzing the resulting neural responses.

CHAPTER IV: *Optogenetic Neuromodulation of Medial Septal GABAergic Neurons and the Impact on Hippocampal Oscillatory Activity in Awake and Behaving Rats* applies our adapted NeuroRighter system to test the hypothesis that GABAergic neurons of the medial septum are responsible for pacing the hippocampal theta rhythm. I demonstrate that rhythmic excitation of the GABAergic population transmits a stimulus-frequency-specific oscillatory rhythm to the hippocampus that drives and controls hippocampal local field potential activity. In contrast, I show that sustained inhibition of this same population does not alter hippocampal oscillatory activity or theta power. This demonstrates that while the MSDB GABAergic neurons can modulate hippocampal oscillations and theta, they are not necessary for theta function in awake and behaving animals, and suggesting that they are not the pacemaker of this oscillatory rhythm.

CHAPTER V: *Optogenetic Modulation of Medial Septal Glutamatergic Neurons and the Impact on Hippocampal Oscillatory Activity in Awake and Behaving Rats* tests the hypothesis that the glutamatergic neurons of the medial septum are responsible for pacing the hippocampal theta rhythm. I demonstrate that rhythmic excitation of this population – much as was demonstrated in the GABAergic population in CHAPTER IV – generates a stimulus-frequency-specific increase in power in the hippocampal local field potential, although not as robustly as was observed in the GABAergic population. I also demonstrate that optogenetic inhibition of this population does not alter hippocampal theta power, but does impact the ability of theta to maintain the phase relationship between cycles, suggesting that the septal glutamatergic neurons may indeed be pacing hippocampal theta.

CHAPTER VI: *Optogenetic Modulation of Medial Septal Cholinergic Neurons and the Impact on Hippocampal Activity in Awake and Behaving Rats* tests the hypothesis that the cholinergic neurons of the medial septum are responsible for pacing and modulating the hippocampal theta rhythm. I demonstrate that neither rhythmic excitation nor constant inhibition of cholinergic neurons modulates hippocampal local field potential in awake animals. I show that rhythmic 35 Hz stimulation, however, can modulate single unit firing rates under anesthesia and in the awake animal. These results suggest that the either the cholinergic hypothesis of hippocampal theta may be incorrect, that this population may act primarily upon single unit firing rates, or that response to cholinergic input is dependent upon specific network states.

CHAPTER VII: *Conclusion*. I conclude the thesis by discussing the implications of this work and its results, and future experimental directions, particularly in the realms of understanding theta and applying our results to epilepsy.

Hardware and software that I have developed during the course of this work will be made publicly available through open access on our website. Portions of this thesis have been published previously or submitted for publication. Chapters based upon published and submitted work are presented here with permission from the relevant publisher (where applicable) and include a citation at the start of the chapter. These chapters are largely unchanged from their original form, with the exception of headings and typographic changes.

CHAPTER II

THE CURRENT STATE OF DEEP BRAIN STIMULATION FOR THE TREATMENT OF EPILEPSY: CIRCUITS, TARGETS, AND TRIALS[*]

Deep brain stimulation (DBS) has proven remarkably safe and effective in the treatment of movement disorders. As a result, it is being increasingly applied to a range of neurologic and psychiatric disorders, including medically-refractory epilepsy. This review will examine the use of DBS in epilepsy, including known targets, mechanisms of neuromodulation and seizure control, published clinical evidence, and novel technologies. Cortical and deep neuromodulation for epilepsy has a long experimental history, but only recently have better understanding of epileptogenic networks, precise stereotactic techniques, and rigorous trial design combined to improve the quality of available evidence and make DBS a viable treatment option. Nonetheless, underlying mechanisms, anatomical targets and stimulation parameters remain areas of active investigation.

---

[*] Laxpati, N.G., Kasoff, W.S., Gross, R.E. Deep brain stimulation for the treatment of epilepsy: circuits, targets, and trials. *NeuroTherapeutics*. 2014.

2.1. INTRODUCTION

2.1.1 The Burden of Epilepsy

Epilepsy afflicts 1% of the world's population, and is medically refractory in 30-40% of cases. (WHO ; Wiebe et al. 2001; Sander 2003; Kwan and Sperling 2009). A substantial portion (10-50%) of medically-refractory patients are candidates for resective surgery (Engel 2013), with postoperative seizure freedom rates of 40-90% depending, in part, on underlying pathology. Nonetheless, there remain millions of patients who either cannot undergo resective surgery or who have recurrent seizures despite surgery (Wiebe et al. 2001; Helmstaedter et al. 2008; Helmstaedter et al. 2011; Engel et al. 2012; Engel 2013). Very few of these will respond to additional medication trials (Beleza 2009), and less than 10% will achieve seizure freedom with vagal nerve stimulation after failed resection (Amar et al. 2004). Thus, there is a pressing need for alternative therapies in medically refractory epilepsy.

Deep brain stimulation (DBS) has proven remarkably effective, safe, and practical in the treatment of movement disorders – primarily Parkinson's disease, dystonia and essential tremor (Hariz et al. 2010; Sironi 2011). These successes have inspired the application of DBS to an ever-broadening range of neurologic and psychiatric disorders, including depression (Holtzheimer et al.), obsessive-compulsive disorder (Blomstedt et al. 2013), and Gilles de la Tourette's syndrome (Kim and Pouratian 2014), as well as epilepsy. This review will examine the use of DBS in epilepsy, including potential targets, mechanisms of neuromodulation and seizure control, clinical evidence and recent clinical trials, as well as future directions and novel therapies.

2.1.2 Rationale: Cortical-Subcortical Networks in Epilepsy

Although partial-onset seizures – the most common seizure type in medically refractory epilepsy – are heterogeneous in onset zone and clinical manifestations, they often propagate along well-defined neural pathways. The networks incorporating these pathways – such as the cortical-striatal-thalamic network (Detre et al. 1996; Guye et al. 2006; Mueller et al. 2010) and the limbic circuit of Papez (Papez 1937; Oikawa et al. 2001) (Figure 2) – provide nodes at which neuromodulatory tools such as electrical stimulation have the potential to regulate the flow of neural information, including pathological signals mediating seizure propagation.

One of the most well-studied of these networks is the circuit of Papez (Papez 1937). Originally characterized for its role in mediating emotions, more recently this circuit has been associated with memory as well as the generation and propagation of limbic (e.g. mesial temporal lobe) seizures (Oikawa et al. 2001; Lega et al. 2010). The circuit originates from the hippocampus and subiculum, projects via the fornix to the mammillary body, then via the mammilothalamic tract to the anterior nucleus of the thalamus (ANT) (Figure 2). The ANT projects to the cingulate gyrus, then to the parahippocampal gyrus, followed by the entorhinal cortex, which finally projects via the perforant pathway back to the hippocampus (Papez 1937; Oikawa et al. 2001). Supporting the notion that neural networks provide multiple points for potential therapeutic interactions, lesions and high-frequency electrical stimulation at several locations along this pathway – including the hippocampus, mammillary bodies, subiculum and ANT – have demonstrated effective modulation of seizure propagation (Velasco et al. 2000; Duprez et al. 2005; Van Rijckevorsel et al. 2005; Fisher et al. 2010; Zhong et al. 2012; Bondallaz et al. 2013).
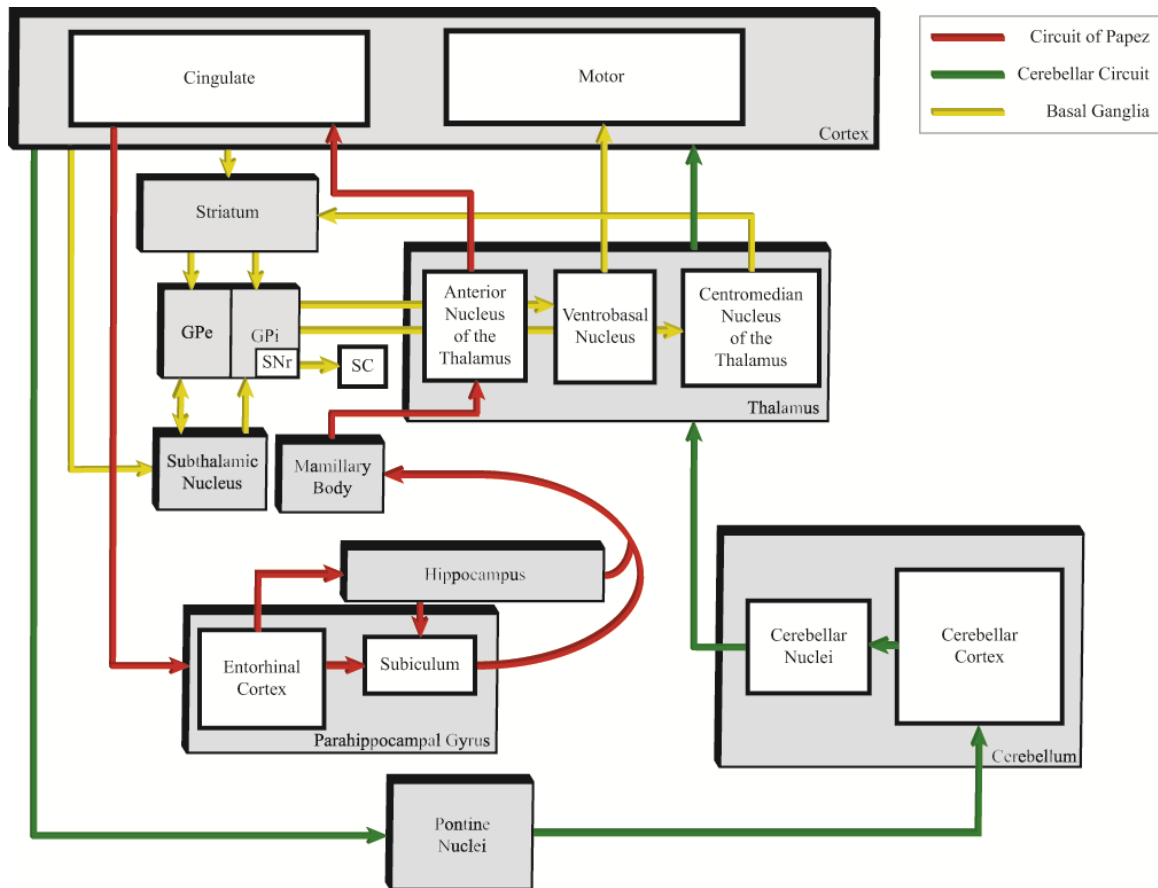
Figure 2: Neural Circuits and Anatomical Targets for Stimulation
Several major neural circuits have been identified and targeted for neuromodulation of epileptic seizures, including the Circuit of Papez (red), the Cerebello-cortico circuit (green), and the basal ganglia (yellow). GPe = external globus pallidus; GPi = internal globus pallidus; SC = superior colliculus; SNr = substantia nigra pars reticulata.

Cortico-thalamo-cortical excitatory loops appear to be involved in absence epilepsy (Lüttjohann and van Luijtelaar 2012) and motor cortex seizures (Detre et al. 1996). In a non-human primate model of chronic focal motor seizures, thalamotomy restricted to the anterior part of the ventro-postero-lateral nucleus was able to produce long-lasting benefit and in most cases led to nearly complete seizure suppression (Mondragon and Lamarche 1990). Thalamic relays are also thought to mediate the benefits from lesions and electrical stimulation of the cerebellum for epilepsy, but this circuit and its influence is less clearly defined (Gale 1992; Fountas et al. 2010; Haneef et

al. 2013). More precise work identifying and manipulating neural signaling within the thalamocortical network is currently being performed (Paz et al. 2013).

These networks, in conjunction with lesional studies and investigations in animal models, have implicated several potential neuromodulatory targets for the treatment of epileptic seizures. To achieve the greatest therapeutic effects and identify the optimum targets and parameters for deep brain stimulation, however, requires a greater understanding of the mechanisms underlying the effects of electrical stimulation.

2.1.3 Mechanism: Neuromodulation via Electrical Stimulation

The stimulation parameters utilized in clinical trials have remained largely empirical in nature – oftentimes unchanged from the arbitrary patterns that were initially explored for each particular anatomical target (Table 1). Only recently have more complex deep brain stimulation parameters begun to be entertained in experiments with human patients (Brocker et al. 2013). A more reasoned approach would be to understand the underlying mechanisms guiding the effects of electrical stimulation on the nervous system, and to implement the most efficacious parameters in clinical trials and practice.

Despite the extensive use of DBS in neuromodulation, its mechanism of action remains poorly understood. The initial observation that high-frequency (>50 Hz) stimulation mimicked the effects of ablative procedures (Benabid et al. 2002) suggested that DBS was inhibitory in nature (Boon et al. 2009), inducing a reversible, functional lesion. Increasingly, however, the functional action of DBS on

Table 1: Published reports of deep brain stimulation for epilepsy

Study	Target	Design	N	Seizure type	Stimulation parameters	Followup	Results	Adverse Events
Cooper et al. 1973; Cooper et al. 1976	Cerebellum	Open-label	15	Variable (6 CPSz, 6 GTC, 3 myoclonic)	Variable (Most 10Hz, 10V; 1-min epochs alternating hemispheres)	11-38 mo	4 of 15 SF at ≥ 30 mo (2 CPSz, 1 GTC, 1 myo) 6 of 15 improved (2CPSz, 2 GTC, 2 myo) 5 of 15 no change	1 broken lead
Van Buren et al. 1978	Cerebellum	Double-blind crossover	5	Variable	10Hz, 10-14V; 8 min ON R/OFF L, 8 min ON L/OFF R	24-29 mo	0 of 5 SF 0 of 5 improved	3 cerebrospinal fluid (CSF) leaks 1 increased CSF pressure
Levy et al. 1979	Cerebellum	Open-label	6	Variable	10Hz, 2-4V; 8 min ON R/OFF L, 8 min ON L/OFF R	7-20 mo	0 of 6 SF 2 of 6 improved	1 infection resulting in explantation All had headaches
Wright et al. 1984	Cerebellum	Double-blind crossover	12	Variable	10Hz, 5-7 mA; 1 min ON R/OFF L, 1 min ON L/OFF R	6 mo	0 of 11 SF 0 of 11 improved	6 patients more than one operation 2 post-op wound infections, 1 resulting in explantation 4 reoperations 1 lead repositioning 1 device failure
Velasco et al. 2005	Cerebellum	Double-blind crossover	5	Variable	10Hz, 3.8mA, PW 450μs, 2.0 μC/cm^2 4 min ON B/l, 4 min OFF B/l	24 mo	3 mo: mean seizure reduction 33% 6 mo: mean seizure reduction 41%	3 reoperations for migration 1 wound infection resulting in removal 1 ataxia and dysmetria 4 electrode migrations

Table 2: continued

Study	Target	Design	N	Seizure type	Stimulation parameters	Followup	Results	Adverse Events
Velasco et al. 2000	HC	Open-label	16	TLE	130 Hz, 0.2-0.4mA, PW 450μs	2 weeks	7 of 10 SF after 6 d 3 of 3 chronic stimulation improved Interictal spikes decreased	N/A
Tellez-Zenteno et al. 2006	HC	Double-blind crossover	4	MTLE	190Hz, 1.8-4.5V, PW 90μs	6 mo	0 of 4 SF 3 mo: median seizure reduction 15%	None reported
Velasco et al. 2007	HC	Open-label	9	MTLE	130Hz, 0.3mA, PW 450μs 1 min ON B/l, 4 min OFF B/l	18 mo	4 of 9 SF 5 of 9 improved	3 skin erosion and local infection, 1 requiring hospitalization 2 explantations
Boon et al. 2007	HC	Open-label	12	TLE	130Hz, 2-3V, PW 450μs	15-52 mo	1 patient exited trial before stimulation 1 of 11 SF 9 of 11 improved (6 of 11 > 50%) 3 of 11 SF after additional leads	1 asymptomatic hemorrhage
McLachlan et al. 2010	HC	Double-blind crossover	2	MTLE	185Hz, "subthreshold", PW 90μs	9 mo	0 of 2 SF 3 mo: mean seizure reduction 33%	None reported
Cukiert et al. 2011	HC	Open-label	6	Variable (5 TLE)	130Hz, 4V, PW 300μs	Acute stimulation only	Clinical outcomes pending 4 of 6 with interictal spikes suppressed	None reported

Table 3: continued

Study	Target	Design	N	Seizure type	Stimulation parameters	Followup	Results	Adverse Events
Boëx et al. 2011; Bondallaz et al. 2013	HC	Open-label	8	MTLE (2 HS)	130Hz, 0.5-2V, PW 450μs	10-74 mo	2 of 8 SF 4 of 8 improved (50-90%)	1 electrode displacement resulting in reimplantation 1 electrode fracture 2 reversible memory deficits with stimulation
Tyrand et al. 2012	HC	Open-label	12	TLE (6 HS)	130Hz 1V peak-to-peak, PW 210 or 450μs	Acute stimulation only	No seizure outcomes reported HS patients demonstrated 51.8% decrease in epileptiform discharges with biphasic stimulation	N/A
Benabid et al. 2002; Chabardès et al. 2002	STN	Open-label	5	Variable	130Hz, 0.8-5.2V, PW 90μs	30 mo	0 of 5 SF 3 of 5 improved (67-80%)	1 infection 1 postimplantation subdural haematoma
Handforth et al. 2006	STN	Open-label	2	CPSz	185Hz, <3.5V, PW 90μs	27 mo	2 of 2 improved (33-50%)	1 repeated surgery 1 hardware failure
Vesper et al. 2007; Wille et al. 2011	STN	Open-label	5	Myoclonic	130 Hz, 3.0V, PW 90μs	12-42 mo	1 of 5 SF 4 of 5 improved (>30%)	
Capecci et al. 2012	STN	Open-label	2	Variable	130Hz, 2-3V, PW 60μs	12-48 mo	1 of 2 improved (65%)	1 patient demonstrated mild balance impairment, dysarthria, severe aboulia, apathy, and mood changes under chronic stimulation

Table 4: continued

Study	Target	Design	N	Seizure type	Stimulation parameters	Followup	Results	Adverse Events
Sramka et al. 1990; Chkhenkeli et al. 1997; Chkhenkeli et al. 2004;	Caudate	Open-label	57	Variable	Variable	Variable	Unclear	N/A
Velasco et al. 1987; Velasco et al. 2000; Velasco et al. 2006;	CMT	Open-label	18	Variable	60Hz, 0.5-0.6mA 1 min ON R/OFF L, 4 min OFF B/l, 1 min ON L/OFF R, 4 min OFF	18 mo	Lennox-Gastaut: 2 of 13 SF, 8 of 13 improved (50-80%) Partial seizures: 2 of 5 improved (>80%)	2 patients explanted due to repeated skin erosions
Fisher et al. 1992	CMT	Double-blind crossover	6	Variable	65Hz, 0.5-10V, PW 90μs 1 min ON, 4 min OFF x 2 hr/day	9 mo	30% mean seizure reduction With stim 24 hr/day, 3 of 6 improved (>50%)	1 connection repair 1 minor hemorrhage with no symptoms or complications
Andrade et al. 2006	CMT	Open-label	2	Variable	100-185Hz, 1-10V, PW 90-120μs,	20-80 mo	1 of 2 improved (>50%)	1 intermittent nystagmus with stimulation 1 possible auditory hallucinations and anorexia during stimulation
Valentin et al. 2013	CMT	Single-blind	11	Variable (6 PGE, 5 FLE)	130Hz, < 5V, PW 90μs	6-72 mo	PGE: 5 of 6 improved (>50%) FLE: 1 of 5 improved (>50%)	1 infection resulting in explantation 1 transient agraphia

Table 5: continued

Study	Target	Design	N	Seizure type	Stimulation parameters	Followup	Results	Adverse Events
Hodaie et al. 2002; Andrade et al. 2006	ANT	Single blind	6	Variable	100-185Hz, 1-10V, PW 90-120μs	50-70 mo	Difficult to interpret; 6 of 6 improved (>50%) by implantation; no further improvement with stim	1 skin erosion requiring wound revision 1 lethargy with continuous stimulation
Kerrigan et al. 2004	ANT	Open-label	5	Variable	100Hz, 1-10V, PW 90-330μs	6-36 mo	Difficult to interpret; non-significant improvement in 4 of 5	1 reimplantation for incorrect positioning
Lim et al. 2007	ANT	Open-label	4	Variable	90-110Hz, 4-5V, PW 60-90μs	33-48 mo	4 of 4 improved (37-75%)	1 resolved mild left-hand weakness associated with hemorrhage 1 scalp erosion resulting in explantation
Osorio et al. 2007	ANT	Single-blind	4	Variable	145Hz, 4.1V, PW 90μs, 1 min ON b/l, 5 min OFF b/l	36 mo	4 of 4 improved (53-92%)	None reported
Fisher et al. 2010 (SANTE)	ANT	Double-blind parallel-group	110	Partial-onset	145Hz, 5V, PW 90μs	4 mo (blinded) 13 -37 mo (open)	4 mo: Median seizure reduction 40.4% with active stimulation, 14.5% with sham stimulation 13 mo: 2 of 110 SF; 43% with >50% response 25 mo: 6 of 81 SF; 54% with >50% response	808 reported in 109 participants, 55 in 40 categorized as serious, 238 of 808 events considered device-related 18.2% paresthesias 14.8% depression during blinded phase 13.0% memory impairment during blinded phase

Table 6: continued

							12.7% implant site infection 10.9% implant site pain 8.2% replaced leads for poor placement 4.5% nonsymptomatic hemorrhages 5 deaths 5 status epilepticus

SANTE = Stimulation of the Anterior Nucleus of the Thalamus in Epilepsy; HC = hippocampus; STN = subthalamic nucleus; CMT = centromedian nucleus of the thalamus; ANT = anterior nucleus of the thalamus; CPSz = complex partial seizure; GTC = generalized tonic-clonic seizure; TLE = temporal lobe epilepsy; MTLE = mesial temporal lobe epilepsy; HS = hippocampal sclerosis; FLE = frontal lobe epilepsy; R = right; L = left; PW = pulse width; b/l = bilateral; SF = seizure-free; myo = myoclonic; PGE = primary generalized epilepsy; CSF = cerebrospinal fluid; N/A = not available
*Follow-up in months unless otherwise specified

neural circuits has been recognized as complex and multifaceted. Stimulation amplitude, frequency and pulse-width play a major role in determining the effects of stimulation, and manipulating other parameters such as waveform and polarity can have significant effects as well (Rolston et al. 2011; Bari et al. 2013).

Early work by Ranck (Ranck 1975) indicated that electrical fields have differential effects on different neuronal structures. Activation thresholds were lowest in myelinated axons, increasing in unmyelinated axons, dendrites, and cell bodies, respectively. Further work by Histed and colleagues, utilizing low-current 250 Hz electrical microstimulation with concurrent 2-photon calcium imaging to identify the location of electrically-activated neurons (Histed et al. 2009), has supported these hypotheses.

Using multi-compartment cable models of neurons coupled to a finite element model of extracellular electric fields, McIntyre et al. (McIntyre et al. 2004) suggest that the majority of cells within ~2 mm of the electrode will generate efferent (axonal) output at the stimulus frequency, whereas those stimulated at sub-threshold levels will be suppressed (McIntyre et al. 2004). Electrical stimulation may consequently be "hijacking" the neural circuit (Cheney et al. 2012) – blocking the extant neural activity and replacing the efferent output with its own. Our own work demonstrates 'entrainment' of downstream (both orthodromic and antidromic) neuronal firing by deep brain stimulation in a Parkinson's patient (R. Gross, K. Mewes, M. DeLong, unpublished data). The consequences of this new efferent output on downstream circuits will depend on their neural connections.

Other mechanisms may be important as well, including neurochemical mechanisms, gene, and protein expression. The anticonvulsant effects of low frequency stimulation have been correlated with changes in adenosine receptor expression (Jahanshahi et al. 2009), and vagal nerve stimulation has been associated with alterations in a variety of neurotransmitters and hormones in cerebrospinal fluid (Hammond et al. 1992). Furthermore, the progressive improvement in outcome associated with electrical stimulation for movement disorders (Krack et al. 2002) and epilepsy (see below) (Fisher et al. 2010; Morrell 2011), suggest that synaptic, neurochemical, and/or expression changes are occurring in response to electrical stimulation of the pathologic neural network.

2.2. TARGETS FOR ELECTRICAL STIMULATION IN EPILEPSY

The history of electrical stimulation for epilepsy has been one of extreme heterogeneity (Table 1), with a great variety of anatomical targets, stimulation parameters, and outcome measures being evaluated. These have primarily been investigated in small case series, and the varying nature of these studies has often made synthesizing conclusions – particularly statistical conclusions – quite difficult. To this end, we attempt here to highlight and summarize the results of these investigations – where possible using the original authors own phrasing with regards to outcome – categorized by anatomical target. In general, the results are described in terms of complete freedom from seizures (seizure-free), a clinically significant reduction in seizure frequency (reduction, response, improvement), or no response (unresponsive, no benefit).

2.2.1 Cerebellum

The earliest subcortical target of stimulation for epilepsy was the cerebellum, which was found as early as the 1950s to modify or halt seizures in animal models of both cortically-induced (Moruzzi 1950; Cooke and Snider 1955) and hippocampal (Iwata and Snider 1959) seizures. The mechanism of action was originally thought to be thalamic inhibition via stimulation-induced Purkinje cell output, but this remains somewhat unclear (Fountas et al. 2010). In the 1970s, Cooper and colleagues were the first to report human cerebellar stimulation for epilepsy. A heterogeneous patient population underwent subdural stimulation of the superior surface of the cerebellar cortex via an inductively-driven system using variable stimulation parameters (Cooper et al. 1973). Of 15 patients, 10 showed significant seizure improvement for up to three years (Cooper Is 1976). However, when Van Buren et al. used a similar technique to perform a double-blind crossover study of 5 patients with intractable epilepsy, no significant differences in seizure frequency were detected (Van Buren et al. 1978). Contemporary results were also published by Levy and Auchterlonie, showing a modest response rate of 33% (2 of 6 patients) (Levy and Auchterlonie 1979). Following these results, Wright et al (Wright et al. 1984) published a prospective, double-blind, crossover study of 12 patients with stable, long-term epilepsy (10 to 32 years) using bilateral 8-contact electrodes inserted over the superior cerebellar surface via occipital burr holes. Patients received 2 months of continuous 5-7 mA 10 Hz stimulation of alternating polarity that alternated hemispheres every other minute (some patient parameters were uniquely adjusted based on their individual responses), 2 months of self-controlled stimulation, and 2 months of no stimulation. There was no observed decrease in the frequency of seizures in the 11 patients available for follow-up. There was a 25% rate of lead migration, a 16.6% rate of

wound infection, and an 8.3% rate of mechanical failure. Interestingly, although there was no objective effect on either seizures or neuropsychological testing, a majority of patients reported that stimulation was beneficial (Wright et al. 1984).

The failure of these two trials, despite the previous apparent clinical successes, led to the cerebellum falling out of favor as a target for epilepsy until revisited by Velasco et al. in 2005 (Velasco et al. 2005). In this double-blind crossover study of 5 patients with medically intractable epilepsy, subjects were implanted bilaterally with 4-contact electrodes on the superomedial surface of the cerebellum. Stimulation parameters were adjusted to deliver a charge density of 2.0 µC/cm^2/phase, with a fixed pulse width of 0.45 ms and current amplitude of 3.8 mA. Stimulation frequency was set at 10 Hz, akin to that explored by Cooper et al. (Cooper Is 1976; Van Buren et al. 1978; Wright et al. 1984). At the end of the three-month blinded evaluation, seizure frequency had decreased by 33% in the group receiving stimulation vs. no reduction in the unstimulated group. At the end of the six-month unblinded stimulation period, the mean seizure reduction rate was 41% (range, 14-75%). Statistical analysis demonstrated a significant reduction in tonic-clonic seizures ($p < 0.001$) and tonic seizures ($p < 0.05$). As with previous trials, there was a high incidence of lead migration (60%).

The small sample sizes, conflicting results and high complication rate of cerebellar stimulation (Van Buren et al. 1978; Wright et al. 1984; Velasco et al. 2005) make its role in the treatment of epilepsy unclear without further investigation. A pooled analysis of prior small series has recently been published by Krauss and Koubeissi (Krauss and Koubeissi 2007), demonstrating a seizure freedom rate of 27% (31 of 115 patients) and at minimum a reduction of seizures in 76% (87 of 115 patients) in the prior,

heterogeneous case series. More rigorously controlled studies across 17 patients found none seizure free, and 5 of 17 with reduced seizures. A detailed review on the subject has also recently been published (Fountas et al. 2010).

2.2.2 Hippocampal formation

Mesial temporal lobe epilepsy (MTLE) is the most common form of medically refractory epilepsy and enjoys a high rate of seizure freedom following amygdalohippocampal resection (Wiebe et al. 2001; Kwan et al. 2011; Engel et al. 2012; Engel 2013). However, hippocampal resection or ablation may be contraindicated in cases of dominant-onset MTLE with preserved verbal memory, cases with bilateral mesial temporal onsets, or recurrent MTLE contralateral to a prior resection. Thus, the ability to prevent or abort seizures arising from the mesial temporal structures without resection or ablation — potentially preserving interictal function — would represent a major advance in the surgical treatment of epilepsy.

The hippocampus is an appealing target for neuromodulation. Although larger than most other DBS targets, and therefore potentially more prone to targeting error and variability, the hippocampus is often stereotactically accessed with recording electrodes and consequently is a relatively familiar target for epilepsy surgeons. Several studies of hippocampal slices and rodent models provided preclinical support for hippocampal DBS (Lian et al. 2003; Ellis and Stevens 2008; Boon et al. 2009; Zhong et al. 2012). The first systematic human studies of hippocampal stimulation came from the Mexico City group of Velasco et al., initially in a pilot study of stimulation prior to temporal lobectomy in 10 patients (Velasco et al. 2000). More recently, the same group reported 18-month follow-up of 9 patients with MTLE, 4 with classic radiological signs of hippocampal sclerosis

(HS) and 5 with normal MRIs, who experienced 15-70 seizures per month (average of 28 seizures) (Velasco et al. 2007). All patients initially underwent invasive monitoring with bilateral 8-contact hippocampal depth electrodes in preparation for amygdalohippocampectomy, but did not undergo resection due to bilateral independent onsets (4 patients) or onsets on the dominant side associated with preserved verbal memory (3 patients). One patient with right-sided onset did not undergo resection due to occasional left-sided epileptiform discharges and another because of bilateral MRI evidence for hippocampal sclerosis. After the completion of the diagnostic phase, the depth electrodes were removed and quadripolar DBS leads (1.5 mm contacts, 0.5 mm spacing) were placed within the long axis of the hippocampus, targeted so that at least 2 contacts were within the identified area (or bilateral areas) of maximal seizure onset. As per their diagnostic findings, 4 patients were implanted bilaterally, 3 unilaterally on the left and 2 unilaterally on the right. Bipolar stimulation within the seizure focus (usually the pes hippocampus or amygdala-pes junction) was performed with 1-minute trains of square wave pulses at 130 Hz, 450 µs duration, and 300 µA amplitude, followed by 4-minute stimulation-free intervals (alternating side-to-side in bilateral cases). Five patients were randomized to an initial one-month, double-blinded period without stimulation in order to investigate possible implantation effects.

Of the 9 patients, 4 (44%) were seizure-free at 18-month followup. Interestingly, these 4 were all in the MRI-normal group, and all showed early and dramatic responses within the first 2 months of stimulation. The fifth patient with a normal MRI also had an immediate, sharp decrease in seizure frequency and, although not seizure-free, continued with only brief, occasional complex partial seizures throughout the study. In contrast, the

4 patients with evidence of hippocampal sclerosis on MRI showed more delayed and partial responses to stimulation, with seizure reduction becoming statistically significant by 8 months and leveling off (with between 50 and 70% reduction) by 10 months. Seizure freedom and levels of seizure reduction were maintained through 18 months of follow-up in all patients.

Important features of the Mexico City series include the use of eight-contact diagnostic depth electrodes followed, in a separate procedure, by DBS placement targeted to the ictal onset zone, which in one case resulted in more posterior DBS placement than would have occurred with standardized placement in the pes hippocampus. As the authors state, a substantial minority (20% in some studies (King et al. 1997)) of MTLE patients demonstrate onset in the posterior hippocampus, and standardized anterior placement of quadripolar electrodes might leave these patients' ictal onset zone outside the area of stimulation. Second, the stimulation paradigm used a constant-current design, which may be more physiologically appropriate in compensating for changes in electrode and/or tissue impedance. Third, in contrast to the study of Boon et al. (Boon et al. 2007) discussed below, better responses were seen in MRI-normal patients than in those with MRI evidence for hippocampal sclerosis. The authors suggest the decreased cell counts and, presumably, lesser network connectivity of a sclerotic hippocampus as an explanation for the delayed effectiveness in these patients. The authors also considered the possibility that tissue impedances may be substantially different in sclerotic vs. normal tissue, but felt this was unlikely, since stimulation artifacts were seen on scalp electrodes at similar threshold voltages in all patients. Finally, a few pieces of evidence support a true effect of stimulation in this trial. The 5 patients who experienced one

double-blind month absent stimulation onset did not show a change in seizure frequency compared to baseline during the first postoperative month, whereas the 4 patients who underwent stimulation during that month showed immediate decreases in seizure frequency. In addition, three patients in whom stimulation was later interrupted (one from battery depletion, two from skin erosion and device removal) showed a partial return to baseline seizure frequency.

The Belgian group of Boon et al. published their experience with acute and long-term hippocampal DBS in patients with refractory TLE (Boon et al. 2007). In twelve patients, two quadripolar DBS electrodes were implanted bilaterally through parieto-occipital burr holes, with one electrode terminating in the amygdala and one terminating in the anterior hippocampus. During the same surgery, recording grid and/or strip electrodes were implanted and monitoring was performed to ascertain seizure onset zone(s). One patient with unilateral mesial temporal onsets exited the trial in favor of resective surgery prior to the stimulation phase. Of the patients that went on to stimulation, 10 had unilateral and 1 had bilateral onsets. All eight contacts across the amygdala and hippocampal quadripolar electrodes on the side of onset were used for stimulation in each unilateral patient; the bilateral patient was stimulated through the bilateral hippocampal electrodes only. Bipolar stimulation was delivered through two pairs of contacts on each electrode, with mean output voltage of 2.3V (range 2-3V), frequency of 130 Hz (1 patient at 200Hz), and pulse width of 450µs. Initial acute stimulation was performed using a temporary external pulse generator, followed by long-term stimulation with an implanted pulse generator if >50% reduction of interictal spike frequency was achieved with temporary stimulation, which occurred in 10 of 11 patients.

Outcome was assessed by comparing each patient's mean monthly seizure frequency during the last six months of follow-up (mean total follow-up 33 months; range 15-52 months) to the pre-intervention baseline. One patient (10%) became seizure free, one had >90% seizure frequency reduction, 5 had seizure reduction >50%, 2 had 30-49% seizure reduction, and one had <30% reduction. Long-term follow-up of the same group plus one additional patient was recently reported, with stimulation adjustments including implementation of bilateral stimulation in 6 patients with <90% response to unilateral stimulation (Vonck et al. 2013). Going from unilateral to bilateral stimulation improved 3 of 5 patients, with one becoming seizure-free, despite onset regions being unilateral. The previous one patient who was seizure-free continued as such, despite stimulation being discontinued at battery end-of-life, and one other patient became seizure-free when stimulation was stopped. Thus, while a total of 6 (55%) patients achieved >90% seizure reduction, the overall 27% rate of seizure freedom (3 of 11) in this long-term follow-up group must be cautiously interpreted. In contrast to the results of Velasco et al. (Velasco et al. 2007), discussed previously, 2 of 3 patients in this study with hippocampal sclerosis became seizure-free (vs. 1 of 11 without), although one of them was the patient that became seizure-free when stimulation was turned off, and the other maintained seizure freedom despite stimulation discontinuation.

The low rate of seizure freedom in this study may have been attributable in part to the proportion of patients (50%) with regional onset in the temporal lobe, rather than a well-defined mesial temporal onset. Another issue may be that stimulation was delivered to only a small region of the hippocampus: the electrodes spanned at most 21 mm (10.5 mm x 2 electrodes) and since the anterior one was in the amygdala, the posterior

electrode did not extend much beyond the hippocampal head. Moreover, bipolar stimulation only delivers cathodic pulses to one of the pair due to the Lilly pulse waveform (charge-balanced biphasic pulses designed to prevent charge deposition and resultant tissue damage (Hauptmann et al. 2009)). It would be interesting to know the effects of using all 8 contacts as cathodes with the case as the anode ("monopolar" stimulation), to affect a larger volume of hippocampal tissue.

Two small series of hippocampal stimulation have been reported by the University of Western Ontario group (Tellez-Zenteno et al. 2006; Boëx et al. 2011). In the first, 4 patients with left mesial temporal seizure onset who were unable to undergo resection (1 due to prior right temporal resection, 3 due to failed intracarotid amobarbital testing) underwent placement of unilateral quadripolar electrodes (3 mm contacts, 6 mm spacing; total span 30 mm) with the first contact in the pes hippocampus and three contacts in the hippocampal body. All four had imaging evidence of hippocampal sclerosis (2 left, 2 bilateral, including the patient with prior right-sided resection). Monopolar stimulation using all four contacts (190 Hz, pulse wide 90μs, voltage adjusted below the patients' conscious thresholds, ranging from 1.8 to 4.5V) was delivered in a double-blinded, randomized, crossover design for 6 months (3 consecutive 2-month periods randomized to ON-OFF vs. OFF-ON). Median seizure frequency reduction between the 3 ON months and 3 OFF months was 15%, although results did not reach statistical significance. No patient was rendered seizure-free, and results were somewhat variable among the 4 patients. This investigation went so far as to explore multiple neuropsychological measures, which importantly did not show any difference between the stimulation-on and stimulation-off states. In their second series, the same group

reported their results in 2 patients with independent, bilateral mesial temporal seizure onset, 1 of whom had a normal MRI and 1 of whom had bilateral MRI evidence for hippocampal sclerosis. Electrode placement and stimulation parameters were similar (with the only difference being stimulation at 185Hz instead of 190Hz). The 2 patients were randomized to undergo 3 months ON and 3 months OFF (in this series, as 3-month blocks) in random order, with a 3-month washout period. Results with bilateral stimulation were slightly more robust than in the earlier, unilateral series, with a mean seizure frequency reduction of 33% in ON periods compared to OFF. Again, no patient was rendered seizure-free. One patient showed declines in verbal and visuospatial learning scores during stimulation. Of note, the volume of tissue modulated in these 6 patients is likely larger than in the Belgian group, since electrodes spanning 3 cm of hippocampal length were used in a "monopolar" configuration.

More recently, the Swiss group of Boëx et al. (Boëx et al. 2011) presented a series of 8 TLE patients (2 with hippocampal sclerosis, 6 non-lesional) who were unable to undergo amygdalohippocampectomy due to bilateral onset (5 patients) or onset ipsilateral to preserved verbal memory (3 patients). All patients received unilateral DBS placement on the side of more frequent seizure onset as determined noninvasively (3 patients) or with intracranial recording (5 patients). A single DBS lead was placed along the long axis of the hippocampus at its junction with the parahippocampal gyrus, with the anterior-most contact at the amygdalo-hippocampal junction. The first 5 patients received quadripolar electrodes (3mm contacts with 6mm spacing; total length 30mm) and the last 3 received octrodes (3mm contacts with 1.5mm spacing; total length 34.5mm). Stimulation was tested in both monopolar configuration, with 4 contacts as the cathode

(130Hz, pulse width 450µs, 1-2V), and in bipolar configuration (130Hz, pulse width 450µs, 0.5-1.5V), using the two contacts with the highest frequency of interictal discharges as cathode and anode.

Of the 8 patients reported, 2 (25%) became seizure-free (one without stimulation, as with Vonck et al. (Vonck et al. 2013), discussed above). Four patients, including the 2 with HS, had 50-90% reduction in seizure frequency, and 2 patients did not show statistically significant seizure reduction. In the 2 patients with presumed hippocampal sclerosis, monopolar stimulation appeared to be more effective than bipolar, but there did not appear to be significant differences between monopolar and bipolar stimulation in non-lesional patients. Interestingly, a subsequent re-analysis of this cohort (Bondallaz et al. 2013) demonstrated that all 6 patients with >50% seizure frequency reduction had active contacts located within 3 mm of the subiculum, whereas the 2 non-responders had electrodes more than 3 mm from the subiculum. Proximity to the presumed seizure onset zone, in contrast, was not associated with outcome, with responders' and non-responders' active contacts located 11 ± 4.3 mm (mean ± SD) and 9.1 ± 2.3 mm from the ictal onset zone, respectively.

Although this study demonstrated significant overall seizure reduction, several inconsistencies make it difficult to interpret. First, the lack of intracranial evaluation in 3 of 8 patients introduces some degree of diagnostic uncertainty, although 2 of these 3 had MRI evidence for hippocampal sclerosis concordant with the side of seizure onset and would have thus proceeded directly to resection were it not for the results of their intracarotid amobarbital testing. Second, the use of two different types of DBS leads and multiple stimulation parameters introduces additional variables; however, this may more

accurately reflect real practice, which will likely require patient-by-patient stimulation adjustments. Third, by the authors' own admission, the use of unilateral stimulation even in cases with documented bilateral seizure onset may have limited the effectiveness of DBS therapy in comparison to the series of Velasco et al. (Velasco et al. 2007) Fourth, stimulation voltages were generally low in comparison to other studies, with maximum amplitude of 2V, potentially limiting the volume of tissue stimulated. Finally, the use of battery depletion as a method of "OFF" testing raises an additional degree of heterogeneity, since the exact timing of "OFF" periods may not be precisely known and will not be consistent, and since variable degrees of neuromodulation may have occurred prior to battery depletion in individual patients.

This group recently published a comparison of biphasic and pseudomonophasic stimulation using hippocampal depth electrodes in 12 patients undergoing intracranial monitoring (Tyrand et al. 2012). Stimulation (1V peak-to-peak, 130 Hz, pulse width 210 and 450 µs) via perpendicular depth electrodes (and, in 3 cases, also via longitudinal DBS leads prior to internalization) was performed in 4-hour epochs during an acute hospital stay. The effect on the interictal epileptiform discharge rate (IEDR) was measured using an automated detection algorithm. In patients with MRI evidence for hippocampal sclerosis, there was a reduction in IEDR of 51.8% +/- 10.3 (mean +/- SD) using biphasic stimulation, but no significant reduction using pseudomonophasic stimulation. In non-lesional patients, neither waveform produced a decrease in IEDR. Thus waveform characteristics, which may select differently-oriented fibers for activation by more heavily weighting cathodic or anodic pulses at each electrode, may play a role along with other DBS parameters in determining the effectiveness of stimulation.

Cukiert et al. (Cukiert et al. 2011) recently reported suppression of interictal spiking with intraoperative test stimulation (130 Hz, 300μs, 4V) in 4 of 6 patients undergoing bilateral hippocampal DBS placement, but associated clinical outcomes have not yet been reported for this cohort.

The above open label studies laid the groundwork for two clinical trials to further evaluate the effectiveness of hippocampal stimulation in epilepsy therapy: the Controlled Randomized Stimulation Versus Resection (CoRaStiR) trial, based in Belgium and Germany (NCT00431457) (University Hospital and Medtronic), and the Medical vs. Electrical Therapy for Temporal Lobe Epilepsy (METTLE) study, based at the University of Calgary (NCT00717431) (Calgary et al.), the latter of which has been terminated due to insufficient enrollment. The CoRaStiR trial will randomize patients with TLE into three arms: immediate amygdalohippocampectomy, immediate hippocampal stimulation, and implantation of hippocampal electrodes with delayed initiation of stimulation by 6 months. Treatment will be unblinded and results compared at 12 months post-surgery using measures of seizure frequency, neuropsychological outcome, mood and quality of life. Also at this period, patients undergoing neurostimulation will have the option to either continue neurostimulation or undergo resective surgery.

Despite promising small series and open label data, the value of hippocampal DBS remains difficult to assess in the absence of larger, prospective data sets. The procedure appears to be safe and does not appear to carry significant neuropsychological risks (Velasco et al. 2007; McLachlan et al. 2010; Miatton et al. 2011). However, as seizure freedom rates have been low in open label trials thus far performed, the prospect for hippocampal DBS achieving a high rate of seizure freedom in blinded controlled trials

is similarly low. This is substantiated by the randomized, double-blind, sham-stimulation controlled trial of responsive neurostimulation (RNS®; Neuropace, Mountainview, CA), in which 50% of the 191 patients with medically refractory seizures had mesial temporal onsets and were implanted with 4-contact leads in the amygdala/hippocampus (Morrell 2011). Overall, 7.1% of patients were seizure-free over the last 3 months of follow-up available (≥ 1 year). In the long-term continuation trial, combining all implanted RNS patients (feasibility plus pivotal trials), this number increased to 13% (31/247); 20.3% had at least one seizure-free period of 6+ months during the trial, albeit not necessarily at last follow-up (Bergey et al., submitted). It should be noted that in this combined group, only 43.4% had seizures arising solely from the mesial temporal lobe. While detailed outcome analysis of the mesial temporal patients was not provided in either report of this trial, seizure localization to the mesial temporal lobe (vs. other locations) was not a significant factor in determining the treatment response, suggesting that there was not a high rate of seizure freedom in MTLE patients in this trial (see Morrell et al., in this issue). Thus, neurocognitive factors notwithstanding, it is likely that hippocampal DBS will emerge as a tool to reduce the frequency of − but not eliminate − seizures in patients who are not candidates for surgical resection or ablation, which remains the gold standard for achieving seizure freedom in MTLE.

2.2.3 Subthalamic Nucleus/Substantia Nigra

Control of limbic seizures in rats by bilateral pharmacological inhibition of the substantia nigra (SNr) was first demonstrated in the early 1980s (Iadarola and Gale 1982; Garant and Gale 1983; Vercueil et al. 1998). Although the mechanisms of such control in animal models is unclear (Vercueil et al. 1998; Dinner et al. 2002; Gross 2008; Zhang et al.

2008), it has been suggested that the release of nigral inhibition of a dorsal midbrain (i.e. superior colliculus) anticonvulsant zone is involved (Loddenkemper et al. 2001) (Figure 2). Thus far, rather than directly modulating SNr with DBS, animal studies have attempted to achieve SNr inhibition via modulation of the subthalamic nucleus (STN) (Vercueil et al. 1998), with the idea that high-frequency stimulation of the STN would reduce excitatory input from the STN to SNr. Although STN DBS was found to be effective in rodent models of epilepsy, more recent evidence that high-frequency stimulation actually *drives* STN activity rather than inhibits it, in addition to supportive neurotransmitter evidence (Zhang et al. 2008), suggests the possibility that inhibitory effects of STN stimulation on SNr were mediated indirectly via activation of GPe (Gross 2008). Resulting elevated GABA levels in SNr from overdriving its GPe afferents would be predicted to dominate any increased glutamate release in SNr from STN driving, due to more proximal location of GABA vs. glutamate receptors on SNr cell bodies (Gross 2008). Additional mechanistic explanations for the use of STN DBS include antidromic neuromodulation of the motor cortex (Dinner et al. 2002; Gross 2008), or other frontal neocortex (Urrestarazu et al. 2009), from STN (Gradinaru et al. 2009).

Several small case series of STN stimulation have been reported (Benabid et al. 2002; Chabardès et al. 2002; Handforth et al. 2006; Lee et al. 2006; Vesper et al. 2007; Franzini et al. 2008; Capecci et al. 2012). In 2002, the Grenoble group reported 5 patients who underwent bilateral STN DBS (some with multiple leads) for inoperable seizures of various types (Benabid et al. 2002; Chabardès et al. 2002). Three patients (all with paracentral neocortical seizures) experienced 67-80% seizure reduction, while 2 patients (one with Dravet syndrome and one with fronto-insular seizures) did not show significant

improvement. In 2006, Handforth et al. (Handforth et al. 2006) reported two patients with refractory partial-onset seizures in whom bilateral STN stimulation (<3.5V, 90μs ,185 Hz pulses) was performed. The first, with partial complex seizures and bitemporal EEG onset, had a 50% reduction in seizure frequency. The second, with post-encephalitic hemiatrophy and left-sided seizure onset, experienced a 33% reduction in seizure frequency and a reduction in seizure severity, including arrest of generalized convulsions, fewer seizure-related injuries, and an improved quality of life. In 2007, Vesper et al. (Vesper et al. 2007) described a single patient with myoclonic epilepsy, who received monopolar stimulation (3.0V, 90μs, 130Hz) via two contacts spanning the inferior STN and SNr bilaterally. At 1-year follow-up, 50% reduction in the severity and frequency of myoclonic seizures was achieved, and the patient's vagal nerve stimulator (VNS) was turned off without recurrence of generalized seizures, which previously had been controlled only with VNS. In 2012, Capecci et al. (Capecci et al. 2012) presented two cases of bilateral STN DBS after failed disconnective surgery. The first case, a patient with widespread cortical atrophy, multiple seizure types, and prior anterior callosotomy, demonstrated a 70% reduction of partial seizures and 85% reduction of secondarily generalized seizures at 1 year with STN stimulation (2.0V, 60μs, 130Hz; stimulator off at night). The second case, a patient with bilateral temporal and occipital cortical and white matter abnormalities, had previously undergone anterior commissurotomy. Continuous stimulation (3.0V, 130Hz, 60μs) was associated with a decrease in tonic-clonic seizures, but a sharp rise in absence seizure frequency, leading to discontinuation of stimulation.

Following their successful 2007 case report (Vesper et al. 2007), Wille and Vesper (Wille et al. 2011) reported a series of five adults with progressive myoclonic

epilepsy who were implanted with STN DBS and followed in an unblinded fashion for 12-42 months. All five experienced improvement, with reduction of myoclonic seizure frequency between 30 and 100% and accompanying improvement in quality of life. Of note, 4 patients were implanted with bilateral Vim thalamus leads in addition to STN, but no benefit was seen with Vim stimulation.

Based on the above case series, STN DBS may be a palliative option, particularly in cases of myoclonic epilepsy. Unfortunately, with the termination of the Grenoble-based STIMEP trial (NCT00228371) due to insufficient enrollment, no larger-scale or randomized trials of STN stimulation appear to be forthcoming.

2.2.4 Caudate Nucleus

With the rationale of modulating the cortico-striato-thalamic network and inducing cortical hyperpolarization, Chkhenkeli et al. (Sramka and Chkhenkeli 1990; Chkhenkeli and Chkhenkeli 1997; Chkhenkeli et al. 2004) tested DBS of the ventral caudate in a large number of patients undergoing stereo-electroencephalography for seizure disorders. Low-frequency (4-8Hz) stimulation decreased cortical and hippocampal interictal spiking and epileptiform activity in a subset of these patients, several dozen of whom subsequently underwent placement of internalized DBS systems. 12 of 21 patients undergoing chronic stimulation of the head of the caudate nucleus (HCN) after resection of the epileptic focus did not provide benefit received a Class IC (Engel et al. 1993) (seizure free) outcome, with the remaining nine achieving worthwhile improvement (class IIIA) (Chkhenkeli et al. 2004). Amongst unlesioned patients, 9 of 17 experienced a IC with chronic therapeutic HCN stimulation, with five experiencing worthwhile reduction and three no improvement. The authors speculated on a suppressive effect due

to inhibitory processes from head of the caudate nucleus activation, although they noted variability in the excitatory and inhibitory effects of stimulation. However, a heterogeneous patient population, varying targets and stimulation paradigms, uncontrolled observations, and insufficient follow-up render this large, single institution series difficult to interpret.

2.2.5 Centromedian Nucleus of the Thalamus

The centromedian nucleus of the thalamus (CMT) has widespread projections to the cortex and plays a central role in wakefulness and cortical excitability (Figure 2) (Al-Otaibi et al. 2011). As these circuits seem to play a role in seizure generation and propagation (Mondragon and Lamarche 1990; Detre et al. 1996; Miller 1996; Lüttjohann and van Luijtelaar 2012), CMT has been explored as a potential target for DBS therapy. It is important to note, however, that CMT also has strong projections to the striatum, and some of its effects, at least in part, may be mediated via the cortico-striato-thalamic circuit (Smith et al. 2014).

Velasco et al. reported their first five cases of CMT DBS in 1987 (Velasco et al. 1987), and larger series in 2000 (Velasco et al. 2000) and 2006 (Velasco et al. 2006), using an alternating left-right stimulation paradigm (60Hz, 500-600µA, 1 minute on/4 minutes off, 24 hours/day). Seizure frequency was measured during a one-month baseline period and monthly for 18 months postoperatively during open label stimulation. Of the 18 patients reported, the most clearly positive results were seen in the 13 patients with Lennox-Gastaut syndrome, 2 of whom became seizure-free, 8 demonstrating 50-80% seizure reduction, and 3 having no response to therapy. Consistent with other observations of progressively decreasing seizure frequency during DBS (Fisher et al.

2010), VNS and RNS (Morrell 2011), seizure frequency decreased immediately after implantation and continued to decline thereafter, reaching its minimum after 6 months of stimulation. Double-blinded 3-month periods of stimulation cessation (between 6 and 12 months after surgery) did not show a return to baseline frequency, whereas open label interruption of stimulation and explantation in two patients with skin erosion and battery depletion after 20 and 39 months on-stimulation, respectively, was associated with increases in seizure frequency to reach or surpass the baseline period. These results a residual antiepileptic effect, possibly due to neural plasticity, however patient bias cannot be excluded. In contrast to the patients with generalized tonic-clonic seizures and consistent with previous results (Velasco et al. 1993; Velasco et al. 1993), 5 patients with partial epilepsy syndromes fared less well, with only 2 of 5 achieving >80% seizure reduction.

Fisher et al. attempted to subject CMT DBS to objective evaluation using a randomized, double-blind, sham-stimulation controlled design. Six patients were enrolled in a cross-over design with 3-month blinded periods; 3-month washout periods were interposed between stimulation periods (Fisher et al. 1992). Although there was a 30% decrease in seizures during stimulation, as compared to an 8% decrease during sham periods, the results were not statistically significant. Several critical factors mitigate interpretation of these findings to support ineffectiveness of CMT DBS. First, the amplitude for active stimulation was set at 50% of the sensory threshold in order to maintain effective blinding. Although details of the actual stimulation amplitude (range 0.5 – 10 V) were not provided, it was likely somewhat below that used in the Mexico City studies where amplitudes 90% of sensory threshold were used. Thresholds were

allowed to increase to this level during the open label extension in the Fisher et al. study; 3 of 6 patients experienced a >50% reduction of generalized tonic-clonic seizures during this phase (Fisher et al. 1992). Moreover, since sensory threshold arises from current spread to the ventrobasal sensory nucleus, it is subject to proximity of the electrode to that structure; low thresholds would lead to correspondingly low stimulation dosages with respect to CMT and would undermine effectiveness. Second, the small number of patients studied place findings at risk of being non-representative (this is true of both studies). Third, the controlled study design may well have affected outcomes. On one hand, the presence of a sham-stimulation period may have limited biasing 'placebo' responses (actually contributed to by both subject and experimenter bias), making the Fisher study more accurate by controlling Type 1 error. Conversely, one patient who was initially randomized to active stimulation had a marked reduction in seizures and refused to undergo sham stimulation, eliminating one of the responders from the data analysis. In the latter context, the controlled study design may have introduced Type 2 error. This early controlled trial of DBS was - if nothing else - highly illustrative that even the ability to perform sham (or "placebo") stimulation does not render DBS trials free of methodological challenges. A cross-over design with a washout period is methodologically rigorous, but is still fraught with difficulties and assumptions, and has rarely been used since publication of this trial.

Additional studies of CMT DBS have been reported. Andrade et al. (Andrade et al. 2006) reported 2 patients in an uncontrolled design, one of whom had >50% seizure reduction. Most recently, Valentín et al. (Valentín et al. 2013) reported 11 patients (5 with frontal lobe epilepsy, 6 with primary generalized epilepsy) treated with CMT DBS

at two centers in London and Madrid. After bilateral implantation, patients underwent single-blinded treatment with 3 months of sham stimulation followed by 3 months of therapeutic stimulation (up to 5 V at 130 Hz with a pulse width of 90 µs), followed by 6 months of open label therapeutic stimulation. Open label stimulation was maintained after 12 months for patients in whom stimulation was thought to be effective. Two patients with generalized epilepsy became seizure-free immediately after implantation, one of whom was maintained off stimulation throughout 50 months of follow-up, and another was seizure free for 12 months, followed by recurrence of seizures that was eliminated with 60 Hz stimulation. All six patients with generalized epilepsy had >50% seizure reduction during the blinded phase, and five of six maintained >50% seizure reduction during the long-term extension phase. The five frontal lobe epilepsy patients did not fare as well, with only one patient with >50% improvement in seizure frequency during the blinded phase. During the open label long-term extension, the frontal lobe patients had a heterogeneous response, with three demonstrating 50-90% reductions in seizure frequency and two showing no clear signs of improvement.

Taken together, these data suggest that CMT DBS may be effective for a subset of patients with generalized epilepsy, namely those with Lennox-Gastaut syndrome or with predominance of tonic-clonic or other generalized seizures. CMT DBS appears to show strong implantation and carry-over neuromodulatory effects even without active stimulation.

2.2.6 Anterior Nucleus of the Thalamus

The anterior nucleus of the thalamus (ANT) in fact consists of several distinct sub-nuclei, some of which have extensive frontal and temporal cortical projections, and others of

which are key stations in the limbic circuit of Papez (Papez 1937). Thus the ANT is an attractive target for both modulation of overall thalamocortical excitability as well as modulation of the limbic seizure network (Lega et al. 2010). Early lesion studies of the ANT in cats and non-human primates demonstrated effective reduction in seizure frequency and duration (Kusske et al. 1972), and human studies began as early as the 1960's (Mullan Ss 1967; Cooper et al. 1980). Several small open label studies throughout the 2000's showed promising decreases in seizure frequency – between ~30-90% – with prominent implantation effects as well as carryover effects with 2-3 months of stimulation cessation (Hodaie et al. 2002; Kerrigan et al. 2004; Andrade et al. 2006; Lim et al. 2007; Osorio et al. 2007).

The promising results of these initial open label studies were the foundation for the Stimulation of the Anterior Nucleus of the Thalamus for Epilepsy trial (SANTE, NCT00101933, Medtronic, Minneapolis, MN), a multicenter, randomized, double-blind trial of bilateral stimulation of ANT for localization-related epilepsy (Fisher et al. 2010). Participants (N=110) with medically-refractory partial seizures – including secondarily generalized seizures – were implanted with bilateral ANT DBS leads and randomized at one month post-surgery to receive either 3 months of stimulation at 5V (90μs pulse duration, 145Hz frequency, 1 minute on alternating with 5 minutes off) or 3 months of sham stimulation. Following the 3-month double-blind period, all patients received open label stimulation for 9 months, with two interspersed office visits at which stimulation parameters could be adjusted in a limited fashion. Following the first year, AEDs and stimulation parameters could be freely adjusted. Of the 110 implanted patients, 108 patients completed the blinded evaluation period, 105 patients were evaluated at the one-

year outcome point and 102 evaluated at 2 years. Two of the implanted patients were excluded from the analysis due to explant of an infected device, one of whom was explanted prior to randomization, and one of whom was randomized to sham-stimulation and – importantly – had only 66 of the pre-specified 70 days of required post-randomization seizure diaries prior to explanation.
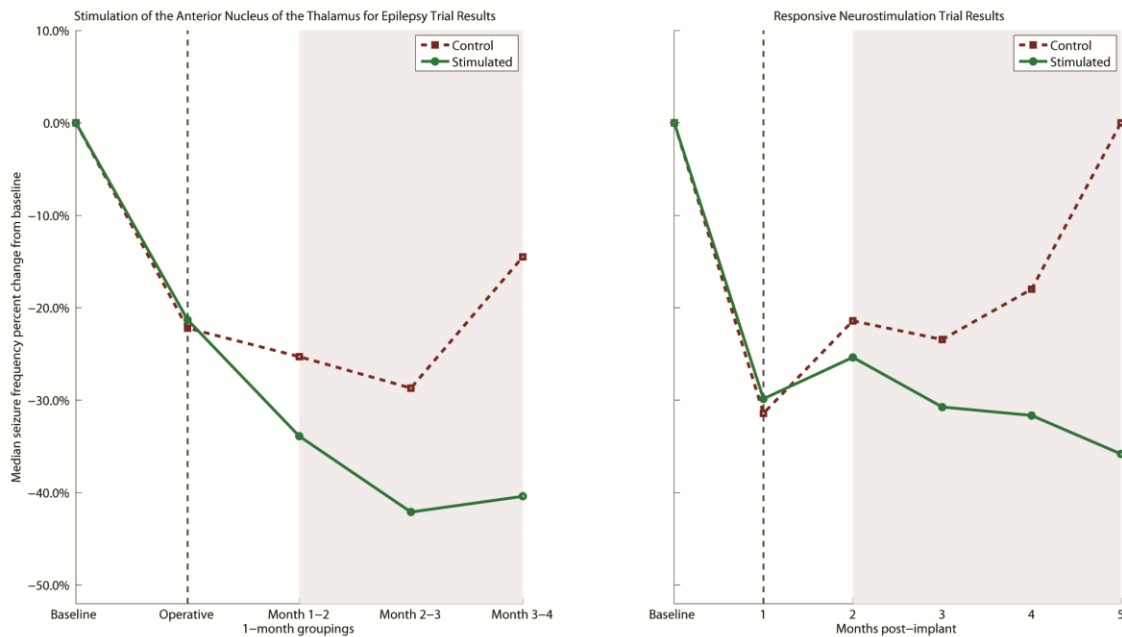
Figure 3: Median percentage change in seizure frequency from baseline during the SANTE and RNS® Trials.
In both trials, stimulation was begun one month after implantation (vertical dashed line). *(left)* Despite an appreciable reduction in seizure frequency with implantation, Control patients (red, dashed line) in the SANTE trial did not improve in seizure reduction during the blinded phase of the trial (gray). This is in contrast to Stimulated patients (green, solid line), who underwent a median 40.4% reduction in seizure frequency in the final blinded month, as compared to a 14.5% reduction in controls. *(right)* Stimulated patients in the RNS® trial demonstrated an appreciable reduction in seizure frequency with implantation as well. Stimulation was optimized for a month before the blinded evaluation phase (gray). During this phase, Stimulated patients underwent a mean 37.9% reduction in seizure frequency, as opposed to a 17.3% reduction in Controls (p=0.012). [Adapted from (Fisher et al. 2010) and (Morrell 2011)]

There were some important statistical issues that warrant discussion. First, as in previous studies, an appreciable implantation effect was noted (although placebo and/or regression to the mean effects could also have been factors): one month following implantation and prior to initiation of the treatment phase patients assigned to both the stimulation and sham-stimulation groups experienced a median 21-22% seizure reduction. As shown in Figure 3, the two groups began to separate beginning with the first month after active- or sham-stimulation and continuing to the end of the blinded period. However, only in the 3rd (and final) month of blinded stimulation was there an unequivocal statistical difference in seizure frequency between the two groups (Figure 3, median 40.4% reduction in seizures in active stimulation as compared to 14.5% reduction with sham-stimulation, p=0.0017), evidently due to continued reduction in the active group and regression towards baseline in the sham group. This finding was in the group of 108 randomized patients who had at least 70 diary days, as pre-specified in the statistical analysis plan. This was not, however, the actual pre-specified primary outcome measure, which was a generalized estimating equation (GEE) model encompassing the entire 3 month blinded evaluation period. The GEE is a useful tool in evaluating biological count data that has a very high variance, as in seizure counts. However, the GEE could not generate a result for this group of 108 patients, due to a treatment-by-visit (i.e. months follow-up) interaction, resulting from the lack of a significant difference between the groups prior to the 3rd month of treatment. This presented a critical challenge in determining whether the study was a success.

To address this issue, two *post-hoc* analyses were additionally performed. First, one patient in the stimulated group was statistically determined to be an "outlier": when

first activated at the protocol-determined 5 V this patient had 210 brief partial seizures during the one-minute on-stimulation phases over 3 days. Although the stimulator was inactivated (and later restored at 4 V with good clinical effect), these seizures disproportionately decreased the difference between the active and sham-stimulation groups. However, when this outlier was excluded from the analysis, the difference between the groups was increased during the first month but was still not statistically significant until the 3rd month (P=0.0023), and the GEE model still indicated a treatment-by-visit effect and again failed to generate a result. The second *post-hoc* analysis excluded the outlier subject, but additionally *included* the patient in the sham-stimulation group who had only had 66 of the 70 required days of seizure diaries prior to explantation, in an 'intent-to-treat' analysis. With this group of 108 patients, the treatment-by-visit interaction was no longer in the GEE model, and a statistically significant treatment effect became evident over the entire blinded evaluation phase (P=0.039).

This use of a *post-hoc* analysis has raised a good degree of debate as to whether this was a successful trial. The primary outcome measure, rather than generating a negative result, simply could not generate a result owing to the time course over which the treatment and placebo groups diverged. In the absence of a result from the pre-specified primary outcome measure, should we discard the important *post-hoc* secondary outcome measure (statistically significant group difference at 3 months) and the non-pre-specified intent-to-treat GEE result? Although "*post-hoc,*" does this truly increase the chance that this finding (P=0.039) represents a Type I error? Or is it more likely that

adopting the stance that the primary outcome measure was not met and the trial was a failure represents a Type II error?

Arguably more relevant than this unresolvable question is the implication that the results are not sufficiently robust to support the usefulness of this treatment. Since there clearly was a statistically significant difference between the groups in the 3rd month of treatment but not the first two, it was not the robustness per se that impaired the GEE analysis, but rather the progressive improvement in the treated group and decline of effect in the non-stimulated group. In fact, seizure frequency continued to decline during the open label stimulation phase: median seizure frequency decreased by 41% at one year, 56% at 2 years (Fisher et al. 2010), and 69% at 5 years (N=74), whereas and the 50% responder rate increased from 43% at one year to 54% at 2 years (Fisher et al. 2010) and 68% at 5 years (N=59) (Salanova et al., in preparation). Nevertheless, seizure freedom was relatively low, with 16% becoming seizure-free for at least 6 months during the first 5 years of the trial. Six subjects (5.5%) were seizure free for over two continuous years and 11 (10%) were seizure free over the last 6 months at the 5 year follow-up.

Complaints of memory impairment occurred in 27% of subjects over the course of the trial (Salanova et al., in preparation). Impairment, which could be confirmed in 50% of the cases, was never serious and occurred in the context of baseline memory impairment in 50%. Conversely, overall group statistics did not show decline in memory measures, but did show improvement in various measures including attention, executive function, and mood.

The complicated statistical issues discussed above may have obfuscated the analysis of the clinical significance of the trial by the U.S. FDA advisory panel. Although

the panel ultimately recommended approval by a 7:5 margin, pre-market approval was not granted and the status of ANT DBS remains in limbo in the United States. Nevertheless, approval was granted by the regulatory agencies in Canada, Europe, Australia and elsewhere. In the wake of the recent approval of the RNS therapy on improbably similar data (Figure 3), it may be worthwhile for the FDA to revisit its decision with respect to ANT DBS.

2.3. FUTURE DIRECTIONS

Despite these significant clinical successes, DBS therapy for epilepsy remains in its infancy. Our limited understanding of the mechanisms of DBS action (McIntyre et al. 2006; Butson et al. 2007; Maks et al. 2009), the epileptogenic networks themselves, and their interaction, as well as the nonselective effects of DBS on heterogeneous populations of neurons, combine to make this promising therapy still relatively unrefined and dependent on careful empiric progress.

Further incremental advances may be gained through technological innovations, such as constant-current and novel devices that may enable more predictable and directed stimulation volumes and better avoidance of stimulation side effects (Chaturvedi et al. 2012; Okun et al. 2012; Gross and McDougal 2013). Additional benefits in device longevity, and perhaps effectiveness and tolerability, may be gained through the use of closed-loop (feedback-controlled) neurostimulation devices and alternative stimulation parameters. One form of closed-loop therapy is the Responsive Neurostimulation System (RNS$^{®}$) (Morrell 2011), which activates electrical stimulation of the previously defined seizure onset zone upon detection of electrophysiological signature of a seizure. Presently

applied directly to the epileptic focus or foci, similar technology could conceivably be applied to modulatory nodes, such as ANT, in response to seizure detection.

An alternate approach, however, is to characterize states that are associated with seizures and mitigate those states with, amongst other approaches, DBS. For example, theta band activity within the septo-hippocampal circuit has been associated with decreased seizures (Colom 2006; Colom et al. 2006), and continuous multimicroelectrode electrical stimulation using theta frequencies in a rat model of temporal lobe epilepsy decreases seizures (Desai, S. A., Gross, R.E. et al., in preparation). Conceivably, the RNS® system could be adapted to accomplish this. Alternatively, using a novel bidirectional stimulation and recording pulse generator unit approved for research in human subjects (Activa PC+S®, Medtronic, Minneapolis, MN), a closed loop state control algorithm was recently tested in a large animal (sheep) model (Stypulkowski et al. 2011). One DBS electrode was implanted in the ANT and a second one in the hippocampus. Spectral power was examined in the latter, which was decreased by stimulation in ANT (Stypulkowski et al. 2013). The sensitivity for evoking seizure activity by stimulation in the hippocampus was decreased in the low power state associated with ANT stimulation as well. Moreover, the power could be continuously kept low in the hippocampus by a closed-loop algorithm that titrated ANT stimulation to hippocampal power, thereby keeping the hippocampus in the less sensitive state for seizure evocation. This paradigm may easily be tested in animal models of epilepsy, or indeed in human subjects with epilepsy, as the safety of both ANT and hippocampal electrode implantation has been thoroughly established. A similar approach is under

study and found to be promising in a non-human primate model of seizures (S. Chabardes, personal communication).

The success to date in ANT DBS for refractory epilepsy likely results in part from the stereotyped pathways for seizure propagation through the ANT in MTLE (60% of patients in the SANTÉ trial had onsets in the temporal lobe (Fisher et al. 2010)) and perhaps forms of frontal lobe epilepsy that may share those pathways. Many foci outside the mesial temporal lobe likely have different propagation networks; *in vivo* studies of epileptogenic networks may therefore allow more rational and patient-specific (Butson et al. 2007) targeting for DBS placement in this heterogeneous and more difficult to treat group of patients. Thus, a true leap forward in neuromodulation therapy will require both a more detailed understanding of epileptogenic networks and the ability to selectively modulate different cell populations within those networks.

Optogenetics, a novel molecular technology utilizing cell-type specific expression of light-sensitive ion channels, is not only capable of millisecond-level precision control, but can also selectively activate and inhibit particular genetically defined subpopulations of neurons within a larger circuit (Yizhar et al. 2011). Activated by particular wavelengths of light, these channels selectively conduct cations or anions across the cell membrane, producing defined depolarization or hyperpolarization in the expressing cells. The resulting technique combines the specificity of pharmacologic therapies with the temporal control of electrical stimulation. Several early studies of optogenetics *in vitro* and in animal models of epilepsy have shown promising results. The earliest application of optogenetics to epilepsy was by Tønneson et al. (Tønnesen et al. 2009), who demonstrated that halorhodopsin – an inhibitory chloride pump – was capable of

suppressing epileptiform activity in hippocampal organotypic slice cultures. More recently, three groups have demonstrated that inhibition of particular targets can interrupt seizures *in vivo* in rat models of epilepsy. Paz et al. (Paz et al. 2012) took advantage of the thalamocortical circuit, inhibiting hyperexcitable thalamocortical neurons in response to epileptic activity in the cortex, arresting the seizure. Wykes et al. (Wykes et al. 2012), on the other hand, targeted the seizure foci directly, again successfully inhibiting seizures. Similarly, Krook-Magnuson et al. (Krook-Magnuson et al. 2013) used a closed-loop approach to directly target the subpopulations of the hippocampus to detect and arrest spontaneous temporal lobe seizures. These early results suggest that optogenetics could play a greater role in future therapeutics. However, there are a number of challenges that currently limit its implementation, such as issues with gene therapy (Henderson et al. 2009), miniaturization of light sources, and channel and light distribution in primate brains. While not insurmountable, these limitations necessitate greater research – particularly with non-human primates, which will better reflect the limitations on human optogenetic therapies.

2.4. CONCLUDING REMARKS

The use of electrical stimulation for epilepsy has been explored for a half-century, and only recently have two therapies successfully obtained regulatory approval for more widespread use in patients: ANT DBS outside of the U.S. (but not within) and RNS within the U.S. (but not outside). Given the complementarity of these two approaches, it would be ideal if all patients in all geographical locations had access to either. For patients with identified foci within functional regions, RNS may be preferable, but is not indicated for multiple (> 2) foci, whereas ANT DBS may be effective in the latter. This

is, however, conjecture, and will remain so for a long period to come. Most proximately, we hope that ANT DBS attains approval in the U.S., either on the basis of a more rational evaluation of the results of the controlled multicenter trial, or as a result of a new trial (which we do not anticipate). While ANT DBS has been approved in Europe and elsewhere, post-approval surveillance data will not likely contribute to U.S. approval, since it is open label and uncontrolled. RNS, on the other hand, is approved only in the U.S. and has not been studied in Europe. The regulatory hurdles for CE Mark approval require safety but not effectiveness data, so it is anticipated that the pathway forward will be less burdensome for RNS approval outside the U.S. Finally, prospects for targets other than the cortex (RNS) and ANT (DBS) are dim, given the difficulty with ANT approval to date and the limited pilot data for alternative targets. CMT DBS would hold the most promise as an adjunct in the treatment of generalized epilepsy, in particular Lennox-Gaustaut Syndrome. Generalized epilepsy remains amongst the most challenging of epileptic syndromes, for which neither RNS nor ANT DBS are likely to be effective, and for which novel therapeutics are much needed.

CHAPTER III

REAL-TIME IN VIVO OPTOGENETIC NEUROMODULATION AND MULTIELECTRODE ELECTROPHYSIOLOGIC RECORDING WITH NEURORIGHTER[†]

Optogenetic channels have greatly expanded neuroscience's experimental capabilities, enabling precise genetic targeting and manipulation of neuron subpopulations in awake and behaving animals. However, many barriers to entry remain for this technology – including low-cost and effective hardware for combined optical stimulation and electrophysiologic recording. To address this, we adapted the open-source NeuroRighter multichannel electrophysiology platform for use in awake and behaving rodents in both open and closed-loop stimulation experiments. Here, we present these cost-effective adaptations, including commercially available LED light sources; custom-made optical ferrules; 3-D printed ferrule hardware and software to calibrate and standardize output intensity; and modifications to commercially available electrode arrays enabling stimulation proximally and distally to the recording target. We then demonstrate the capabilities and versatility of these adaptations in several open and closed-loop experiments, as well as demonstrate spectrographic methods of analyzing the results, as well as discuss artifacts of stimulation.

_____

3.1. INTRODUCTION

Optogenetic techniques provide powerful tools for precise manipulation of complex nervous system circuitry. Selective excitation and inhibition with light of a genetically-targeted neuron population − without directly perturbing the neighboring untargeted cells − has provided the means to elegantly explore a number of important neuroscience questions (Aravanis et al. 2007; Carter et al. 2009; Gradinaru et al. 2009; Kravitz et al. 2010; Yizhar et al. 2011; Packer et al. 2012; Wykes et al. 2012; Paz et al. 2013). When combined with electrophysiological recording techniques, optogenetic control can provide unprecedented insight into neural connectivity and function (Bell et al. 2013), as well as suggest potential therapeutic strategies (Gradinaru et al. 2009; Paz et al. 2012; Wykes et al. 2012; Krook-Magnuson et al. 2013).

Optogenetics combines a number of techniques in molecular biology, electrophysiology, optics, and neuroscience, the mastery of which can prove a barrier to easy adoption. Significant efforts have been made to expand the toolbox of optogenetic channels, constructs, and viral techniques (Chow et al. 2010; Gunaydin et al. 2010; Diester et al. 2011), as well as to develop complex custom-designed optoelectric neural interfaces (Fan et al. 2013; Voigts et al. 2013). However, commercial electrophysiology hardware and software has lagged behind these developments, and often fails to incorporate support for complex stimuli, real-time multielectrode closed-loop control (Newman et al. 2013), and customized experimental configurations in awake and behaving animals. In addition, the cost of these systems is often prohibitive, particularly for investigators looking to initiate a new line of research with limited funding. There is consequently a need for a customizable, adaptive, and low-cost optoelectrophysiology system for *in vivo* experimentation.
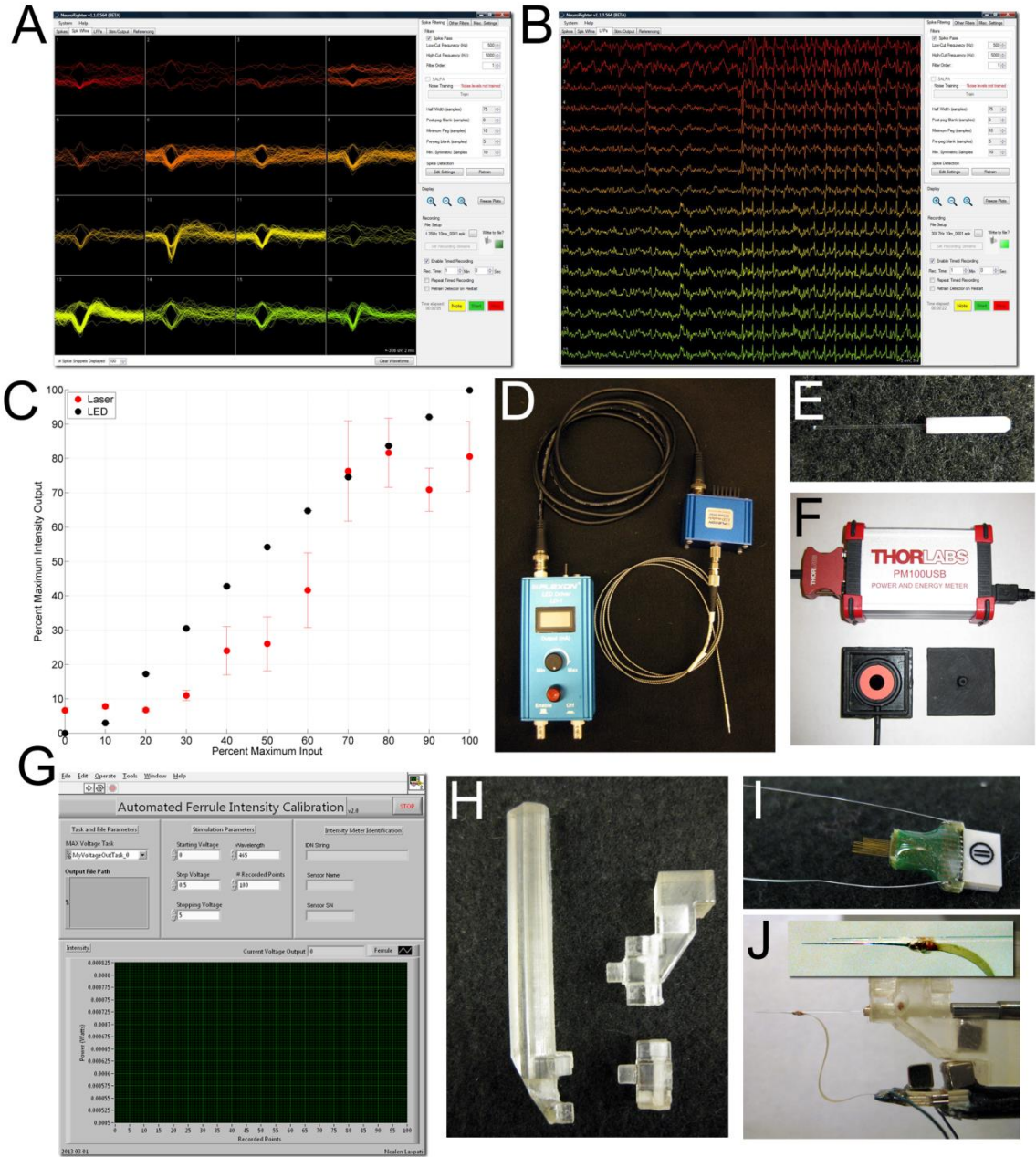
Figure 4: NeuroRighter software and hardware for calibration, optical stimulation, and recording.

NeuroRighter's main application window enables real-time isolation of single units (**A**) and local field potentials (**B**) from multielectrode arrays. A number of settings and customizations are available, and have been described in detail elsewhere (Rolston et al. 2009; Rolston et al. 2009; Newman et al. 2013). Note that, in the example view in (**B**), optical stimulation of the medial septum began half-way through the recording, generating readily visible evoked potentials.(**C**) A comparison between the intensity generated by 473 nm Blue DPSS Laser (Shanghai Dream Laser) output (red) and 465 nm Blue LED (Plexon, Inc.) output (**black**). 100 samples of power output were measured at each input step using our calibration setup, and the mean (**dot**) and standard deviation (**error bars**) plotted. Note the high variance associated with the laser output as

compared to the LED (present for the LED but smaller than the data point marker) despite the similar inputs, and the non-linear nature of the laser output. This variation is an inherent property of the laser. The maximum intensity output generated by the LED was 80 mW/mm^2, and for the laser was 30 mW/mm^2. **(D)** Plexon LED Driver, 465 nm Blue LED module, and 200µm 0.67NA armored patch fiber cable. **(E)** Custom-made optical ferrules utilizing 200 µm diameter 0.37NA fiber optic. **(F)** Thorlabs PM100USB Power and Intensity Meter **(top)**, with accompanying S120C Intensity Meter and 3D-printed Intensity Chamber. Custom-designed ferrules **(E)** plug into the chamber **(F, bottom right)** which overlays the S120C detector **(F, bottom left). (G)** Our Labview-based program for Automated Ferrule Intensity Calibration. Light wavelength, the range of voltages over which to calibrate, and the number of samples taken at each point can be customized with this graphical user interface to generate output vs. input plots **(C)**. **(H)** A 3D-printed implantation post has multiple modules to enable ferrule implantation alone **(H, bottom right)** or coupled to an array **(H, top right, J)**. **(I)** TDT 16-channel MEA, which was implanted in the dorsal hippocampus. **(J)** A H-style NeuroNexus 16 channel shank array was manually coupled to a calibrated ferrule **(J, inset)**, enabling simultaneous stimulation and recording from the same target site.

3.2. NEURORIGHTER PLATFORM

We developed our optoelectrophysiology platform based on the existing hardware

and software for electrical stimulation and electrophysiology system, NeuroRighter.

NeuroRighter is a low-cost open-source electrophysiology system written in C-Sharp

and intended for open and closed-loop neural interfacing *in vivo* and *in vitro* (Rolston et

al. 2009; Rolston et al. 2009; Rolston et al. 2010). The software, compatible with 32- and

64-bit Windows operating systems (Microsoft Corp., Redmond, WA) is free and the

source code is available on a publicly accessible repository[‡]. The hardware is also open-

source, utilizing printed circuit boards (PCBs) and commercially-available components,

National Instruments (NI; National Instruments Corp, Austin, TX, USA) data acquisition

hardware (NI PCI-6259, PCIe-6259, PCIe-6353, and PCIe-6363) and driven with NI's

hardware control library, DAQmx. The design, construction, and performance of this

---

[‡] http://code.google.com/p/neurorighter

electrophysiology platform – which meets or exceeds the performance of many commercial alternatives – is well documented (Rolston et al. 2009; Newman et al. 2013).

Recently, the NeuroRighter platform has been enhanced for improved usage with closed-loop multichannel interfacing experiments for electrical stimulation (Newman et al. 2013), as well as *in vitro* optogenetic stimulation (Newman et. al, under review). NeuroRighter is capable of recording single-unit (Figure 4A) and local field potential (Figure 4B) activity from multielectrode extracellular arrays, as well as delivering complex and customizable patterns of electrical stimulation through analog and digital outputs (Rolston et al. 2009; Rolston et al. 2010; Newman et al. 2013). NeuroRighter is consequently well-positioned to incorporate customized optogenetic hardware and provide a low-cost solution to the problems facing optoelectrophysiology. Here, we summarize the adaptations we have made to NeuroRighter to produce a system that enables real-time optogenetic neuromodulation and multielectrode electrophysiology *in vivo* in awake and behaving rodents using low-cost components. We describe two example experiments, one in which the site of optical stimulation is distant from the electrode recordings (medial septum and dorsal hippocampus, respectively), and the other in which optical stimulation and electrophysiologic recording is performed in the same location (dorsal hippocampus). In the former, we provide examples of the complex stimuli that can be performed with NeuroRighter, and present descriptive results. In the latter, we demonstrate and discuss some of the issues concerning optically-induced artifacts.

3.2.1 Design

3.2.1.1 Design criteria

We designed our optoelectrophysiology system to adapt the capabilities of NeuroRighter into the optogenetic purview *in vivo*. In so doing, we wished to maintain the standards established in its original design – that the system be 1) inexpensive, interfacing with commercially-available hardware as well as custom-designed solutions; 2) maintain the high spatial and temporal resolution required in electrophysiology; 3) function robustly in a number of different experimental environments; and 4) be open-source.

3.2.1.2 Optical stimulation

While many of the initial efforts with optogenetics relied on the use of lasers (Yizhar et al. 2011), high-intensity Light-Emitting Diodes (LEDs) have increasingly proven an attractive alternative, particularly for *in vivo* experiments. Lasers tend to be large and cumbersome, and many setups require careful collimation and alignment for proper function and maintenance of consistent output within and between experiments. These designs are sensitive to the slight perturbations generated from connections to awake and behaving animals. Commercially-available collimated LEDs, however, are compact, robust, and readily portable, making them easy to integrate into behavioral experiments. In addition, LEDs have a more precise input/output relationship than lasers. LED luminance output can be well approximated by a logarithmic or linear function with respect to input current. In contrast, similarly-priced DPSS lasers have a nonlinear sigmoidal relationship with input voltage (Figure 4C) (Cardin 2012). Furthermore, the light intensity generated by lasers can be unstable and demonstrate transient peaks and fluctuations (Cardin 2012). The output intensity of LEDs, in contrast, is much more stable and better approximates a square wave, with much less variation over time. Indeed,

we have determined that the variability in 465 nm Blue LED output intensity is less than that of a comparable-cost laser 475 nm DPSS Laser (Shanghai Dream Lasers, China; Figure 4C). While the standard deviation of the laser intensity output could be over 10% of the maximum output, the standard deviation of the LED intensity output was small enough to be obscured by the datapoint marker. It should be noted that the outputs of lasers and LEDs are influenced by temperature as well. Without proper heat dissipation, output efficiency will decrease and consistency will no longer be maintained (Newman 2013). Controller properties also largely influence these input dynamics: more advanced and more expensive controllers can linearize outputs, in particular when coupled with optical feedback. Indeed, for experiments in which long-term stimulation may prevent heat dissipation, it is recommended that an optical feedback controller be used to maintain consistency in optical stimulation output. High-intensity LEDs thus enable precise experimental standardization and repeatability while also retaining the high-intensity output and dynamic range that make lasers desirable for optogenetic experiments. Consequently, we designed our platform to make use of low-cost high intensity LEDs in optogenetic *in vivo* experiments in awake and behaving animals.

To this end, we made use of the Plexon PlexBright™ Optogenetic Stimulation System (Plexon Inc., Dallas, Texas; Figure 4D). Similar LEDs are available from other suppliers (Thorlabs, Newton, New Jersey). The PlexBright™ system consists of an LED Voltage to Current Controller, a 465nm Blue LED Module, and a patch fiber cable connected via FC/PC connection to the LED Module and protected by steel jacketing. The LED controller received input from one channel of the analog output from a National Instruments (NI) SCB-68 screw-terminal connector box. This output ranged from 0-5 V,

which was converted by the controller to 0-300 mA of current. This system was capable of driving 465 nm Blue LED light output at intensities of up to 80 mW/mm^2 in custom-made implantable optical ferrules (Figure 1C,E) – well within the acceptable window for non-damaging optical stimulation (Cardin et al. 2010). As each analog output of NeuroRighter can be accessed independently, four LEDs can be simultaneously controlled with NeuroRighter configuration on a single supported NI data acquisition card (NI PCI-6259, PCIe-6259, PCIe-6353, PCIe-6363 16-bit 1M sample/sec). The modular nature of the system enables the addition of additional NI data acquisition cards to increase the number of LED outputs, in addition to recording inputs.

Custom-made implantable optical ferrules (Figure 4E) were constructed from 1.25 mm long 230 μm inner diameter ceramic stick ferrules (Precision Fiber Products, Milpitas, CA) in a fashion based on a previously-described design (Sparta et al. 2012). 200 μm diameter 0.37 Numerical Aperture optical fiber (Thorlabs) was carefully stripped of its protective coating and cleaved. Heat-cure epoxy (Precision-Fiber Products) was mixed and applied to the concave end of the ferrule, through which the cleaved fiber segment was subsequently threaded. After wiping off the excess, a heat gun was applied to quickly cure the epoxy, and the ferrules were then allowed to finish curing overnight at room temperature. The ferrule connector was polished using a polishing disk and increasingly fine grades of polishing paper (Thorlabs), with frequent inspection to ensure transmission quality. Once polished, the free end of the fiber was scored and cleaved to 10-12 mm in length.

Custom hardware and software was designed in order to standardize the variations in output intensity and calibrate each ferrule. An Intensity Calibration Device (ICD;

Figure 4F, bottom) was designed in Solidworks 2011, 3D-printed on an Objet Eden 250 from FullCure 720 model resin, and painted black. A S121C Silicone Diode (Thorlabs) was placed within the central cavity of the ICD and connected to a PM100USB intensity meter (Figure 4F, top). Custom-written LabVIEW 2009 software (National Instruments, Austin, Texas; Figure 4G) steps the LED through user-defined output voltages and measures the power on the S121C Silicone Diode. LED output power passing through the ferrule is thus correlated to the analog input voltage signal to the LED controller. The program then calculated intensity from power based on the diameter of the fiber optic and linearly correlated to the voltage input. This standardized the output of each ferrule based on intensity rather than voltage input, enabling precise stimulation at accurate intensities across all experimental subjects. Custom-written Matlab scripts then converted standard output intensities to the appropriate signal voltages for each test subject.

Ferrules were attached to the patch fiber cable by means of 1.25 mm inner diameter Ceramic Split Sleeves (Precision Fiber Products). These were reinforced by threading them through trimmed heat shrink tubing (Digi-Key, Thief River Falls, MN), and subsequently heating them. These reinforced sleeves were superior to the bare split-sleeves in resisting breakage due to vigorous movement of some subjects. This ceramic split sleeve was the most common breaking point in the connection, conveniently leaving the implanted ferrule and patch fiber cables intact.

3.2.1.3 Electrode Arrays
Two electrode array configurations were used in these experiments. For recording of the dorsal hippocampus while simultaneously stimulating the medial septum, 16-channel microwire multielectrode arrays (Tucker Davis Technologies (TDT), Alachua, FL., USA;

MEA) were constructed from sixteen 33 μm diameter tungsten electrodes with polyimide insulation (Figure 4I). The electrodes were arranged in two rows of eight electrodes with 1 mm between rows and 175 μm of space between the electrodes within a row. Ground and reference wires were separated on the array and routed through two stainless steel wires, which were affixed to separate skull screws during the implantation surgery. The two rows were cut to different lengths, 4.0 mm and 3.0 mm, to target and record simultaneously from the hippocampal CA3 and CA1 regions, respectively, enabling multiunit and local field potential recording from the hippocampus distantly from the optical stimulation site in the medial septum.

NeuroNexus (Ann Arbor, Michigan, USA) 16-channel shank arrays were coupled with optical ferrules to record and stimulate simultaneously in the hippocampus. A single-shank H-style arrays was used, with 16 177 μm^2 contacts spaced 100 μm apart along a 5 mm shaft. This length was sufficient to record simultaneously from the CA1 and CA3 layers. The shaft was connected to an Omnetics connector via a 21 mm flexible cable. Ground and reference wires were again separated from the contact sites and routed through stainless steel wires. NeuroNexus "activated" the electrode contacts via iridium oxide - a process that reduced impedance and they suggested would reduce optical stimulation artifacts (personal communication). Both the NeuroNexus and TDT arrays made use of a magnet-based coupling technique to the 16-channel 100 gain tethered recording headstage (Triangle Biosystems, Durham, NC, USA) to reduce movement artifacts, a technique we have described previously (Rolston et al. 2009; Rolston et al. 2010). Once the magnet was attached with superglue, the array could be situated onto our custom-designed and 3D-printed implantation holder (Figure 4H, J). This enabled the

array shank and contacts to be positioned in parallel to the optical fiber, and cemented in place with quick-drying super glue.

The implantation device consists of a single post compatible with a Kopf Universal Holder (David Kopf Instruments, Tujunga, California, USA) with a single-prong plug that enabled easy swapping and customization depending on the implant configuration (Figure 4H). This allowed us to use the device to implant an optical ferrule in isolation – as in the medial septum – or in conjunction with a NeuroNexus array (Figure 4J) – as in the dorsal hippocampus.

3.2.2 Methods
3.2.2.1 Surgeries
2 month old adult male Sprague-Dawley rats (250-300g) were purchased from Charles River Laboratories (Wilmington, MA, USA). All animals were maintained within a 12/12 light/dark cycle vivarium with unlimited access to food and water. This work was conducted in accordance with Emory University's Institute for Animal Care and Use Committee.

Each subject underwent two surgical procedures. The first survival surgery introduced the optogenetic viral vector to the stimulation target – either the medial septum or the dorsal hippocampus. For medial septal stimulation, rats were anesthetized with 1.5-4% inhaled isoflurane, and a craniectomy was made 0.40 mm anterior and 2.00 mm lateral to bregma on the right side of the skull. A pulled-glass pipette attached to a stereotactically mounted injector (Nanoject; Drummond Scientific Co., Broomall, PA, USA) was used to inject 1.8 μL of 10^{12} particles/mL AAV5-hSynapsin-hChR2(H134R)-EYFP (UNC Vector Core Services, Chapel Hill, NC, USA). The injection was made at a

20° angle to the dorsal-ventral axis (0.40 mm anterior, 2.12 mm lateral at the 20° angle, 5.80 mm ventral to pia along the rotated axis) in order to target the medial septum without damaging the medially-located central sinus. After 5 minutes of equilibration the injection was made over 7 minutes with the pipette remaining in place an additional 10 minutes post-injection to prevent reflux. Once withdrawn, the scalp was stapled closed, ketofen was administered as an analgesic (3-5 mg/kg) to minimize pain, and the rats were quarantined for 72 hours before returning to normal housing. Hippocampal injections were similarly performed, but the craniectomy was made 3.30 mm posterior and 3.20 mm lateral over the right dorsal hippocampus. An injection of 1.8 µL of 10^{12} particles/mL AAV2-CaMKIIα-hChR2(H134R)-mCherry was made along the dorsal-ventral axis at 3.10 mm depth to pia to target the hippocampal pyramidal neurons. Identical closure and quarantine procedures were performed.

The second survival surgery was performed two weeks later, which we have found to provide ample time for robust channel expression. For the medial septal stimulation experiments, a second craniectomy was made over the right dorsal hippocampus centered at 3.50 mm posterior and 2.80 mm lateral to bregma. The dura was incised with a sterile curved scalpel blade. The TDT array was positioned at a 50° angle to midline, with the posterior end swung laterally, to match the positioning of the hippocampal pyramidal cell layers (Rolston et al. 2010). The MEA was lowered while simultaneously recording single unit and local field potential (LFP) activity to attain the ideal positioning (Rolston et al. 2009). When the electrophysiologic recordings stabilized, the original injection craniectomy was reopened, and a calibrated optical fiber ferrule was implanted at a 20° angle to the dorsal-ventral axis (0.40 mm anterior, 2.12 mm lateral in

the rotated axis). Stimulation was performed as the ferrule was implanted, with the resulting recordings immediately analyzed spectrographically. Descent was halted when a strong stimulus-response signal was observed in the spectrogram, or when the optical ferrule reached a depth of 5.50 mm from pia along the rotated axis.

For the hippocampal stimulation experiment, the previous craniectomy was reopened and expanded, and the combined optical fiber and NeuroNexus electrode array (Figure 4J) was inserted while similarly stimulating. Stimulation artifacts were noted in the upper cortical layers where there was no viral expression, and were recorded for later artifact analysis. A local field potential response was visible in the hippocampus in addition to the artifact and so the implantation was halted at 2.80 mm at the shank tip. In both experiments, once the electrodes and ferrules were in place, the craniectomy was sealed with dental acrylic (OrthoJet; Lang Dental; Wheeling IL), securing the array/electrode and ferrule in place. The rats were administered ketofen (3-5 mg/kg) to minimize pain and returned to normal housing to recover for 3-5 days.

3.2.2.2 Optical stimulation and electrophysiologic recordings
Using our adapted NeuroRighter system, electrophysiologic recordings were sampled at 25 kHz with a 1-9,000 Hz bandwidth. LFPs were isolated online with a 1-500 Hz 1-pole Butterworth band-pass filter and downsampled to 2000 Hz. Action potentials were isolated both online (Newman et al. 2013) and offline, with the offline results presented here. Action potentials were detected offline using custom-written adaptations to the automated spike-sorting Wave_clus scripts (Quiroga et al. 2004). The raw data was band-pass filtered offline from 500-5000 Hz. For the TDT electrodes, the median signal was removed across the CA3 and CA1 electrodes, respectively. For the NeuroNexus Array,

the median signal was removed across all electrodes. Positive and negative thresholds were applied at 5x the standard deviation of the signal, and the resulting waveforms were matched, sorted, and isolated using superparamagnetic clustering. Power spectra and spectrograms were computed using the Chronux suite of analysis tools and multitaper analysis (Bokil et al. 2010), with a moving window size of 4s stepping in 0.5s increments, T=1, W=4 and 3 tapers. Data were recorded intraoperatively and for up to four weeks postoperatively.

To stimulate awake and behaving animals, calibrated ferrules were connected via armored patch fiber cables (200 µm diameter, 0.67 NA, Plexon). Square-wave stimulation pulses varied between 10, 30, and 50 mW/mm^2; 7, 11 (theta), 17, 23, 35 (beta), and 42 (gamma) Hz; and 2, 5, and 10 ms pulse widths. NeuroRighter enables custom-designed stimulation times and amplitudes to be defined via Matlab script (Newman et al. 2013). We leveraged this customizability to develop several other stimulation patterns, including varying frequency, Poisson distributions, and continuous sinusoids, which are described in more detail as they are presented. In all cases, the experimental protocol consisted of repeated one minute recordings of 20 seconds of background, 20 seconds of stimulation with a particular pattern, and a subsequent 20 seconds of additional background. Stimulation protocols were performed in random order and repeated numerous times over several recording sessions. This setup was able to stimulate and record LFP and single-unit responses from awake and behaving animals uninterrupted for several hours and over several days.

3.2.2.3 Histology

Histology was performed after experimentation to verify microelectrode recording locations and light-sensitive ion channel expression. Rats were deeply anesthetized with an overdose of Euthasol (5ml/kg, Virbac, Fort Worth, TX, U.S.A.) injected intraperitoneally. They were then transcardially perfused with 0.9% saline followed by 4% paraformaldehyde in 0.1M phosphate buffer at pH 7.2. The heads, still containing the electrodes and ferrules, were then separated and post-fixed at 4°C overnight. The next day, the brains were dissected out, removed, and cryoprotected with 30% sucrose at 4°C. Frozen transverse (horizontal) sections were made of 50 µm thickness on a sliding microtome and collected in 0.1M PBS. Sections were mounted on glass slides and mounted with Vectashield mounting medium with DAPI (Burlingame, CA, U.S.A.) for visualization of nuclei. Sections were imaged in the NIS-Elements software (Nikon Instruments, Inc., Melville, NY, USA) using a Nikon DS-Fil color digital camera on a Nikon E400 microscope equipped with TRITC, FITC, and DAPI fluorescence cubes.

3.3. RESULTS

3.3.1 Histologic validation of channel expression and electrode placement

Channelrhodopsin-2 expression in the medial septum (Figure 5A, green) and hippocampus (Figure 5B, red) was robust upon histologic evaluation. From the medial septum, axonal projections to the hippocampus (Figure 5A, C) were readily apparent, coinciding with the passage of the electrodes (Figure 5C, red and white arrows) and the hippocampal pyramidal cell layer (Figure 5, yellow arrow). The NeuroNexus array also passed alongside the expressing pyramidal cell layer of the hippocampus (Figure 5B).

Consequently, we would expect our recordings to appropriately reflect the influence of optogenetic stimulation on these respective neuron populations.
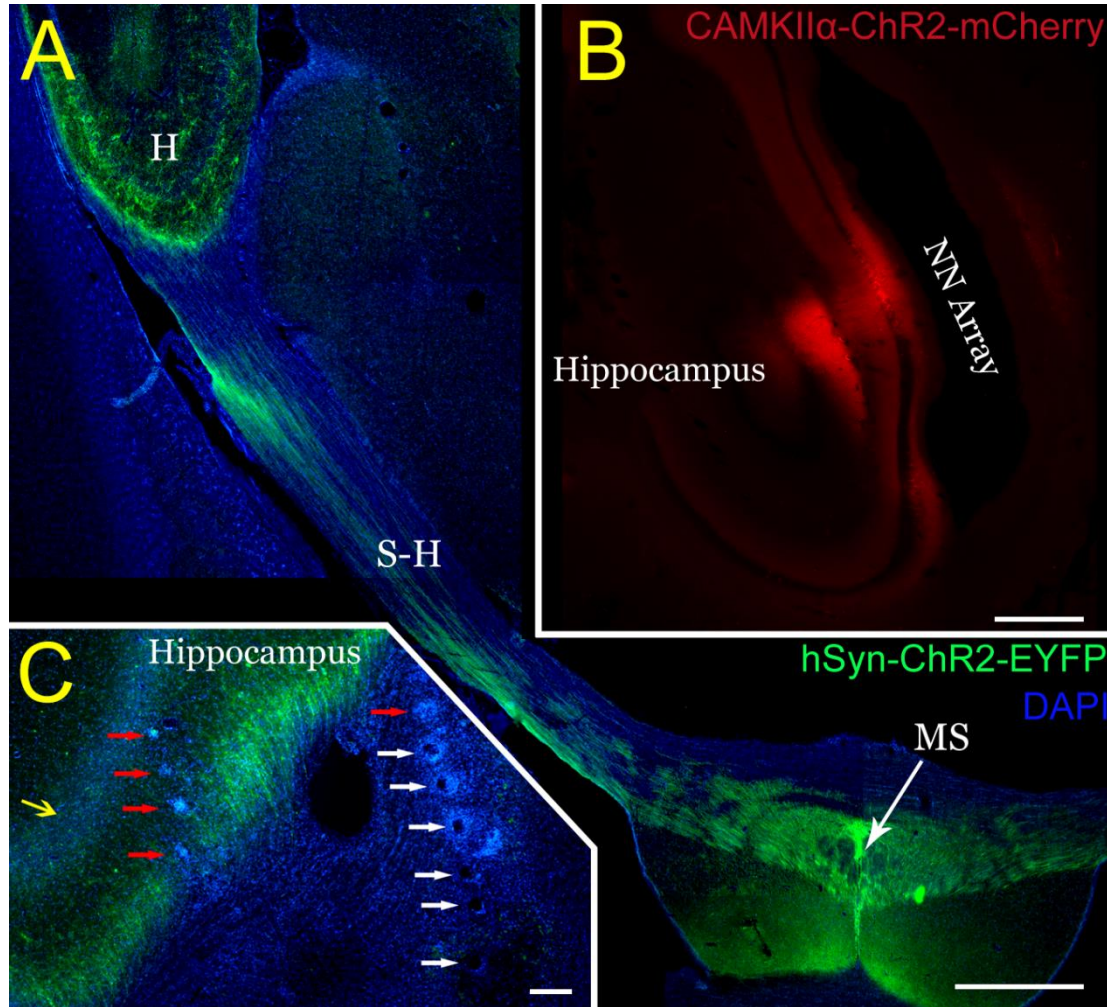
Figure 5: Robust expression of ChR2 on transverse section histology and verification of electrode placement.
(**A**) AAV5-hSyn-ChR2-EYFP injection into the medial septum (**MS**) produced robust ChR2-EYFP expression (**green**) in the MS. Axons from the MS could be tracked along the septohippocampal pathway (**S-H**) and into the hippocampus (**H**). Scale 1 mm. (**B**) Similarly, injection of AAV2-CaMKIIα-ChR2-mCherry into the dorsal hippocampus (**red**) selectively expressed in the pyramidal cell layer and their projecting axons/dendrites. The NeuroNexus array implantation site was localized alongside the expressing pyramidal cell layer by the damage it generated. Scale 0.5 mm (**C**) TDT arrays in the dorsal hippocampus were localized similarly by tracking their passage (**white arrows**) and endpoints (**red arrows**). Note the axons from the MS (**green**) expressing surrounding the pyramidal cell layer (**yellow arrow**) and the electrode array. Scale 200 mm.

3.3.2 Validation of hippocampal response to pulsatile stimulation patterns in the medial septum

To validate the effectiveness of the platform, we first explored the LFP response in the dorsal hippocampus to square-wave pulsatile stimulation of the medial septum (Figure 6). At 50 mW/mm^2, stimulation of the medial septum produced readily visible delayed pulsatile responses in the hippocampal LFP in both the CA1 and CA3 layers during the stimulation epoch (Figure 4B, Figure 6A). This delay is likely the result of synaptic conduction. These responses did not persist into the post-stimulation epoch, but instead were highly time-locked to the stimulus onset and offset. In order to examine the waveform of the LFP response, a peristimulus average was constructed by determining the mean LFP signal between 5 ms preceding and 40 ms following onset of each stimulus pulse. These were calculated across every stimulation parameter to produce the mean (solid line) and standard deviation (filled area) (Figure 6B). As expected, the stimulation parameter specifications had a large impact on response waveform amplitude, shape, and timing. Increasing the amplitude of the stimulus pulse tended to generate a more rapid time to peak response. Intriguingly, while increasing the pulse width at lower frequencies increased the amplitude of the response, at higher frequencies (23+ Hz) this was not the case. Indeed, the response to a 35 or 42 Hz, 10ms stimulus looked remarkably similar regardless of stimulation intensities, with the primary differences manifesting in phase. Biphasic responses were also noted at higher intensities, whereas unipolar depolarization was most common at 10 mW/mm^2.

To further characterize the hippocampal LFP response to pulsatile stimulation, we examined the spectral properties of the mean signal from six trials of 50 mW/mm^2, 10ms stimulation pulses at 7, 23, and 35 Hz. (Error! Reference source not found.). In all cases,
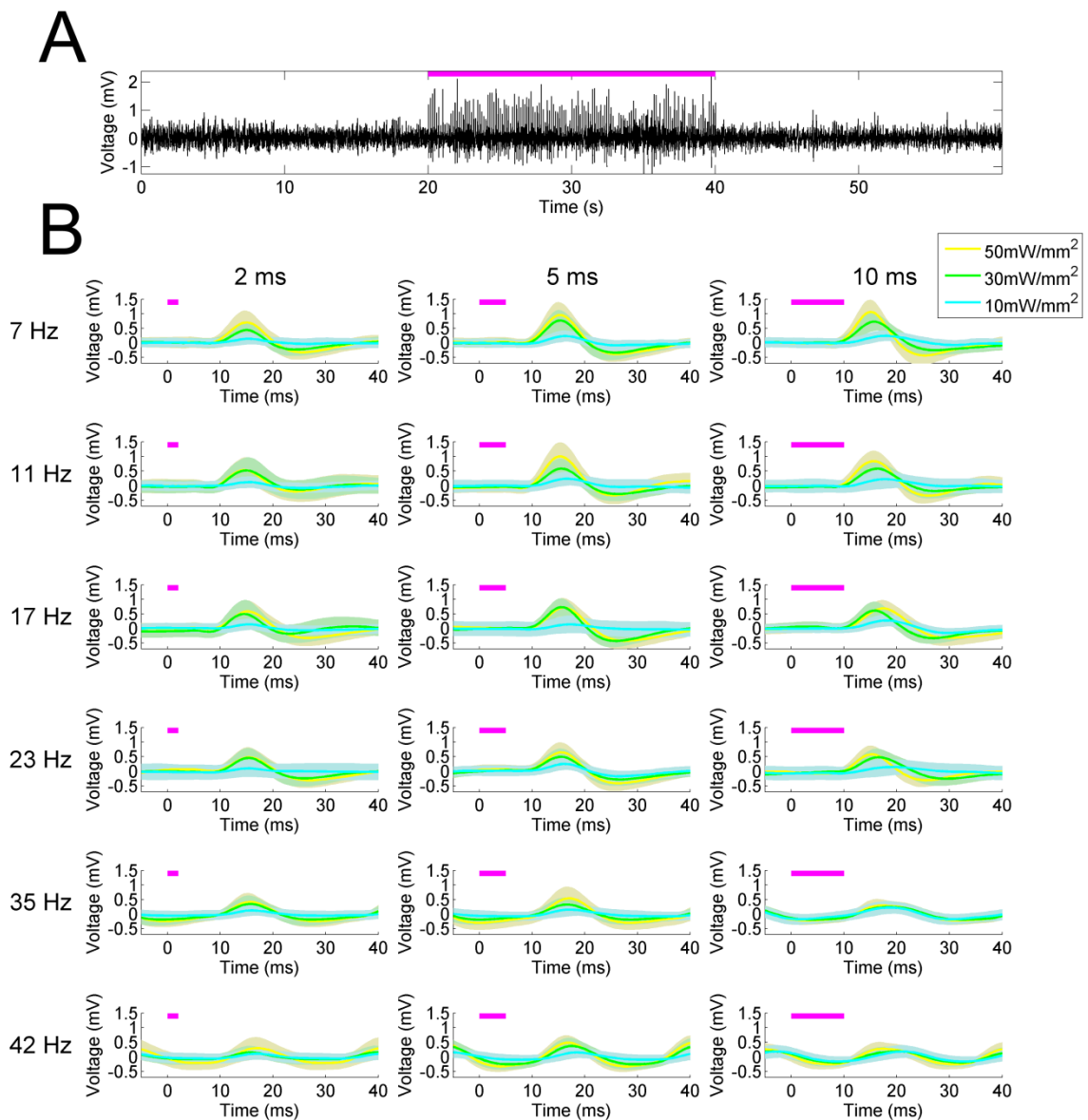
Figure 6: Peristimulus average hippocampal LFP responses to medial septal stimulation reveal the influence of stimulation parameters on waveform shape.
(**A**) Hippocampal LFP response to 50 mW/mm^2, 7 Hz, 10ms square-wave optical stimulation of the medial septum (**magenta bar**). (**B**) Responses to stimuli at different frequency (rows), pulse width (columns), and intensities (**blue, green, yellow, respectively**). Lines indicate the mean response and the shaded areas indicate the standard deviation. Note the decrease in amplitude of the response waveform with increasing stimulation frequency, as well as the increasingly sinusoidal response at higher frequencies. The time-to-peak response was influenced not only by the stimulation intensity, but also by the pulse width. At 10 ms pulse widths at higher frequencies, a notable delay in the time-to-peak was observed that was not present at 2 ms pulse widths. Pulse widths at low frequencies also had an influence on response amplitude, with longer pulse widths associated with a larger amplitude response waveform.

multitaper spectrograms were generated using seven tapers (T=4 W=1) and a four second long moving window iterating at 0.5 second. This wide temporal window resulted in some temporal blurring of the stimulation onset and offset into the non-stimulation epochs, but allowed us to more precisely resolve the frequency domain. A clear increase in power in the spectrum corresponding to the stimulation frequency was apparent during the stimulation epoch as compared to the pre- and post-stimulus epochs in all cases
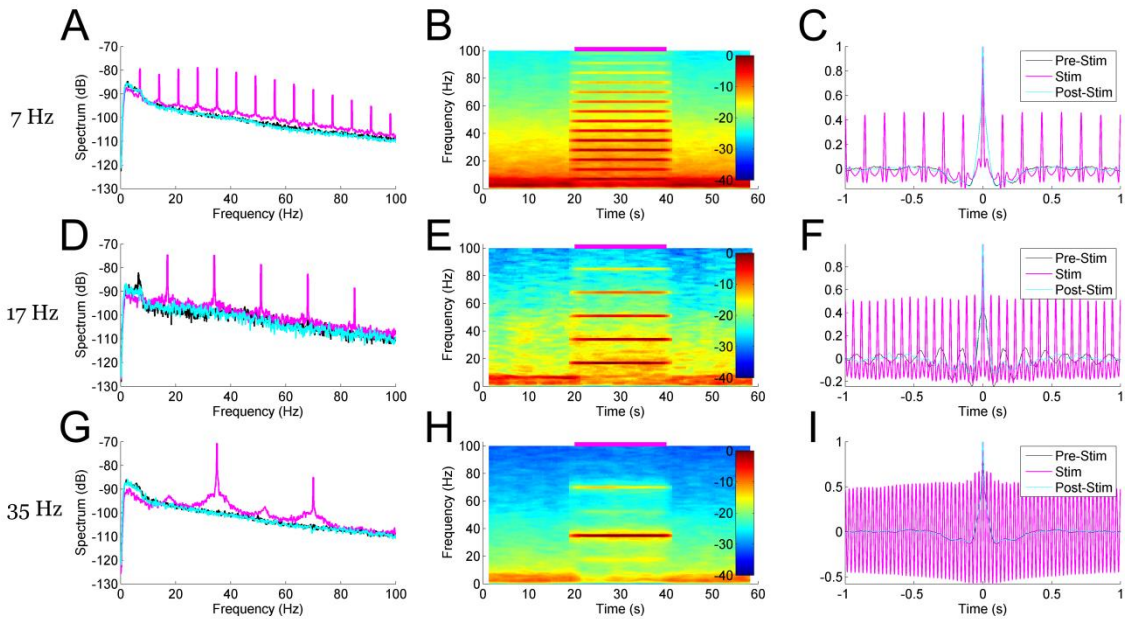
Figure 7: Spectral and correlational response of the CA3 hippocampal LFP to medial septal pulse stimulation demonstrate time-locked and frequency specific responses.
Stimulation at 50 mW/mm^2, 10ms pulse width, and 7 Hz **(A-C)**, 17 Hz **(D-F)**, and 35 Hz **(G-I)** each produced unique and frequency-specific responses in the spectrum **(A, D, G)**, spectrogram **(B, E, H)**, and autocorrelation **(C, F, I)** of the LFP signal. The spectral analysis demonstrates a time-locked and frequency-specific response to stimulation onset. Blurred edges near stimulus onset and offset are a result of a wide (4s) moving window that better resolved the frequency-specificity of the response. Note the presence of increased power at harmonics of the stimulation frequency; these are further analyzed in **Figure 5**. The autocorrelation demonstrates a highly correlated LFP signal at stimulation time points, suggesting a locking of oscillatory phase to the stimulus.

(Figure 7A, D, G). A spectrogram of each case revealed the temporal precision of this response (Figure 7B, E, H), as well as some of the interactions with power at other frequencies. In all cases low-frequency (1-10Hz) power was reduced as compared to the pre- and post-stimulus epochs, presumably via stimulation-controlled hijacking of the LFP signal. Examining the mean autocorrelation lends further support to this idea: during stimulation in all cases, the signal became highly correlated at stimulation frequencies (Figure 7C, F, I). At higher frequencies the oscillatory nature of the LFP response dominated (Figure 6B), resulting in a highly correlated and almost sinusoidal signal that indicated the LFP rhythm was largely dominated and locked to the stimulus frequency and phase.

Aside from increases in power at the stimulation frequency, there were concomitant increases of power at harmonics of that frequency. In the case of 7 Hz stimulation, power was also increased at 14 Hz, 21 Hz, and so forth (Figure 7A-B). We suspected that these were a result of the Fourier decomposition of the response waveform, and not evidence of other neurologic oscillatory responses, as neurologic oscillations are not typically so rigidly locked in frequency bandwidth. In order to distinguish the roles these harmonics play in the signal compared to the primary signal at the stimulation frequency, we systematically removed the harmonics from the LFP (rmlinesc.m, Chronux) (Bokil et al. 2010). The time-series signal is converted to frequency space, and then the spectrum is interpolated across at the defined frequencies, removing significant sine waves from continuously recorded data without altering phase properties as would happen with a notch filter. This has been used to remove the line noise resulting from nearby electronics and power sources (Viswanathan and Freeman

2007). As we progressively removed harmonics from the LFP response to 50 mW/mm^2, 7 Hz, 10ms stimulation, the peristimulus average became increasingly sinusoidal, centered on the stimulus frequency (Figure 8). The harmonics therefore play an integral role in generating the waveform of the LFP pulse response, particularly as the waveform deviates from the pure sinusoid of the stimulation frequency, but likely should not be interpreted as coupling between frequencies.
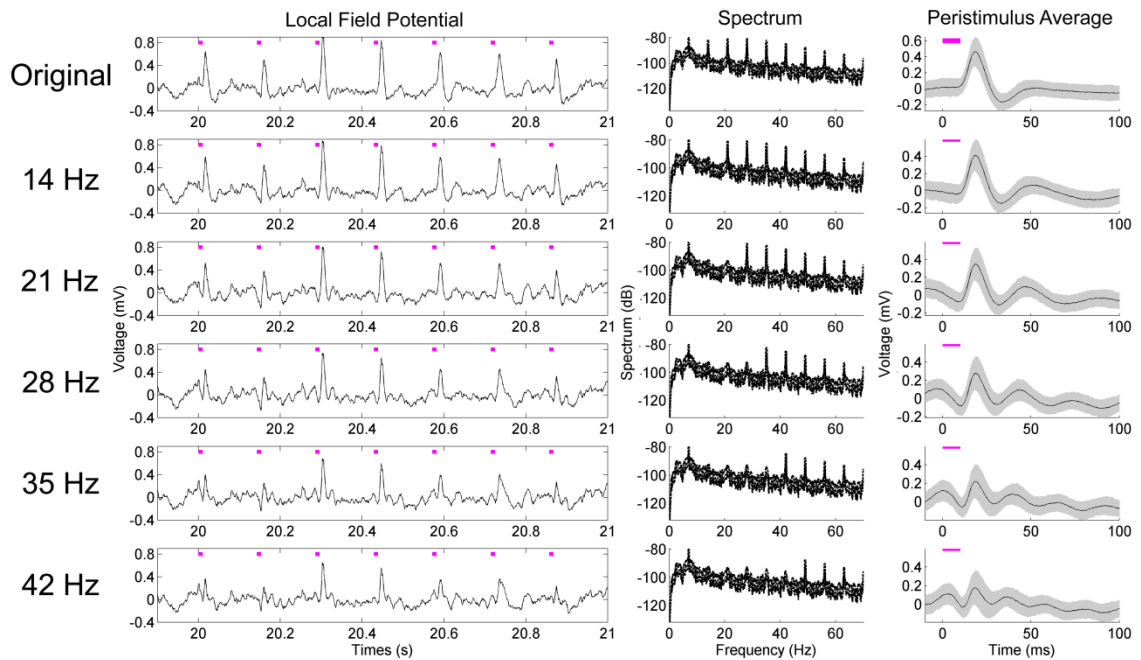
Figure 8: Harmonic deconstruction demonstrates their participation in non-oscillatory dynamics of the hippocampal pulse response.
The original LFP response to 50 mW/mm^2, 7 Hz, 10 ms stimulation pulses demonstrates a stereotyped biphasic waveform, with several harmonics present in the spectrum during the stimulation epoch. Successively removing each of these harmonics (14, 21, 28, 35, and 42 Hz) results in alterations to the waveform shape – as demonstrated in the peristimulus average – that reveal the importance of the harmonics in producing the non-sinusoidal aspects of the original response waveform.
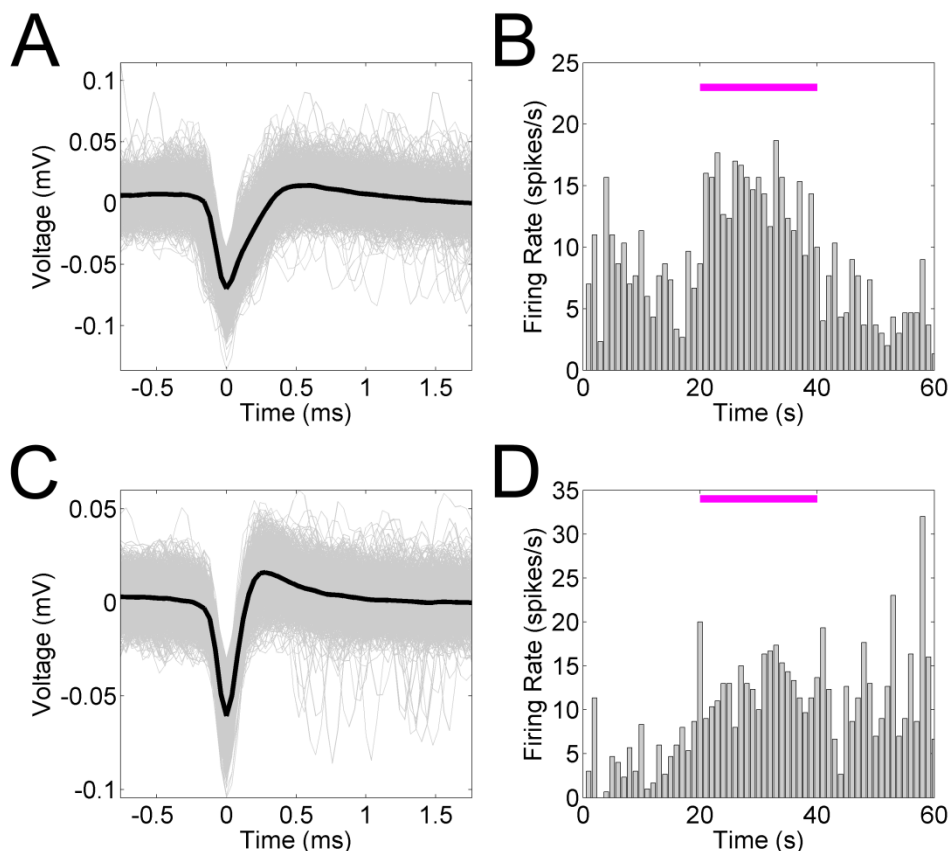
Figure 9: Hippocampal single unit firing rates increase in response to optical stimulation of the medial septum.
Mean firing rates for two single units (**A, C**) identified from 50 mW/mm^2, 23 Hz, 10 ms stimulation trials. Mean firing rate (**B, D**) tended to increase during the stimulation period. In the second case (**C**), the increase in firing rate remained increased during the post-stimulation epoch (**D**).

We next examined the hippocampal single-unit responses to medial septal optogenetic stimulation (Figure 9). NeuroRighter is capable of identifying and sorting units online (Newman et al. 2013). In a demonstration of its flexibility, however, we isolated units offline from 25kHz sampled data using Matlab scripts combining wavelet transformation and superparamagnetic clustering (wave_clus) (Quiroga et al. 2004). Two example units were analyzed for waveform (Figure 9A, C) and mean firing rate (Figure 9B, D) properties before, during, and after a 50 mW/mm^2, 23 Hz, 10ms stimulus train. In

both cases the mean firing rate increased during the stimulation epoch, as calculated across several trials. The firing rate returned to baseline for the first unit (Figure 9A-B), whereas the second unit maintained the new average firing rate during the post-stimulus epoch (Figure 9C-D). As these are only examples of the capabilities of NeuroRighter to explore single-unit activity, this study was not powered to statistically compare these results, but it was noted that several units demonstrated a trend towards increased firing rate during the stimulation epoch.

3.3.3 Alternative, customizable stimulation patterns

NeuroRighter is capable of generating complex and customizable stimulation patterns using scripted protocols (Newman et al. 2013). In order to demonstrate examples of this capability, we demonstrate how alternative optical stimulation patterns in the medial septum could alter hippocampal neural activity in our *in vivo* septohippocampal axis experiments. The results are presented from the combined analysis of several trials.

3.3.3.1 5 Hz jitter

In Figure 4 and 5, each stimulus pulse occurred at the same frequency during the stimulation epoch, producing a very frequency-specific increase in power in the hippocampal LFP. In the first experiment in alternative stimulation patterns, we introduced a jitter in the interpulse interval based on a random normal distribution of up to 5 Hz surrounding the arbitrarily-examined stimulus frequency of 23 Hz (**Error! eference source not found.**A). The resulting 50 mW/mm^2, 10 ms pulsed stimulus produced similar depolarization/hyperpolarization responses to that of the fixed-frequency pulsed stimulation, as seen in the peristimulus averages generated (**Error!**

eference source not found.B), but notable differences were observed spectrographically

(**Error! Reference source not found.**C). First, a broader response was
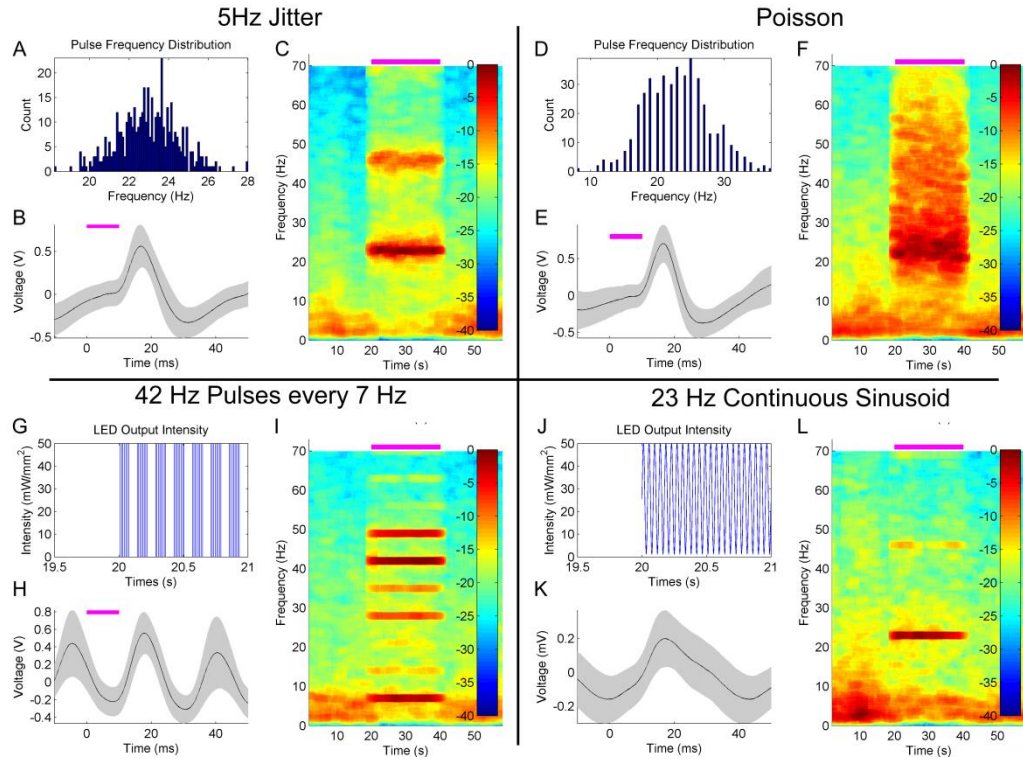
Figure 10: Hippocampal LFP response to alternative, customizable optical stimulation patterns in the medial septum.
(A-C) Varying the frequency of 50 mW/mm^2, 10ms stimulation pulses ±5 Hz within a normal distribution centered on 23 Hz **(A)** produced a peristimulus average waveform **(B)** similar to that seen with fixed-frequency simulation **(Figure 6)**, but also generated a broader peak in the spectrogram **(C)** with variations in the peak response frequency during the stimulation time. Interestingly, this stimulation in the beta frequency range reduced the power at frequencies <10 Hz. **(D-F)** Poisson 50mW/mm^2 10ms pulses generated with a frequency of 23 Hz **(D)** also demonstrated a similar LFP peristimulus average response **(E)**. However, the spectrogram **(F)** revealed a broadband increase in power peaking at the Poisson distribution frequency that did not influence <10 Hz power. **(G-I)** 50 mW/mm^2, 10 ms pulses were generated in bursts of four pulses at 42 Hz, with the burst frequency set to 7 Hz **(G)**. This pattern generated a sinusoidal peristimulus waveform **(H)** similar to that seen with constant 42 Hz stimulation **(Figure 6)**. While harmonics of the 7 Hz oscillation were noted **(I)**, the amplitude of these harmonics varied widely, most likely due to constructive and destructive interference. **(J-L)** A continuous sinusoidal oscillation in light intensity through the implanted ferrule **(J)** was also capable of generating a LFP response. The peristimulus average of the response was largely sinusoidal **(K)**, and also lower in amplitude that that of pulsed stimulation. Power was concentrated at the stimulus frequency in the spectrogram **(L)**, with the presence of harmonics much reduced.

observed that varied over time within the stimulation epoch. This is reflective of the variability introduced to the stimulation signal. Note that a harmonic is also apparent, with similar variability as seen in the primary signal. The spectrogram also demonstrates an increase in power across frequencies greater than 25 Hz during the stimulation, and a concomitant reduction in power at frequencies less than 10 Hz.

3.3.3.2 Poisson distribution

In our next example experiment, we stimulated the medial septum with a Poisson distribution of 10 ms pulses at 50 mW/mm^2, generated at an average frequency of 23 Hz independent of the previous stimuli (**Error! Reference source not found.**D). A imilarly-stereotyped peristimulus average response was observed (**Error! Reference source not found.**E). However, the increase in spectral power was much broader than that generated by fixed or jittered-frequency stimulation (**Error! Reference source not ound.**F). A smear of increased power was observed during the stimulation epoch, extending from ~15 Hz to 70 Hz, peaking at the stimulation frequency average of ~23 Hz. Also observed was a reduced impact on low-frequency (<10 Hz) power as compared to fixed and jittered stimulation pulses.

3.3.3.3 Cross-frequency stimulation

Cross-frequency interactions, such as those between theta and gamma frequencies, are thought to play an important role in neural processing, such as perception and memory (Jensen and Colgin 2007). In order to try and artificially generate a theta-gamma coupled state, we stimulated the medial septum at 50 mW/mm^2 with four 10 ms pulses at 42 Hz with the cycle occurring at a frequency of 7 Hz (**Error! Reference source not found.**G).

his produced a highly sinusoidal pattern in the LFP, as demonstrated by the peristimulus average (**Error! Reference source not found.**H) and consistent with what has been bserved previously (Figure 6). Spectral analysis demonstrated a complex response dominated by power bands at 7 and 42 Hz (**Error! Reference source not found.**I). armonics of the 7 Hz response were visible, but the amplitude varied considerably and in a pattern unlike that previously encountered (Figure 7, Figure 8). It is likely that constructive and destructive interference between the harmonics of the 7 Hz and 42 Hz components of the response are responsible for the particular patterning observed.

3.3.3.4 Continuous sinusoidal
Continuous optical stimuli, as opposed to pulsed stimuli, can introduce stimulus currents that better mimic natural synaptic bombardment (Tchumatchenko et al.). Therefore, we also explored stimulating with a continuous 23 Hz sinusoidal signal (**Error! Reference ource not found.**J). The average response was more sinusoidal than fixed frequency (**Error! Reference source not found.**K). As in other stimulation cases, power was argely concentrated at the stimulus frequency as well, with a reduced harmonic component as compared to the fixed-frequency pulses (**Error! Reference source not ound.**L). Intriguingly, this stimulation pattern seemed to alter the LFP at frequencies other than just the stimulation frequency, with stimulation onset correlating with a consolidation of power at theta frequencies into two discrete bands as calculated across several trials.

3.3.4 Validation of hippocampal response to pulsatile stimulation patterns in the hippocampus

In our second example experiment, we explored stimulation and recording from the same site, namely, the dorsal hippocampus (Figure 5B). NeuroRighter is compatible with a wide variety of electrode configurations, as evidenced in our use of the combined NeuroNexus array and optical ferrule in this example (Figure 4J). Optically stimulating and electrically recording in the same location does possess a significant caveat, in the form of optically-induced artifacts on the recording electrodes (Ayling et al. 2009; Han et al. 2009; Cardin et al. 2010) that must be separated from the true neurologic signal. This has long been a problem with electrical stimulation and recording, where the multi-fold difference between the stimulation and recording regimes readily obscures or saturates the signal (Wagenaar and Potter 2002; Rolston et al. 2010). The photoelectrochemical artifact, or Becquerel effect (Khurram and Seymour 2013), is not of the same magnitude; it is typically on the same order as the electrophysiologic signal (Figure 11A). However, these artifacts still pose a potential problem – can they be separated from the underlying neural signal in order to resolve the LFP and single-unit responses to optical stimulation?

We first set out to characterize the artifact *in vivo*, and then to separate the artifact from the underlying electrophysiologic signals (Figure 11). Stimulating in non-ChR2-expressing cortical tissue, we were able to define the stereotypical artifact waveform at 10, 30, and 50 mW/mm^2, which appeared in the LFP as charge/discharge depolarization/hyperpolarizations at the beginning and end of the stimulus pulses (Figure 11A, red). We did not note DC offsets as seen by Cardin et al. (Cardin et al. 2010), perhaps due to our particular ground and reference configurations. The electrodes also possessed an iridium oxide coating, as this had been indicated by NeuroNexus Tech

(personal communication) to potentially reduce optically-induced artifacts. Note that as the intensity increased, so too did the artifact amplitude, but otherwise the waveform was largely stereotyped in appearance. The immediacy with which these artifacts appeared, as well as the steps we took to prevent optically-induced artifacts, suggests that they were actually a result of direct electrical coupling. Since these were unobserved on the TDT microwire arrays and the impedance values between the arrays were similar, we suspect that they resulted from the 21mm ribbon cable attaching the electrode shank to the Omnetics connector. The cable could be acting as an antenna, picking up the driving current to the LED, and amplifying this noise alongside the neurologic signal.
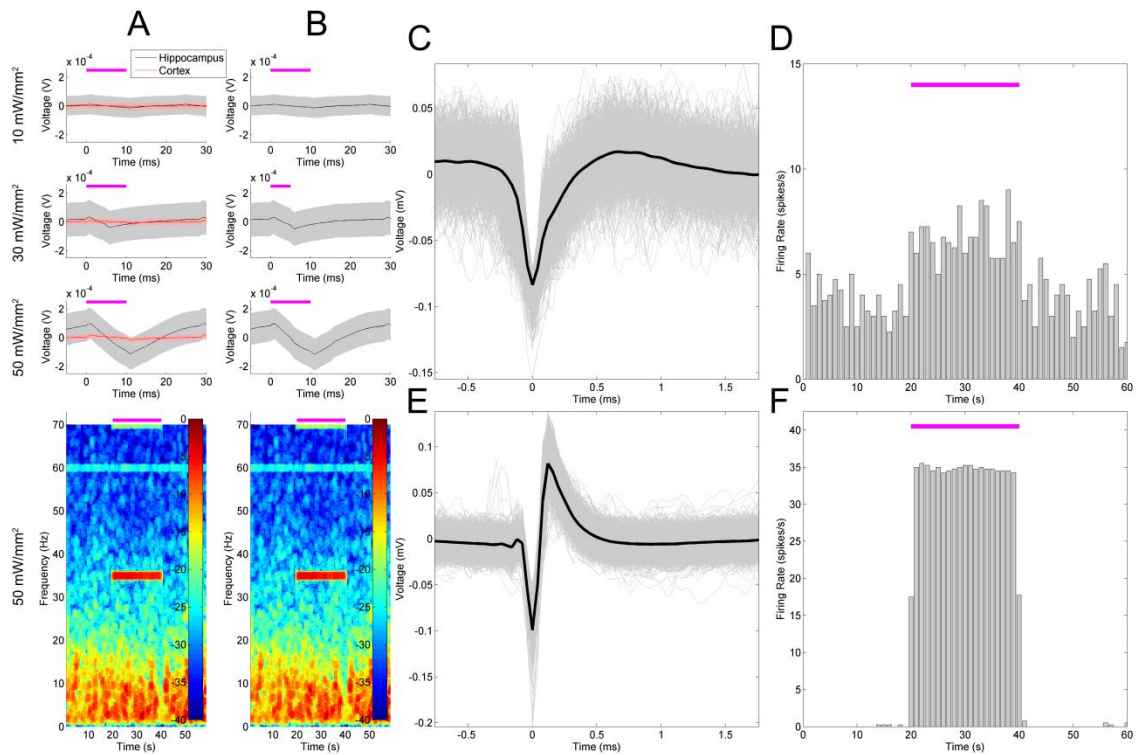
Figure 11: Stimulation and recording within the hippocampus.
The dorsal hippocampus was stimulated with the combined NeuroNexus array and ferrule (shown in **Figure 4J**) with 35 Hz, 10 ms pulses at 10 mW/mm^2, 30 mW/mm^2, and 50 mW/mm^2. Artifacts of stimulation (**A, red**) that were intensity-dependent were noted and characterized in the cortex during implantation. The peristimulus average of the raw hippocampal LFP (**A, top**) is thus a combination of a LFP response and stimulation artifact. This makes it difficult to interpret the

corresponding spectrogram **(A, bottom)**, as it is unclear whether or not the response is due to the artifact or the neurophysiologic activity. We removed the mean artifact from each stimulation time point **(B)**, assuming that it would remain consistent between the locations, and suggesting the remaining signal was a true neurophysiologic response to stimulation. A single unit **(C)** increased in firing rate during stimulation **(D)**, but returned to basal firing rate in the post-stimulus epoch. In contrast, **(E)** shows an artifact from the stimulation signal that resembles a single unit waveform, but the firing rate was locked to the stimulation frequency **(F)**.

In the ChR2-expressing regions of the LFP of the dorsal hippocampus (Figure 11A, gray), a delayed LFP response to the stimulation was apparent along with the artifact, peaking approximately 11 ms after stimulus onset. Note that this LFP waveform response was only observed in the ChR2-expressing hippocampus. Similarly to medial septal stimulation (Figure 7), these responses generated an increase in LFP power at the stimulation frequency (Figure 11A, bottom). However, with the artifact still present in the recorded signal, it is unclear whether this increase in power was due to the presence of the artifact, or the underlying electrophysiological response.

In order to remove the artifact, we assumed that the artifact wouldn't significantly change between non-expressing tissue and expressing tissue, in part due to its stereotypy. To remove the artifact signal offline, we then subtracted the mean artifact recorded from the cortex from the LFP recording in the hippocampus (Figure 11B). As the neurophysiologic response was much larger than the artifact, the resulting spectrographic analysis remained largely unchanged (Figure 11B, bottom).

While the artifacts in the LFP were readily identifiable from the underlying neurophysiologic signal, the single-unit responses proved difficult to resolve. While common median referencing was employed to attempt to improve the signal to noise ratio of the action potentials (Rolston et al. 2009), it remained difficult to distinguish true single-units from artifacts. This is demonstrated in (Figure 11C-F), wherein a unit believed to be real, and a unit believed to be an artifactual response, are presented. The first detected unit (Figure 11C-D) had a basal firing rate preceding the stimulus that increased during the stimulation epoch in successive trials. The second detected unit (Figure 11E-F) also increased its firing rate during the stimulus, and appeared to be

largely locked to stimulus onset. However, the latter unit failed to be detected outside of the stimulation epoch, and despite the favorable appearance of its waveform, appeared to have been consequent to high-pass filtering of the stimulation artifact on this electrode. Without an accompanying intracellular waveform, or a tetrode-based identification scheme, it remains very difficult to clearly define a unit in this fashion. This is particularly a problem if the unit only appears during stimulation, and is locked to the stimulation frequency.

3.3.5 Closed-loop stimulation

We used NeuroRighter for closed-loop stimulation of medial septum in which hippocampal theta-rhythm was used as a control signal to trigger the stimulation of the medial septum. The control system was implemented using a dynamic link library (dll) based on the NeuroRighter application programming interface (API) (Newman et al. 2013). The API contains a set of tools for interacting with NeuroRighter's input and output streams. In this framework the dll accesses the NeuroRighter data servers, performs computation on the neural data, and then generates and introduces stimulation protocols into the stimulation servers, enabling real-time and closed-loop functionality. Latency is largely determined by the called hardware and software − NeuroRighter's double-buffered StimSrv output had a response latency of 46.9 ± 3.1,s − but this was reducible to 7-9 ms with alternative triggers, stimulation hardware, and less-complex outputs (Newman et al. 2013). Our implementation made use of StimSrv, which we found to be fast enough for most of our closed-loop requirements, and nicely integrated with the existing LFP data stream without significant hardware or software complexity.

The LFPs from the 16 channel microelectrode array were sampled by the API and analyzed in this fashion to estimate the power spectral density of theta oscillations (6-10Hz, Figure 12) over time, relative to the total power of the signal in each time window. The power spectral density was estimated using the signal processing libraries of the Accord.net framework. When the normalized theta power dropped below a defined threshold a predefined stimulation profile ($50mW/mm^2$, 35Hz, 10ms for 30 seconds) was generated and sent to the NeuroRighter stimulation servers. The stimulation parameters and threshold can be adjusted in run-time through a graphical user interface. This arbitrarily-designed closed-loop system worked quite robustly, generating readily-identifiable increases in power at 35 Hz following periods of low-theta power relative to the total signal (Figure 12, magenta arrow). In this particular case, theta power did appear to recover by the end of the stimulus, but more robust testing will be necessary to determine whether or not this effect was a consistent one.
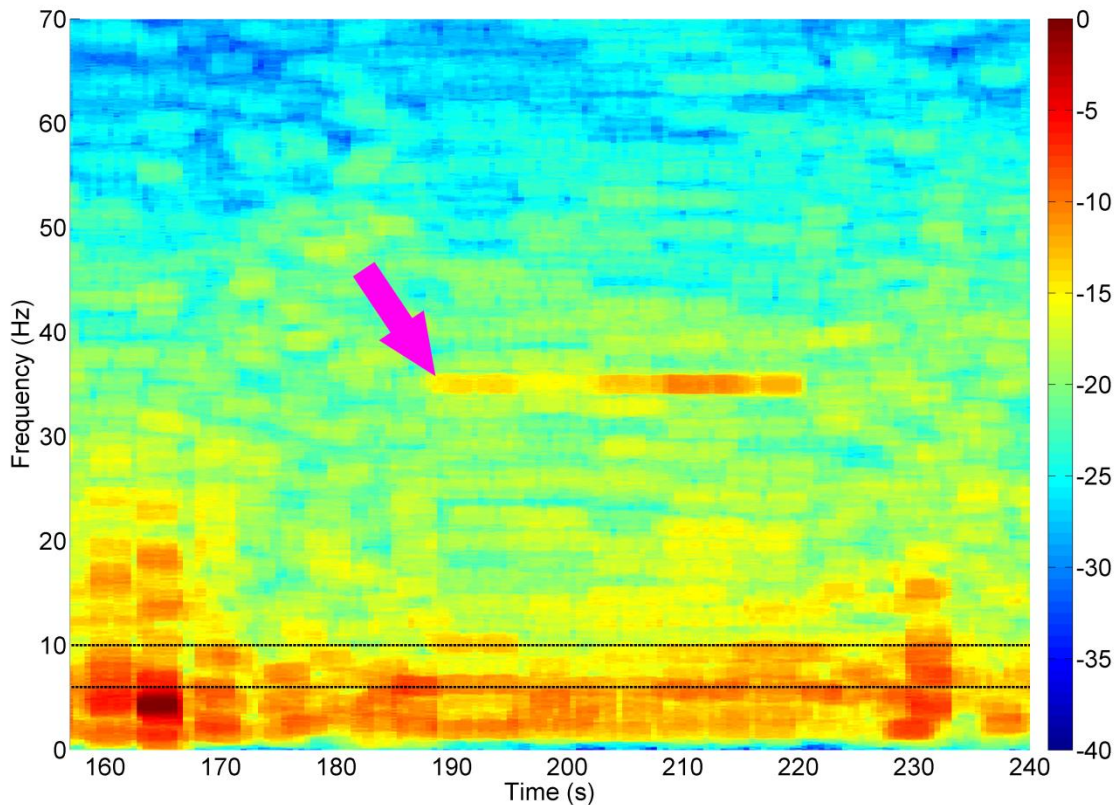
Figure 12: Closed-loop stimulation of the medial septum in response to decreased theta power.
As an example of the closed-loop capabilities of NeuroRighter, theta power (6-10Hz, within black dotted lines) was evaluated in a closed-loop dll produced for use with NeuroRighter. 50 mW/mm^2, 35sHz, 10 ms stimulation pulses were produced for 30 seconds in response to a decrease of power within the theta band below threshold relative to the total power in the time window. This response was readily identifiable in the spectrogram (magenta arrow).

3.4. DISCUSSION

NeuroRighter has been demonstrated to be an adept and versatile platform for real-time, *in vivo* awake and behaving experiments with optogenetic neuromodulation and electrophysiologic recordings. It is capable of open- and closed-loop optical stimulation in a wide variety of user-defined patterns, and provides single-unit and LFP outputs, which are easily and readily analyzed. Through our example experiments and

analyses we have demonstrated the capabilities of this system, and imply future endeavors that are worthy of exploration.

As we suspected, the parameters of square-wave optical stimulation in our medial septal stimulation experiments had a significant impact on response waveform properties (Figure 6). As we are stimulating in the medial septum and recording in the hippocampus, the LFP responses we detected were likely the result of post-synaptic potentials generated via medial septal axons (Buzsáki et al. 2012). At higher stimulation frequencies the response became increasingly sinusoidal and decreased in amplitude. There has long been evidence that ChR-2-infected neurons have difficulty following stimulation patterns at >40 Hz (Yizhar et al. 2011). A decrease in LFP response amplitude might therefore be assumed at frequencies >40 Hz as a result of less reliable spike generation: fewer neurons are following the stimulus and generating action potentials, so the signal conducted to the hippocampus – manifested in the hippocampal post-synaptic LFP – is reduced. However, the stimulation frequencies we explored are within this experimentally-determined acceptable window. We hypothesize instead that the pattern of decreasing amplitude with increasing stimulation frequency is instead a consequence of the photocycle of ChR2. ChR2 is believed to possess a four-stage photocycle consisting of two open states with different ion conductances, and two closed states (Berndt et al. 2010). The first open state, which is triggered by sudden light intensity changes, results in the non-specific conduction of several ionic species. The second open state, which occurs with prolonged illumination, follows the first open state and is associated with a decrease in the total conductance, in part due to increased selectivity for H^+ ions, as well as the accumulation of channels in nonconducting states. The waveform response properties we observed may

then be a result of similar accumulation of ChR2 channels in these non-conducting states, whereas low-frequency stimulation is able to more maximally activate a recycled and conductive population of light-sensitive ion channels. This hypothesis also provides an explanation for the observation that longer pulse widths altered the time-to-peak responses with different intensities. With short pulse widths the primary conductive mediator would be the first, fast open state. With longer pulse widths the second, slower conducting open state could come into play, delaying the time-to-peak with a later contribution to the response waveform. Computer modelling of these dynamics could provide more quantitative hypotheses that would better reveal the influence of stimulation parameters on these responses, as well as greater insight into the ChR2 channel.

Increasingly, alternative stimulation patterns are being explored for use in clinical deep brain stimulation therapies (Brocker et al. 2013). Indeed, the regimented frequency-specificity of our existing therapies and experiments appear quite artificial when compared with the natural oscillations within these neural circuits. Alternative stimulation patterns that better approximate neurologic signals, such as those presented here (Error! Reference source not found.), may prove more effective in eliciting ehavioral and experimental outcomes.

The artifacts of optical stimulation that we and others have observed (Figure 11), while of significantly less magnitude than equivalent electrical stimulation artifacts, do obscure and potentially influence the underlying neurophysiologic activity. In our hands these artifacts have proven very array-dependent, and others have suggested some mechanisms for reducing and removing them (Cardin et al. 2010). As they can prove

quite insidious, leading to false detections as single units, robust methods for preventing, defining, and removing such artifacts will be necessary to limit improper conclusions.

3.5. CONCLUDING REMARKS

The NeuroRighter platform provides a low-cost, open-source, real-time solution for optogenetic neuromodulation and multielectrode electrophysiology in awake and behaving animals. It is readily customizable to a number of applications, including open- and closed-loop experimentation with a variety of stimulation patterns, recording electrodes, and behavioral tasks.

CHAPTER IV

OPTOGENETIC NEUROMODULATION OF MEDIAL SEPTAL GABAERGIC NEURONS AND THE IMPACT ON HIPPOCAMPAL OSCILLATORY ACTIVITY IN AWAKE AND BEHAVING RATS

4.1. INTRODUCTION

Substantial evidence implicates the medial septum-diagonal band complex (MSDB) in the generation and maintenance of the hippocampal theta rhythm (Stewart and Fox 1990; Tóth et al. 1997; Buzsáki 2002). Three genetically-distinct neuron subpopulations have been identified within the MSDB – GABAergic, glutamatergic, and cholinergic neurons – all of which project to the hippocampus and may play a role in modulating hippocampal activity and theta oscillations (Freund and Antal 1988; Sotty et al. 2003; Yoder and Pang 2005; Huh et al. 2010; Bell et al. 2013), individually or in a coordinated fashion. The GABAergic subpopulation in particular possesses several anatomical and electrophysiologic features that suggest it may play a definitive role in driving and pacing hippocampal theta.

Histological investigation of the septohippocampal axis demonstrated that the GABAergic MSDB population selectively innervates most of the GABA-containing interneurons throughout the hippocampus, establishing basket-like formations around cell

bodies and proximal dendrites (Freund and Antal 1988). These synaptic contacts are found in all hippocampal layers, but were predominantly observed in the strata oriens and radiatum of CA3 and the hilus and granule cell layers of the dentate gyrus.

No hippocampal glutamatergic pyramidal cells were found that received multiple synaptic inputs from the GABAergic projections (Freund and Antal 1988). Consequently, it was hypothesized that activity in MSDB GABAergic neurons would inhibit GABAergic interneurons of the hippocampus, effectively disinhibiting the pyramidal neurons they in turn synaptically contact. Rhythmic synchronous disinhibition sponsored by the medial septum could then generate periods of inhibition and disinhibition, manifesting as an oscillatory rhythm.

Electrophysiological investigations lent support to the hypothesis that the MSDB GABAergic neurons were capable of pacing theta oscillations in the hippocampal local field potential (LFP). In cleverly prepared septohippocampal slice preparations, Tóth et al. stimulated either the medial septal nucleus or at the septal end of the fimbria in the presence of muscarinic and excitatory amino acid antagonists, while concurrently recording intracellularly from neurons in the CA3 field (Tóth et al. 1997). Single or repetitive stimulation of the MSDB reduced the frequency of inhibitory post-synaptic potentials (IPSPs) in CA3 pyramidal neurons. In contrast, hippocampal inhibitory interneurons experienced IPSPs in response to septal stimulation, in some cases abolishing spontaneous firing. Furthermore, Toth et al. determined that rhythmic (5 Hz) septal stimulation generated a conserved period of oscillating hippocampal synaptic oscillation driving hippocampal LFP. During this period, the authors also noted that

despite the lack of increase in pyramidal cell firing frequency, action potentials were strongly entrained to the peak of the artificial disinhibitory oscillation.

Coupled with work from Stewart and Fox that identified a rhythmically bursting neuron population in the MSDB (Stewart and Fox 1990), it was hypothesized that the GABAergic MSDB neurons in this disinhibitory circuit pace hippocampal theta oscillations. However, it was unclear whether this bursting neuron subpopulation was indeed composed of the MSDB GABAergic neurons, as the correlation between neurochemical identity and electrophysiologic properties had yet to be established. In fact it would soon become clear that despite this work an entirely novel population of glutamatergic neurons was unrecognized.

Significant progress towards elucidating these facts was accomplished by Sotty et al, in a thorough series of elegant experiments (Sotty et al. 2003). The authors coupled whole-cell recordings with single-cell reverse-transcription polymerase chain reaction (RT-PCR) to simultaneously characterize both the electrophysiologic and genetic characteristics of the MSDB neurons they sampled. They characterized four distinct firing populations – slow-firing, burst-firing, fast-firing, and slow/cluster-firing – alongside three major neurochemical profiles, and a few multi-neurochemical profiles. The choline acetyl-transferase (ChAT) positive cells (cholinergic) were identified as the slow-firing neurons, whereas the novel VGLUT-positive neurons (glutamatergic) demonstrated a stimulus-dependent slow/cluster firing rate. GAD67 expressing neurons (GABAergic), as hypothesized, were found to consist of both burst- and fast-firing populations. Despite these findings, it should be noted that sustained rhythmic bursting – necessary for the maintenance of an oscillatory rhythm – was not observed in these

populations. In addition, several of their genetically-identified neurochemical groups also demonstrated cross-reactivity, including VGLUT reactivity. The authors thus hypothesized that either the bursting GABAergic neurons or cluster-firing glutamatergic neurons were contributing to pacemaker activity in the hippocampus, but could not establish a definitive argument for either of them.

One concern with these investigations is that they were performed in deafferented septohippocampal slices, a preparation which might change the firing properties of the investigated neurons and the associated physiologic rhythms (Stewart and Fox 1990; Williams and Kauer 1997). However, in a similar series of *in vivo* juxtacellular recording experiments in anesthetized rats, Borhegyi et al. used cytoplasmic filling to perform immunocytochemical identification (Borhegyi et al. 2004). They identified two distinct populations of highly regular, constitutively bursting medial septal GABAergic neurons whose activity was correlated to either the peak or trough of the hippocampal theta oscillation. Investigating the axonal arborizations revealed the presence of numerous collaterals within the medial septum, suggesting that the bursting MSDB GABAergic neurons could synchronize the activity of the entire septohippocampal network.

While these investigations asked whether the GABAergic populations of the MSDB were capable of driving hippocampal theta activity, Yoder et al. investigated their *necessity* to the oscillatory rhythm (Yoder and Pang 2005). The authors selectively lesioned the MSDB GABAergic and cholinergic neurons chemically and examined the impact on hippocampal theta in two states – urethane anesthesia and awake locomotion. Urethane anesthesia is associated with theta II, a theta oscillatory rhythm sensitive to arrest from the competitive muscarinic antagonist atropine. A second type of

hippocampal theta, theta I, co-occurs with theta II during locomotion, and is resistant to elimination by atropine (Vanderwolf 1975; Montoya and Sainsbury 1985; Yoder and Pang 2005). Intraseptal injections of kainic acid or 192 IgG-saporin were utilized to selectively destroy MSDB GABAergic and cholinergic neurons, respectively (Yoder and Pang 2005). We should note that they did not assess the impact of either of these interventions on the glutamatergic population, which may have been affected. Either of these interventions greatly reduced hippocampal theta power under urethane anesthesia, suggesting that both populations are each necessary for type II (atropine-sensitive) hippocampal theta. Theta during locomotion was less reduced by the same interventions, suggesting that contribution to theta during awake behavior may also stem from another source. The authors postulated that the source of this input may be glutamatergic projections from the entorhinal cortex, and that the reduction in theta power during locomotion was due to elimination of intermixed type II theta (Yoder and Pang 2005). Combinatorial lesions – including of entorhinal cortex projections – suggested that each of these sources was involved in theta I, with the MSDB GABAergic cells – in conjunction with the MSDB cholinergic neurons – providing the atropine-sensitive component (theta II).

Additional work correlated disruption of medial septal GABAergic activity with alterations to hippocampal theta (Villette et al. 2010). In this study, Villette et al. introduced amyloid β into the dorsal hippocampus of rats. They subsequently observed a reduction in theta power and detuning of theta oscillations, as well as a significant impairment of long term memory. Intriguingly, the alterations to the theta oscillations

were found to be in conjunction with a reduction in the rhythmic bursting activity of theta-phase locked MSDB GABAergic neurons, but without any accompanying cell loss.

Most recently, Kaifosh et al. attempted to characterize the synaptic population dynamics of MSDB GABAergic projections during awake behavior (Kaifosh et al. 2013), an important step as the work by Yoder et al suggests that theta behaves differently under anesthesia (Yoder and Pang 2005). Utilizing an AAV-hSynapsin-GCaMP5 injection into the medial septum of mice, the authors selectively expressed the Ca^{2+} indicator in the MSDB GABAergic population. In the postsynaptic hippocampal interneurons, they then expressed tdTomato fluorescent protein for targeting purposes and head-post fixed the animal with a chronic imaging window above CA1. This enabled fluorescence signals from axonal varicosities to be examined with two-photon microscopy during a treadmill task. During running episodes simultaneous extracellular field recordings demonstrated increased bouton fluorescence correlating with increased theta power – supporting the evidence from slices and anesthetized animals implicating the MSDB GABAergic neurons role in hippocampal theta.

Despite these efforts, the role of the MSDB GABAergic neurons in hippocampal theta remains less than clear, particularly in the light of novel glutamatergic cell populations. This confusion stems from issues of selectivity in lesioning studies, awake vs. anesthetized models, and the effects of electrical stimulation on nervous system tissue. To best assess the role of MSDB neuron subpopulations in hippocampal oscillatory activity, several experimental aspects are optimal: 1) experimentation in awake and behaving subjects 2) genetically and temporally selective excitation of the neurochemically defined MSDB GABAergic neurons to investigate the capability of

modulating hippocampal theta, and 3) genetically and temporally selective inhibition of the MSDB GABAergic neurons to investigate their necessity to hippocampal oscillatory theta activity.

To evaluate the hypothesis that the medial septal GABAergic neuron population pace hippocampal theta activity, we investigated optogenetic excitation and inhibition of the MSDB GABAergic neurons in unrestrained awake and behaving rats. Optogenetic tools provide a powerful methods for genetically and temporally precise manipulation of complex heterogeneous nervous system circuitry (Aravanis et al. 2007; Carter et al. 2009; Gradinaru et al. 2009; Kravitz et al. 2010; Yizhar et al. 2011; Packer et al. 2012; Wykes et al. 2012; Paz et al. 2013). When combined with electrophysiological recordings, optogenetic control can provide unprecedented insight into neural connectivity and function (Bell et al. 2013), particularly in awake and behaving animals (Gradinaru et al. 2009; Liu et al. 2012).

4.2. METHODS

4.2.1 Surgeries

2-3 month old adult male Sprague-Dawley rats (250-300g) were purchased from Charles River Laboratories (Wilmington, MA, USA). 2-3 month old adult male Long-Evans rats were bred as the non-expressing cage-mates of a Chat-CRE transgenic rat colony. Three rats apiece were used in each experimental group. No differences were seen between the strains, so the animals were grouped for all analyses. All animals were maintained within a 12/12 light/dark cycle vivarium with unlimited access to food and water. This work was conducted in accordance with Emory University's Institute for Animal Care and Use Committee.

Each subject underwent two surgical procedures. The first survival surgery introduced the viral vector to the medial septum and provided time for expression of the optogenetic channel. Rats were anesthetized with 1.5-4% inhaled isoflurane, and a craniectomy was made 0.40 mm anterior and 2.00 mm lateral to bregma on the right side of the skull. A pulled-glass pipette attached to a stereotactically mounted injector (Nanoject; Drummond Scientific Co., Broomall, PA, USA) was used to inject 1.8 µL of 10^{12} particles/mL AAV5-hSynapsin-hChR2(H134R)-EYFP or AAV5-hSynapsin-eNpHR3.0-EYFP (UNC Vector Core Services, Chapel Hill, NC, USA). This promoter has been described as selectively expressing in the GABAergic neurons of the MSDB (Kaifosh et al. 2013). The injection was made at a 20° angle to the dorsal-ventral axis (0.40 mm anterior, 2.12 mm lateral at the 20° angle, 5.80 mm ventral to pia along the rotated axis) in order to target the medial septum without damaging the medially-located central sinus. After 5 minutes for equilibration, the injection was made over 7 minutes with the pipette remaining in place an additional 10 minutes post-injection to prevent reflux. Once withdrawn, the scalp was stapled closed, ketofen was administered as an analgesic (3-5 mg/kg), and the rats were kept in BSL2 housing for 72 hours before returning to normal housing.

The second survival surgery was performed two weeks later. A second craniectomy was made over the right dorsal hippocampus centered at 3.50 mm posterior and 2.80 mm lateral to bregma. The dura was incised with a sterile curved scalpel blade. In order to record from the dorsal hippocampus 16-channel microwire multielectrode arrays (Tucker Davis Technologies (TDT), Alachua, FL., USA; MEA) were constructed from sixteen 33 µm diameter tungsten electrodes with polyimide insulation (Figure 4I).

The electrodes were arranged in two rows of eight electrodes with 1 mm between rows and 175 µm of space between the electrodes within a row. Ground and reference wires were separated on the array and routed through two stainless steel wires, which were affixed to separate skull screws during the implantation surgery. The two rows were cut to different lengths, 4.0 mm and 3.0 mm, to target and record simultaneously from the hippocampal CA3 and CA1 regions, respectively, enabling multiunit and local field potential recording from the hippocampus distantly from the optical stimulation site in the medial septum. The array was positioned at a 50° angle to midline, with the posterior end swung laterally, to match the positioning of the hippocampal pyramidal cell layers pyramidal cell layers (Rolston et al. 2010). The MEA was lowered while simultaneously recording single unit and local field potential (LFP) activity to attain the ideal positioning (Rolston et al. 2009). When the electrophysiologic recordings stabilized and the CA1 and CA3 layers were identified, the original injection craniectomy was reopened, and a calibrated optical fiber ferrule (Figure 4E, H) was implanted at a 20° angle to the dorsal-ventral axis (0.40 mm anterior, 2.12 mm lateral in the rotated axis). Stimulation was performed as the ferrule was implanted, with the resulting recordings immediately analyzed spectrographically. Descent was halted when a strong stimulus-response signal was observed in the spectrogram, or when the optical ferrule reached a maximum depth of 5.50 mm from pia along the rotated axis.

Once the electrodes and ferrules were in place, the craniectomy was sealed with dental acrylic (OrthoJet; Lang Dental; Wheeling IL), securing the array and ferrule in place in their respective targets. The rats were administered ketofen (3-5 mg/kg) to

minimize pain and returned to normal housing to recover for 3-5 days before optical stimulation and recording experiments were performed.

4.2.2 Optical stimulation and electrophysiologic recordings

Using our adapted NeuroRighter system (CHAPTER III), electrophysiologic recordings were sampled at 25 kHz with a 1-9,000 Hz bandwidth. LFPs were isolated online with a 1-500 Hz 1-pole Butterworth band-pass filter and downsampled to 2000 Hz. Action potentials were isolated online (Newman et al. 2013) and sorted using spike-sorting Wave_clus scripts and superparamagnetic clustering (Quiroga et al. 2004).

To stimulate awake and behaving animals, calibrated ferrules were connected via armored patch fiber cables (200 µm diameter, 0.67 NA, Plexon) to the NeuroRighter platform. ChR2 animals were stimulated with a 465 nm blue LED module. Square-wave stimulation pulses varied between 10, 30, and 50 mW/mm^2; 7, 11 (theta), 17, 23, 35 (beta), and 42 (gamma) Hz; and 2, 5, and 10 ms pulse widths. eNpHR3.0 animals were inhibited with a 620 nm orange LED module. Square-wave stimulation pulses varied between 10, 30, 50, 70, and 90 mW/mm^2; 7, 11 (theta), 17, 23, 35 (beta), and 42 (gamma) Hz; and 2, 5, and 10, 20, and 50 ms pulse widths. Continuous stimulation at 50, 70, and 90 mW/mm^2 was also performed. The experimental protocol consisted of repeated one minute recordings of 20 seconds of pre-stimulation background, 20 seconds of stimulation, and a subsequent 20 seconds of additional post-stimulation background. Stimulation protocols were performed in random order and repeated several times over multiple recording sessions. This setup was able to stimulate and record LFP and single-unit responses from awake and behaving animals uninterrupted for several hours and over several days. Subjects were introduced into an open-field environment for the duration of

the experiments. Data were recorded intraoperatively and for up to four weeks postoperatively.

4.2.3 Data analysis

We isolated recording days where we simultaneously recorded CA1 and CA3 single units, and selected those contacts with the highest amplitude and best-isolated single units for further analysis. Power spectra, spectrograms, coherence, and coherograms were computed from the LFP on these channels using the Chronux suite of analysis tools and multitaper analysis (Bokil et al. 2010). For spectrum and coherence calculations, T=1, W=5 with 9 Slepian tapers. A Jackknife approach was used to calculate 95% confidence intervals for statistical testing purposes. For spectrogram and coherogram analysis a moving window size of 4s was stepped in 0.5s increments, T=1, W=4 and 7 Slepian tapers. Note that these parameters sacrifice temporal specificity to gain greater resolution in frequency. As a result, edge transitions in spectrograms and coherograms will be blurred into the pre and post-stimulation epochs. Mean autocorrelation and cross-correlation between CA1 and CA3 were performed to assess alterations in theta phase during the stimulation and non-stimulation epochs, with 95% confidence intervals calculated and presented alongside the mean for statistical testing.

4.2.4 Histology

Histology was performed after experimentation to verify microelectrode recording locations and light-sensitive ion channel expression. Rats were deeply anesthetized with an overdose of Euthasol (5ml/kg, Virbac, Fort Worth, TX, U.S.A.) injected intraperitoneally. They were then transcardially perfused with 0.9% saline followed by

4% paraformaldehyde in 0.1M phosphate buffer at pH 7.2. The heads, still containing the electrodes and ferrules, were then separated and post-fixed at 4°C overnight. The next day the brains were dissected out, removed, and cryoprotected with 30% sucrose at 4°C. Frozen transverse (horizontal) sections were made of 50 μm thickness on a sliding microtome and collected in 0.1M PBS. Sections were mounted on glass slides and mounted with Vectashield mounting medium with DAPI (Burlingame, CA, U.S.A.) for visualization of nuclei. Sections were imaged in the NIS-Elements software (Nikon Instruments, Inc., Melville, NY, USA) using a Nikon DS-Fil color digital camera on a Nikon E400 microscope equipped with TRITC, FITC, and DAPI fluorescence cubes.

4.3. RESULTS

4.3.1 Histologic verification of channel expression

Injection of AAV5-hSynapsin based viral vectors resulted in robust expression in the medial septum (Figure 13, Figure 5A, green). The hSynapsin promoter has demonstrated specificity for the GABAergic neurons of the medial septum (Kaifosh et al. 2013). From the medial septum, axonal projections to the hippocampus (Figure 13C, Figure 5A, C) were visible, coinciding with the passage of the electrodes (Figure 5C, red and white arrows) and the hippocampal pyramidal cell layer (Figure 5C, yellow arrow). AAV5-hSynapsin-eNpHR3.0 expression is not shown because those animals have yet to be sacrificed and processed histologically.
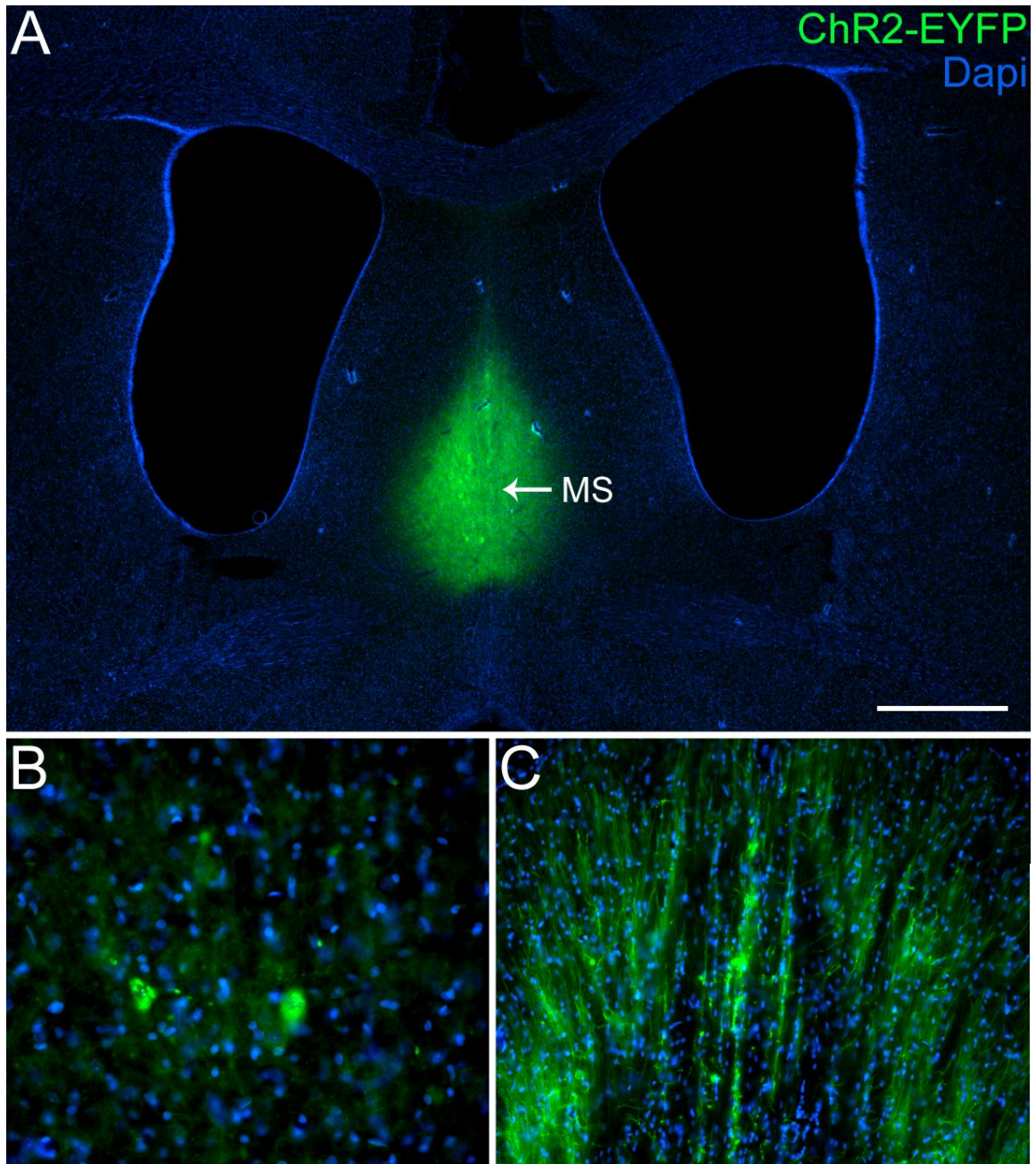
Figure 13: Robust expression of ChR2-EYFP in the medial septum.
(**A**) AAV5-hSynapsin-ChR2-EYFP injection into the medial septum (**MS**) produced robust ChR2-EYFP expression (**green**). Scale 1 mm. Expression was noted specifically within individual cells (**B**) and in their axonal projections (**C**).

4.3.2 Rhythmic excitation of GABAergic MSDB neurons

4.3.2.1 Evoked LFP response waveforms to excitation are highly influenced by stimulation parameters.

To address the question of whether GABAergic MSDB neurons can modulate hippocampal oscillatory activity, we selectively excited this population with hChR2(H134R) in pulse trains of varying width, amplitude, and frequency, and examined the resulting hippocampal LFP response. Stimulation produced evoked field potentials in both the CA1 and CA3 layers. These evoked potentials were readily visible in the local field potential recording (Figure 14A). Averaging the response from each pulse across all parameters (peristimulus average) indicated that the evoked potential waveform was highly dependent upon stimulation parameters (Figure 14B). Stimulating at lower frequencies (7-23 Hz) produced defined evoked potentials which increased in amplitude with light intensity and longer pulse-widths. However, at high beta (35 Hz) and low gamma (42 Hz) frequencies, the response to stimulation was visibly sinusoidal and no longer dependent upon stimulation intensity.
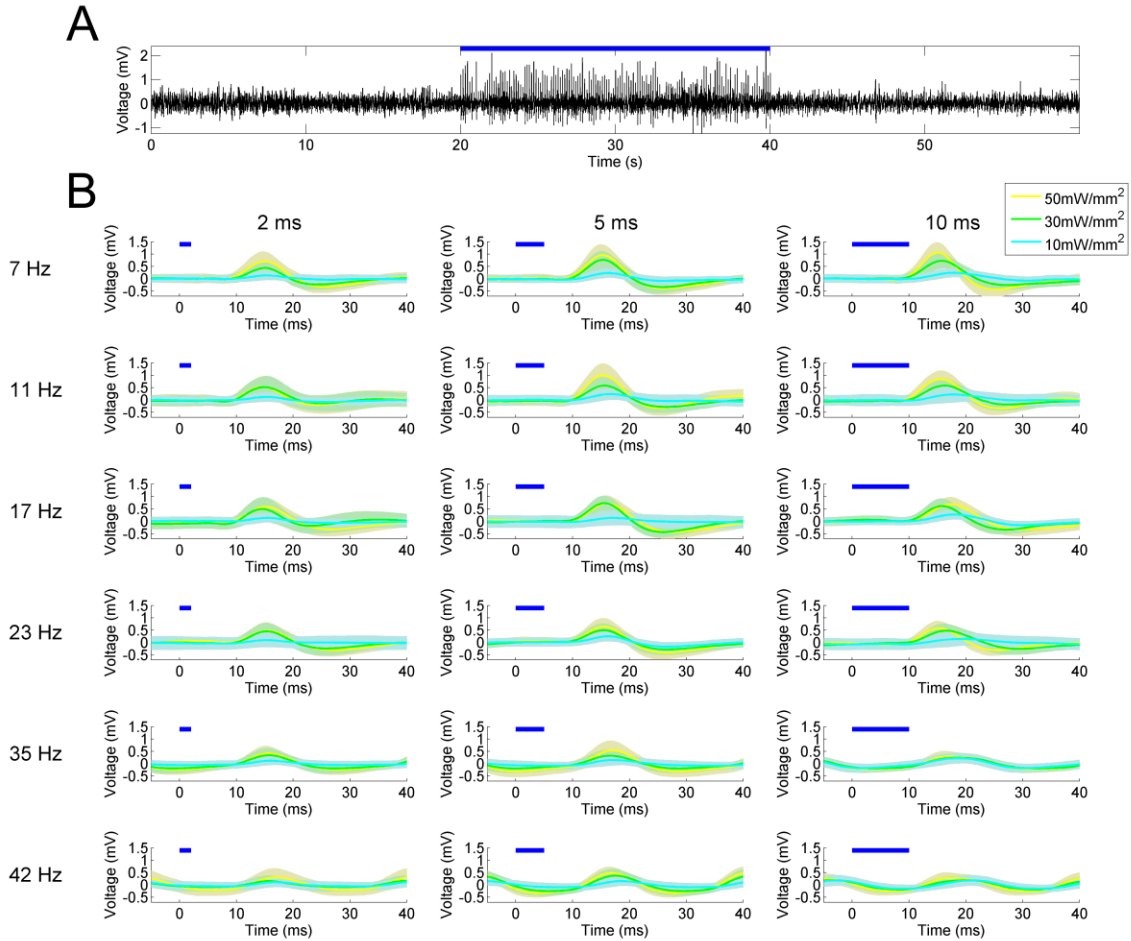
Figure 14: CA3 LFP response as a function of stimulus intensity, frequency, and pulse width.
Stimulation of the GABAergic neurons of the medial septum resulted in pronounced evoked potentials in the hippocampal LFP. **(A)** An example CA3 LFP recording during 50 mW/mm^2, 7 Hz, 10ms excitation (blue bar). **(B)** Calculating the peristimulus average (thick line is mean, shaded area is standard deviation) response in CA3 across each of the stimulation protocols demonstrated that the evoked potential waveform was highly dependent on the stimulation parameters. Low-frequency stimulation (7-23 Hz) produced defined waveform peaks, particularly at high stimulation intensities and long pulse-widths. At higher frequencies (35-42 Hz), however, the response was largely sinusoid and independent of stimulus intensity. Note that at higher frequencies the interpulse interval reduces such that each 50ms window features multiple pulse responses, which is likely what is driving the sinusoidal response.

3.2.2 Frequency-specific responses to optical excitation in both layers

Spectral analysis was performed to evaluate the effect of stimulation at theta frequencies on hippocampal oscillatory activity. The primary result observed during the stimulation epoch was a statistically significant stimulus-frequency specific increase in power

relative to the pre-stimulation epoch, as well as harmonics of that stimulation frequency (Figure 15). The harmonics necessarily derive from the Fourier decomposition of the non-sinusoidal evoked potentials (Figure 8). Also notable was a significant decrease in theta power below the stimulation frequency, and a general increase in power at >20 Hz, again as compared to the pre-stimulus epoch. The lack of coherence at the stimulation frequency is potentially a result of indiscriminate grouping of the subjects.
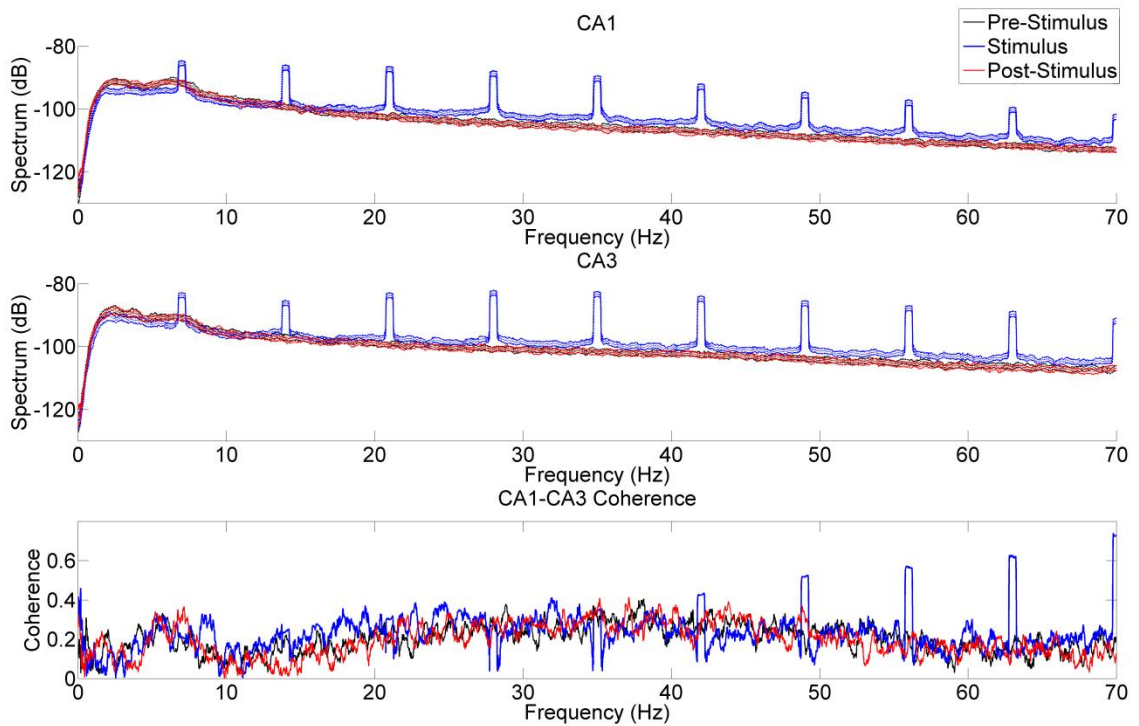
Figure 15: CA1 and CA3 demonstrate stimulation theta frequency-specific increases in power with 7 Hz stimulation.
Stimulation was performed at 50 mW/mm^2, 7 Hz, and 10 ms, and the pre-stimulus **(black)**, post-stimulus **(red)** and stimulus **(blue)** epochs across all trials were separated and spectrally examined for changes in power. 95% confidence intervals were calculated for each epoch using a Jackknife approach (dashed lines). Statistically significant (p<0.05) increases in power at the stimulus frequency were demonstrated in both the CA1 **(top)** and CA3 **(middle)** layers, alongside stimulation harmonics. Power at frequencies less than 7 Hz was significantly reduced during stimulation, and increased above 20 Hz. No significant difference in power was noted between the pre- and post-stimulation epochs. CA1-CA3 coherence at the stimulation frequency **(bottom)** only slightly increased, but more prominent peaks were noted at stimulus harmonics.

Stimulating the GABAergic neurons at other frequencies also generated a significant (p<0.05) stimulus-frequency specific response in the hippocampal LFP (Figure 16). The GABAergic neurons of the MSDB, when synchronously and rhythmically activated, transmitted the frequency pattern to the hippocampal LFP in all cases. With high beta stimulation (35 Hz, Figure 16) a significant decrease in power at theta (~ 7 Hz) was noted alongside a general increase in power >15 Hz in CA1, and less so in CA3. Also notable was an increase in CA1-CA3 coherence at the stimulation frequency.
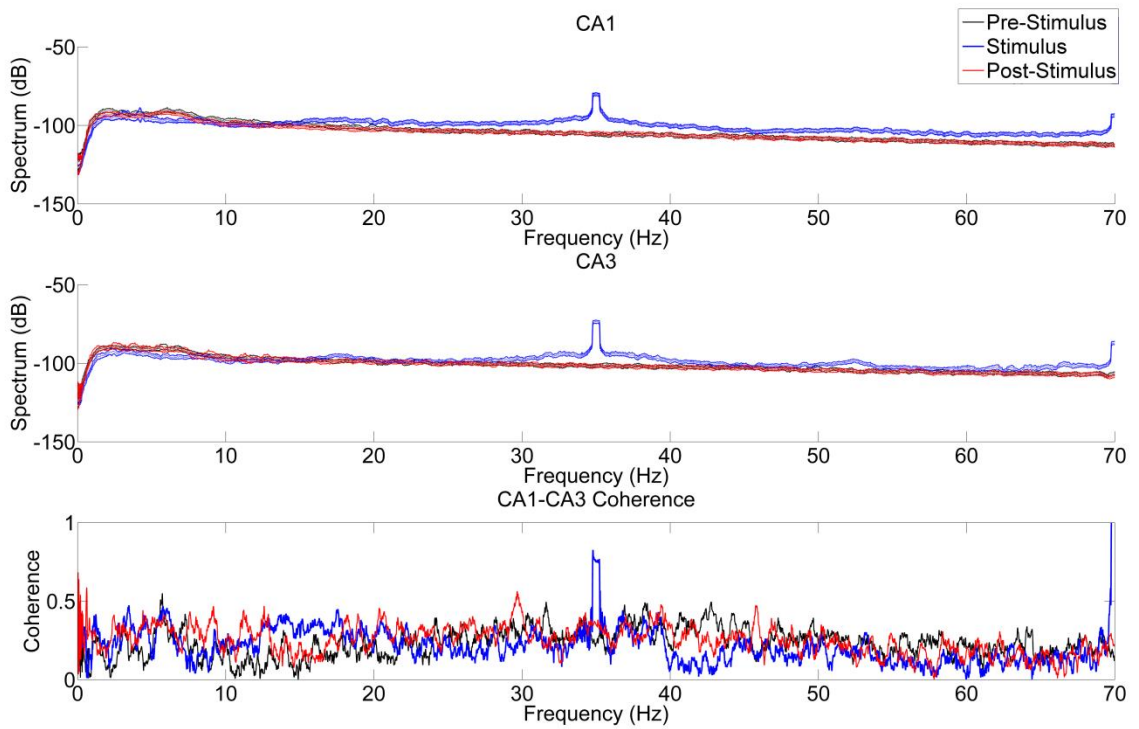
Figure 16: Stimulus-frequency specific increases in spectral power with 35 Hz stimulation.
 Stimulating with 50 mW/mm^2, 35 Hz, 10 ms pulses also significantly (p<0.05) increased power at the stimulus frequency, as well as reduced hippocampal theta power. CA1 demonstrated a significant increase in power at frequencies >15 Hz, but CA3 was not as robust in this aspect. Unlike 7 Hz stimulation **(Figure 15)**, 35 Hz resulted in a large increase in CA1-CA3 coherence.

Examining the spectrogram of the same recordings also demonstrated the consistent stimulation-frequency specificity of the LFP response in CA1 and CA3 layers, as well as the temporal specificity of the stimulation onset and offset (Figure 17, Figure 18). The post-stimulation epoch was not impacted by the stimulation epoch – increase in hippocampal oscillatory power at the stimulus frequency was not entrained and ended with the stimulus. Decreased spectral power at non-stimulus theta frequencies was observed in both stimulation paradigms, and a significant increase in CA1-CA3 coherence was observed with 35 Hz stimulation. A consistent phase relationship during the stimulation epoch was also observed for each stimulation frequency (significant only for 35 Hz), suggesting GABAergic MSDB stimulation may lock hippocampal CA1-CA3 phase relative to each other.
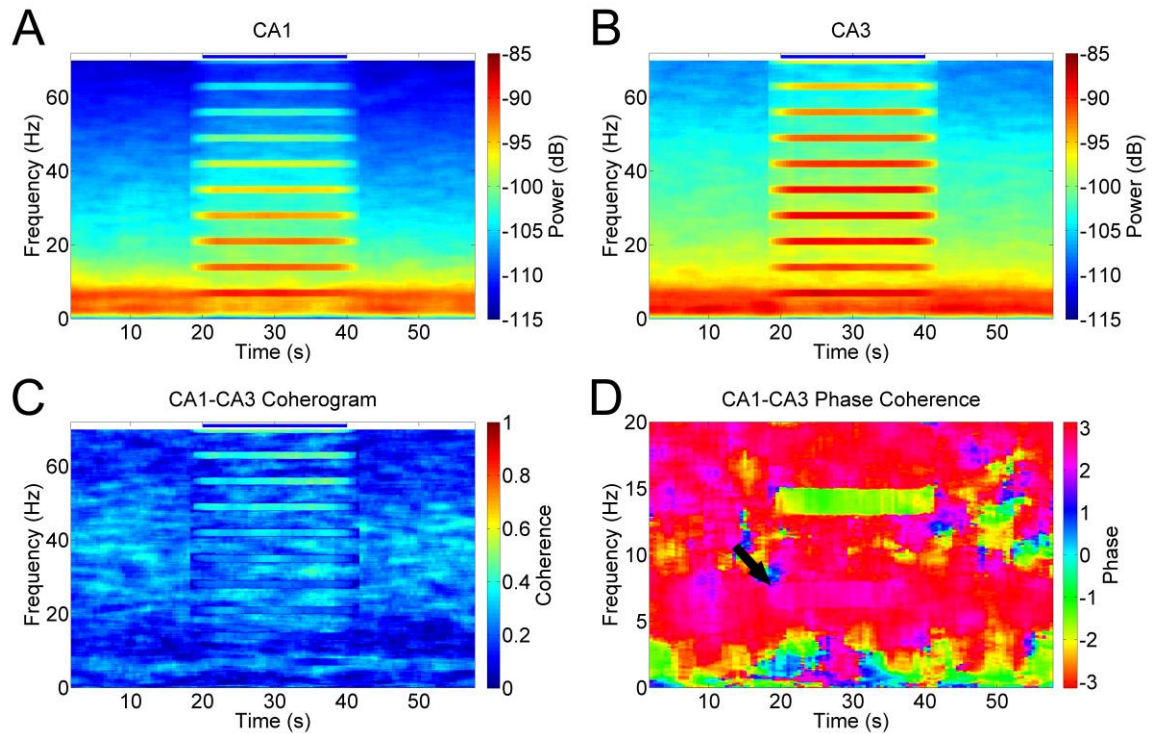
Figure 17: Temporal specificity of the spectrographic and coherence response to 7 Hz stimulation.
Stimulation of MSDB GABAergic neurons with 50 mW/mm^2, 7 Hz, 10 ms pulses **(blue bar)** consistently increased hippocampal power at the stimulus frequency in both CA1 **(A)** and CA3 **(B)**, alongside decreased power <7 Hz. While there was a non-significant (p>0.05) increase in coherence amplitude **(C)** at the stimulation frequency, examination of the angle of the coherence **(D, black arrow at stimulus frequency)** suggests that the responses in CA1 and CA3 was locked in a particular phase relationship during stimulation. Note no lasting effects from stimulation into the post-stimulation epoch. Blurring of the edges is due to the wide moving window used in spectral analysis (4s), necessary to properly resolve the frequency bandwidth (1 Hz).
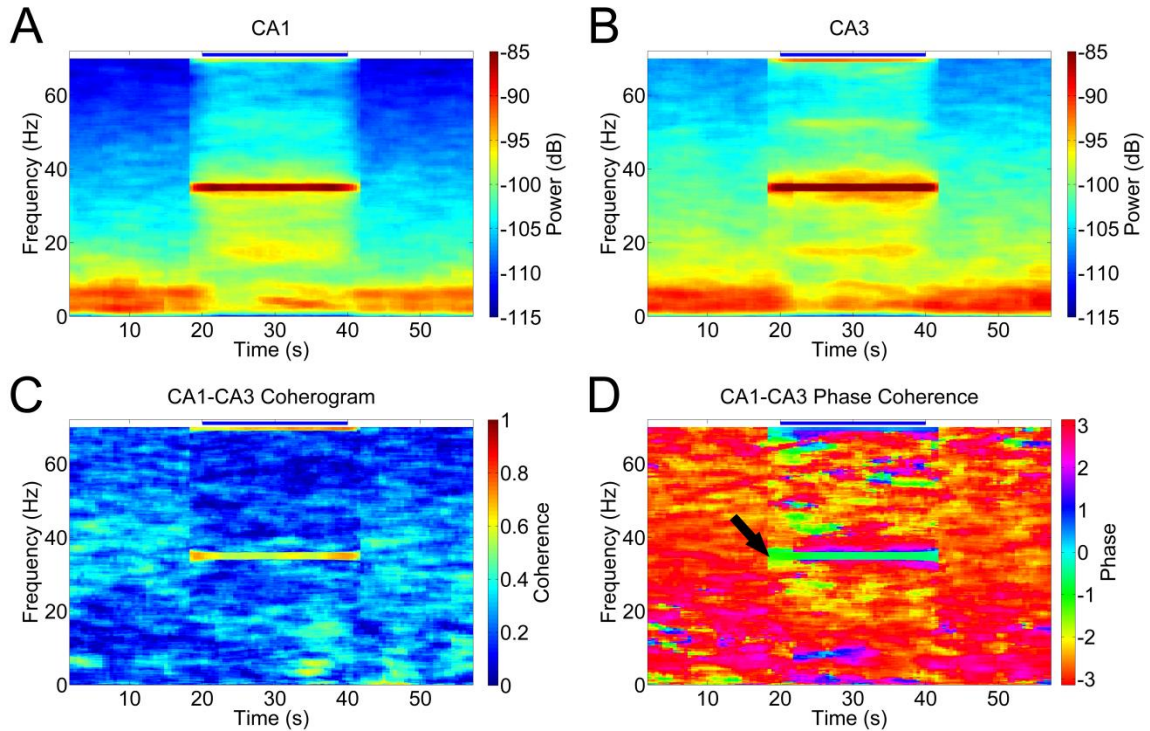
Figure 18: Temporal specificity of the spectrographic and coherence response to 35 Hz stimulation.
Stimulation of MSDB GABAergic neurons with 50 mW/mm^2, 35 Hz, 10 ms pulses **(blue bar)** also consistently and robustly increased hippocampal power at the stimulus frequency in both CA1 **(A)** and CA3 **(B)**, as well as decreased theta power. In contrast to 7 Hz stimulation (Figure 17), there was a significant ($p<0.05$) increase in coherence amplitude **(C)** at the stimulation frequency. This was accompanied by a very consistent phase relationship **(D, black arrow)**.

4.3.2.3 Phase-locking to the theta stimulus pattern

To examine the impact of MSDB GABAergic stimulation on hippocampal phase more thoroughly, we evaluated the autocorrelation of the CA1 and CA3 signals in response to theta (7 Hz) stimulation, as well as the cross-correlation between the layers (Figure 19). If the oscillation was locked in phase and amplitude throughout the stimulation epoch (Figure 19, blue), then we would observe peaks in the correlation at stimulation lag times. Both CA1 and CA3 demonstrated significantly ($p<0.05$) correlated peaks at lags corresponding to the stimulus frequency (Figure 19). These peaks were consistent well

into the lag in both layers, indicating that LFP phase was locked to the stimulation. The

CA1-CA3 correlation did suggest (not significant, p>0.05) a stimulation-imposed phase-

relationship between the CA1 and CA3 layers, wherein the correlation peak was shifted

into the negative lags, suggesting the CA3 LFP response slightly preceded the CA1 LFP

response.
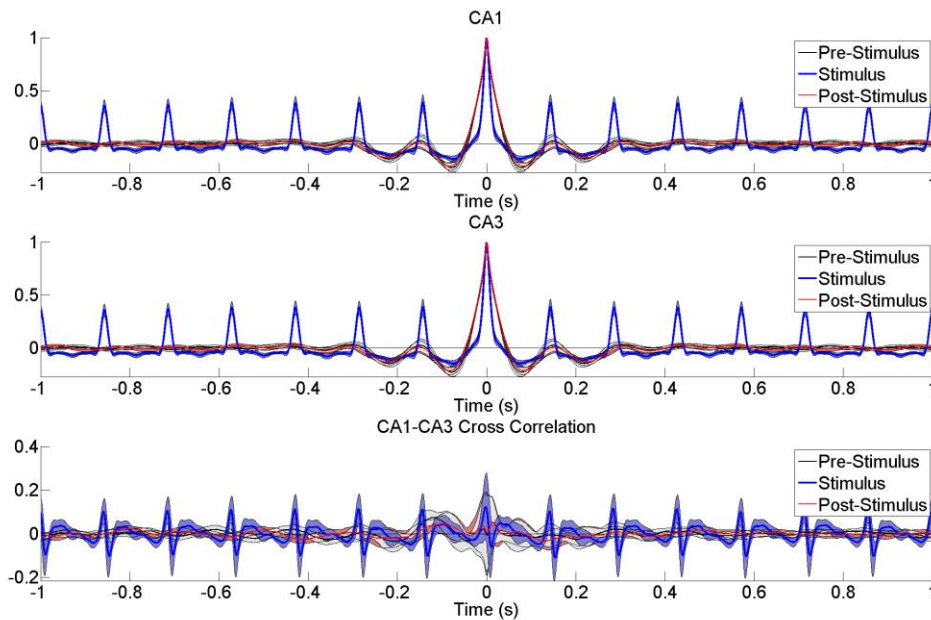
Figure 19: Auto and cross-correlation properties indicate phase-locking to stimulus pulses.
Autocorrelation of the CA1 and CA3 LFP-signal demonstrated a consistently significant (p<0.05)
increase in correlation at the stimulus frequency – as compared to the pre and post-stimulus
epochs, suggesting that the LFP response was phase-locked to the stimulus pattern. Cross-
correlation between CA1 and CA3 was not significant (p>0.05) at zero lag, but was so at
successive lag times, suggesting a phase relationship between CA1 and CA3 wherein CA3
preceded CA1. Dark line is the mean. Shaded area is 95% confidence interval.

4.3.3 Inhibition of MSDB GABAergic neurons

Whereas the preceding experiments explored the *capability* of the MSDB GABAergic neurons to modulate and drive hippocampal oscillatory activity, the following work utilizes optogenetic inhibition to assess the *necessity* of MSDB GABAergic neurons for hippocampal theta oscillations in the awake animal.

4.3.3.1 Rhythmic 35 Hz inhibition of MSDB GABAergic neurons produces a concurrent increase in power at the stimulus frequency.

Rhythmic 90 mW/mm^2, 35 Hz, 10 ms inhibition of MSDB GABAergic neurons was performed. This pattern produced a statistically significant ($p < 0.05$) increase in hippocampal LFP power at 35 Hz in both the CA1 and CA3 layers (Figure 20), with the effect more pronounced in CA3. This effect was not nearly as robust as that seen with excitation of the MSDB GABAergic neurons (Figure 16), but indicates successful inhibition of MSDB GABAergic neurons.
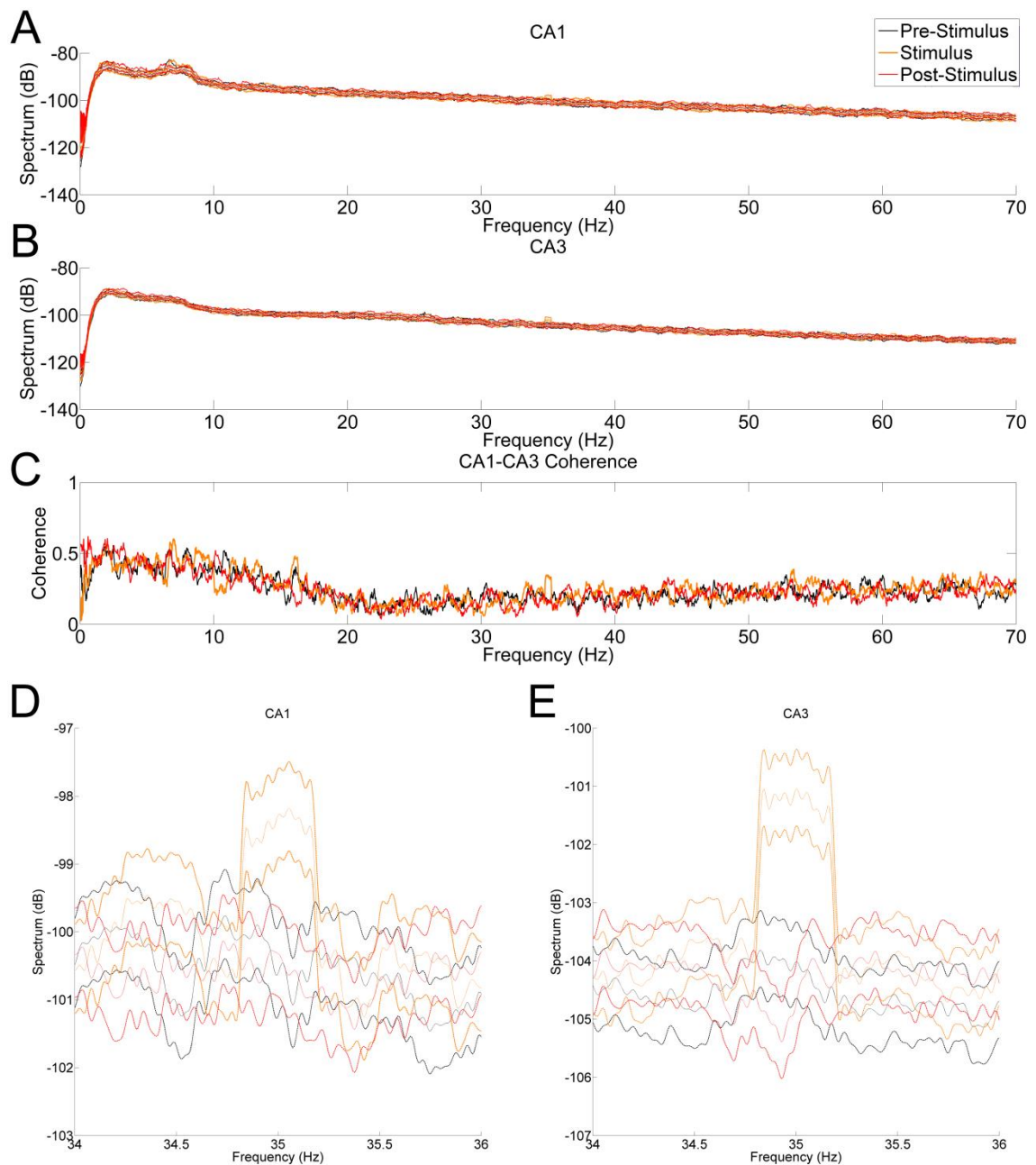
Figure 20: Rhythmic inhibition significantly increases power at the inhibition frequency.
Inhibitory stimulation was performed at 90 mW/mm^2, 35 Hz, and 10 ms, and the pre-stimulus **(black)**, post-stimulus **(red)** and inhibitory stimulus **(orange)** epochs across all trials were separated and spectrally examined for changes in spectral power. 95% confidence intervals were calculated for each epoch using a Jackknife approach **(dashed lines)**. Statistically significant (p<0.05) increases in power at 35 Hz were demonstrated in both the CA1 **(A,D)** and CA3 **(B,E)** layers. Changes at other frequencies were not observed, and no significant difference in power was noted between the pre- and post-stimulation epochs. CA1-CA3 coherence at the stimulation frequency **(C)** only slightly increased.
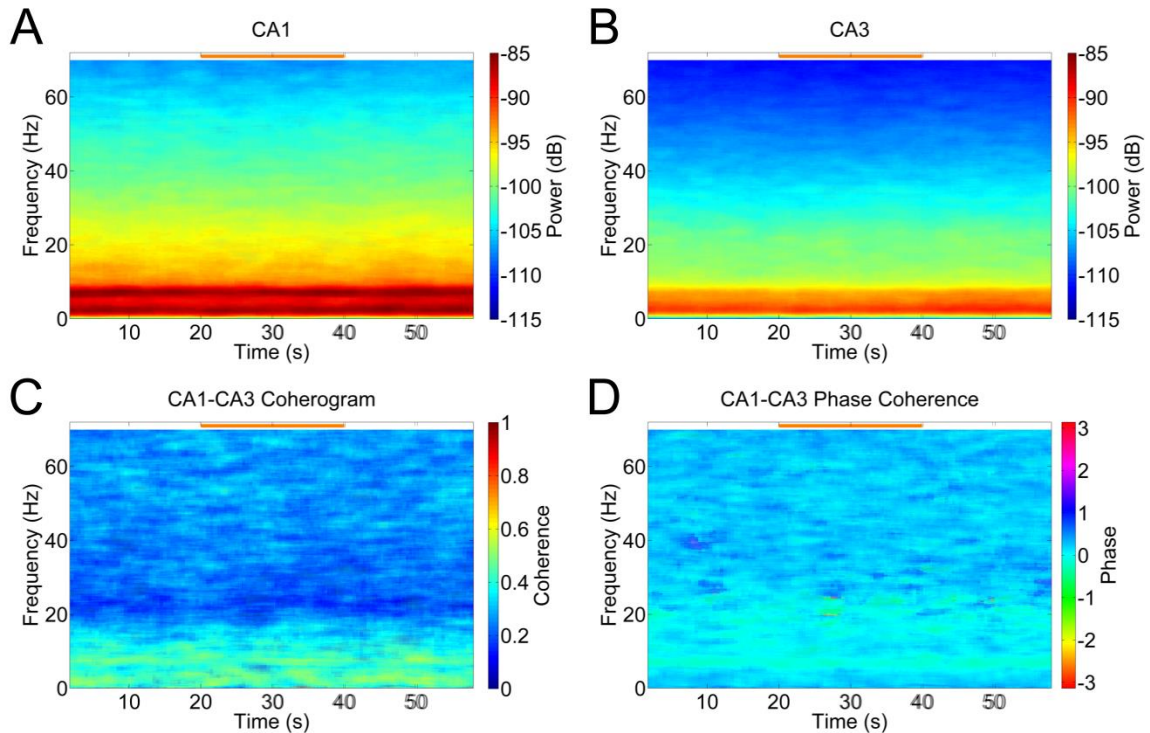
Figure 21: Constant inhibition of MSDB GABAergic neurons does not alter hippocampal oscillatory power.
Constant inhibition of the MSDB GABAergic neurons for 20 seconds at 90 mW/mm^2 **(orange bar)** failed to significantly alter hippocampal power at any frequency in either CA1 **(A)** and CA3 **(B)** from the pre-stimulus epoch. Similarly, no alterations between the pre-stimulus and post-stimulus epochs were seen in the coherogram **(C)** or the phase coherence **(D).** Theta power was not altered in the awake and behaving animal in either hippocampal layer.

4.3.3.2 Constant 90 mW/mm^2 inhibition of MSDB GABAergic neurons does not alter hippocampal LFP.

To examine the necessity of MSDB GABAergic neurons for hippocampal oscillatory

activity, we performed constant 90 mW/mm^2 inhibition for 20 seconds. Inhibition in this

fashion did not alter hippocampal spectral power at any frequency (Figure 21 A, B), nor

coherence between CA1 and CA3 (Figure 21 C, D). It also failed to significantly alter

phase relationships as assessed by autocorrelation and cross-correlation (Figure 22). It is

unclear whether or not inhibition completely arrested MS GABAergic activity.
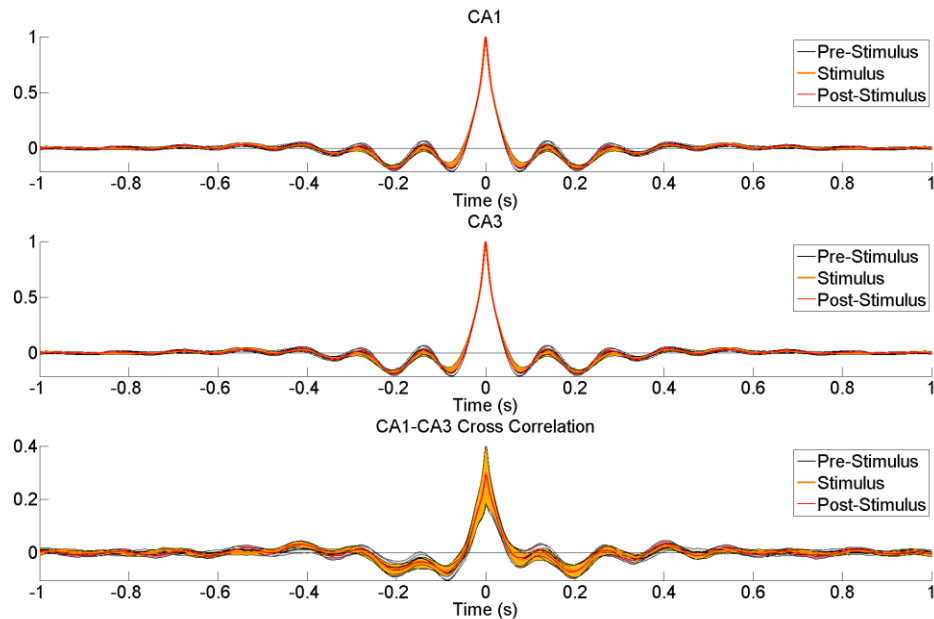
Figure 22: Constant inhibition of MSDB GABAergic neurons does not significantly alter hippocampal phase.
No significant changes between the pre-stimulus (black), stimulus (orange), and post-stimulus (red) epochs was seen during constant 90 mW/mm^2 inhibition.

4.4. DISCUSSION

Rhythmic optogenetic stimulation of the GABAergic MSDB neurons in awake rats effectively transmitted the frequency pattern of stimulation to the hippocampal LFP across both the CA1 and CA3 layers. This is in agreement with previous work in septohippocampal slice preparations (Tóth et al. 1997), and provides additional support for the disinhibitory hypothesis. In addition, we determined that this response was not dependent upon stimulation frequency – GABAergic stimulation effectively conveyed theta, beta, and low gamma patterns to the hippocampal LFP (Figure 14, Figure 17, and Figure 18). This might be expected from the disinhibitory circuit MSDB GABAergic neurons are acting through, as the structure of the circuit, supported by these results,

suggest that there is nothing inherent about the circuit that necessitates its oscillation at theta frequencies.

Our stimulation pattern was additionally associated with a phase-locking effect (Figure 19), wherein the hippocampal LFP in both CA1 and CA3 demonstrated significantly increased correlation at stimulation lag-points. This implicates a role for synchronous firing in the MSDB GABAergic neurons subpopulation in altering hippocampal oscillatory phase, which might prove important in theta phase resetting (Suthana et al. 2012).

The experimental evidence from this study and others suggest that the medial septum GABAergic neurons are capable of modulating hippocampal oscillatory activity. However, this does not necessarily mean that these neurons are necessary for theta. Work from Yoder et al. suggests that the MSDB GABAergic neurons are not majorly involved in theta in awake and behaving animals (Yoder and Pang 2005). In fact, their work implies that the anesthetized and slice-preparations most commonly used reflect an altered non-physiologic state of the septohippocampal axis.

Thus to effectively examine the necessity of the MDSB GABAergic neurons in hippocampal oscillatory activity, we optogenetically inhibited this population in the medial septum and examined the effects on hippocampal LFP. Rhythmic 35 Hz inhibition produced a frequency-specific response in the hippocampal LFP (Figure 21) suggesting that our intervention effectively modulated MSDB GABAergic neurons. This frequency-specific response may be due to filtering of fast-firing neurons action potentials, but electrophysiologic reports of the medial septum do not indicate the glutamatergic neurons firing at a high enough rate for this to be likely (Sotty et al. 2003; Borhegyi et al. 2004;

Simon et al. 2006). Instead, we hypothesize that the oscillation was generated from rebound bursting in the burst-firing MSDB GABAergic neurons (Sotty et al. 2003). Inhibition of the MSDB GABAergic population would be followed by synchronized rebound excitation, which would then be transmitted to the hippocampus.

In contrast, constant 90 mW/mm^2 inhibition failed to significantly alter hippocampal LFP power, coherence (Figure 21), and phase (Figure 22). Of particular note, no changes in hippocampal theta power or phase in response to inhibition were observed. This supports the observations by Yoder et al. that theta in awake and behaving animals is resistant to lesions of GABAergic neurons in the medial septum (Yoder and Pang 2005), and supports the conclusion that the GABAergic population is not necessary for hippocampal theta. However, it is unclear how successful our inhibitory paradigm was at arresting MS GABAergic activity, and the lack of effects may be a result of an inability to completely abolish extant neural activity in this population.

This does not rule out a modulating or synchronizing role for MSDB GABAergic neurons − this subpopulation may be particularly state-dependent. Indeed, the role of MSDB-derived theta has well established associations with learning and memory (McNaughton et al. 2006; Colom and Garrido-Sanabria 2007; Lipponen et al. 2012). Performing these same experiments under a memory behavioral paradigm (e.g. Morris water maze) could provide greater insight into MSDB GABAergic function.

In addition, combinatorial effects cannot be ruled out. Yoder et al. observed that combined GABAergic and cholinergic lesions produced a greater decrease in theta power than either alone (Yoder and Pang 2005). As septal inactivations and lesions can reduce

or abolish theta (Colom and Garrido-Sanabria 2007), there appears to be a role for the medial septum in theta.

In addition, pulsatile stimulation may not best reflect the physiologic activity of the MSDB GABAergic neurons. Pulses may overly synchronize activity – note the differences at the first theta lag in the LFP autocorrelation between the stimulus and pre- and post-stimulation epochs (Figure 19). Instead, stimulating with a continuous sinusoid (**Error! Reference source not found.**) could better reflect the electrophysiologic signal hysiologically conveyed from the medial septum to the hippocampus.

Finally, the demonstrated ability of the GABAergic population to tightly regulate phase in the hippocampus suggests that the GABAergic population may be serving to amplify a pacemaking signal and coordinate it within the hippocampal circuitry. The hippocampus is capable of theta-like oscillations in the deafferented state (Konopacki et al. 1987), and it is possible the GABAergic input from the MSDB acts upon extant hippocampal oscillatory activity to shape and modulate it. Indeed, stimulation consolidated power in the hippocampus at the stimulus frequency abolishing pre-stimulus theta oscillations.

4.5. CONCLUSIONS

Medial septal GABAergic neurons, when synchronously activated optogenetically, produce stimulation-frequency specific activity in the hippocampal CA1 and CA3 local field potential. This enables these neurons to modulate theta oscillations – as well as other frequencies – and indicates that the MSDB GABAergic neurons are capable of pacing theta, as well as other frequencies. However, inhibition of MSDB GABAergic neurons failed to alter hippocampal oscillatory activity at any stimulation

frequency, suggesting that the GABAergic neurons of the medial septum do not modulate

or pace theta in isolation.

CHAPTER V

OPTOGENETIC MODULATION OF MEDIAL SEPTAL GLUTAMATERGIC NEURONS AND THE IMPACT ON HIPPOCAMPAL OSCILLATORY ACTIVITY IN AWAKE AND BEHAVING RATS

5.1. INTRODUCTION

Substantial evidence implicates the medial septum-diagonal band complex (MSDB) in the generation and maintenance of the theta rhythm in the hippocampus (Stewart and Fox 1990; Tóth et al. 1997; Buzsáki 2002; Huh et al. 2010). Three genetically-distinct neuron subpopulations have been identified within the MSDB – GABAergic, glutamatergic, and cholinergic neurons – all of which project to the hippocampus and may play a role in modulating hippocampal activity and theta oscillations (Freund and Antal 1988; Sotty et al. 2003; Yoder and Pang 2005; Huh et al. 2010; Bell et al. 2013). The glutamatergic neurons of the medial septum have only recently been discovered (Lin et al. 2003; Sotty et al. 2003; Wu et al. 2003), but the implications for their role in the septohippocampal axis, and in theta modulation, is profound.

Definitive histologic evidence for the existence of the glutamatergic population in the MSDB would stem from immunohistochemical investigations for vesicular glutamate

transporter-2 (VGLUT2), a neuron-specific marker for the transport of glutamate (Lin et al. 2003). Many of the connections these glutamatergic neurons have were local, synapsing onto parvalbumin-immunoreactive dendrites as well as parvalbumin-positive cell bodies, and appeared to mediate the effects of nicotine on septohippocampal GABAergic neurons (Wu et al. 2003).

The first electrophysiologic investigation of the glutamatergic neuron population was performed by Sotty et al. (Sotty et al. 2003). The authors coupled whole-cell recordings with single-cell reverse-transcription polymerase chain reaction (RT-PCR) to simultaneously characterize both the electrophysiologic and genetic characteristics of the MSDB neurons. They described four distinct firing populations – slow-firing, burst-firing, fast-firing, and slow/cluster-firing – alongside the three major singular neurochemical profiles. The choline acetyl-transferase (ChAT) positive cells (cholinergic) were identified as the slow-firing neurons, while the GAD67 neurons (GABAergic) were found to consist of burst and fast-firing populations. The novel VGLUT-positive neurons (glutamatergic) – identified via the sole presence of vGLUT1 and/or vGLUT2 mRNA – demonstrated a stimulus-dependent slow/cluster firing rate. Small depolarizations resulted in the slow-firing activity, while depolarizations of up to -45 mV (from a baseline of -60 mV) resulted in cluster firing and subthreshold membrane oscillations between clusters. This raised the question of whether these neurons – which were also thought to project to the hippocampus (Manns et al. 2001) – might be providing pacemaker activity to the hippocampal theta rhythm. Their connectivity with the parvalbumin neurons of the MSDB (Wu et al. 2003) suggests that they could also drive the disinhibitory GABAergic circuitry.

More extensive histologic investigation of this population was then performed by Colom et al., who estimated a population of approximately 16,000 glutamatergic neurons concentrated in the medial septum (Colom et al. 2005). Fluorogold-based retrograde tracing of injections from the CA1, CA3, and dentate gyrus demonstrated that MSDB glutamatergic neurons send projections to each region, comprising ~23% of the total septo-hippocampal projection. This suggests that this population may primarily be involved in local circuitry of the medial septum, but this contribution to septohippocampal circuitry cannot be discounted. Indeed, the authors hypothesized that the glutamatergic population was providing a necessary excitatory background for theta rhythm generation onset and maintenance (Colom et al. 2005). Manseau et al. would further explore this hypothesis (Manseau et al. 2005), demonstrating that glutamatergic neurons within the local MSDB network could generate excitatory inputs to cholinergic and GABAergic neurons, and that these glutamatergic neurons were in turn activated by muscarinic cholinergic inputs.

Huh et al. further investigated the electrophysiologic properties of the MSDB glutamatergic neuron subpopulation, including their synaptic projections to the hippocampus, in septal and septohippocampal slices from transgenic mice expressing VGLUT2-driven enhanced green fluorescent protein (eGFP) (Huh et al. 2010). MSDB glutamatergic neurons demonstrated a broad range of firing patterns in this study. Cluster firing was again uniquely observed in this population, but the largest proportion of the subpopulation was fast firing. They also observed burst and slow firing subsets. All three of these firing patterns were shared with their GABAergic counterparts, and the fast-firing glutamatergic neurons were extremely electrophysiologically similar to fast-firing

GABAergic neurons. Huh et al. also found that 21% of the fast-firing glutamatergic MSDB neurons recorded fired spontaneously at 4-12 Hz, with the remaining demonstrating little to no spontaneous firing. In contrast, 75% of fast-firing GABAergic neurons demonstrated spontaneous theta-range firing rates. The authors also demonstrated that at least a subset of glutamatergic MSDB neurons spontaneously fired at theta frequencies in the presence of both excitatory and inhibitory synaptic blockers. However, it should be noted that a greater proportion of the GABAergic neurons tested under the same conditions demonstrated spontaneous theta firing patterns.

Huh et al. examined the glutamatergic projections from the medial septum to the hippocampus in a septohippocampal slice preparation (Huh et al. 2010). NMDA microinfusions into the MSDB directly stimulated the glutamatergic neurons, resulting in monosynaptic AMPA receptor-mediated glutamatergic responses in CA3 pyramidal neurons. The authors hypothesize – based on the presence of delayed IPSPs with electrical fornix stimulation – that the MSDB glutamatergic neurons also acted upon the hippocampal GABAergic interneurons. They proposed that the glutamatergic MSDB neurons serve to induce fast depolarizations that trigger hippocampal pyramidal cell firing, which if synchronous could contribute to theta oscillations. The local and projecting nature of these glutamatergic neurons may serve to contribute local excitatory drive in both the MSDB and the hippocampus, and coordinate oscillatory activity in the septohippocampal axis.

In order to determine the contribution of MSDB glutamatergic neurons to hippocampal oscillatory activity, and evaluate the hypothesis that medial septal

glutamatergic neurons drive hippocampal theta activity, we optogenetically excited and inhibited this population in unrestrained awake and behaving rats.

5.2. METHODS

5.2.1 Surgeries

2-3 month old adult male Sprague-Dawley rats (250-300g) were purchased from Charles River Laboratories (Wilmington, MA, USA). 2-3 month old adult male Long-Evans rats were bred as the non-expressing cage-mates of a Chat-CRE transgenic rat colony. Recordings from four rats were used in the excitation protocol, and three rats were used for inhibition. No differences were observed between the animals, and so the strains were grouped for all analyses. All animals were maintained within a 12/12 light/dark cycle vivarium with unlimited access to food and water. This work was conducted in accordance with Emory University's Institute for Animal Care and Use Committee.

Each subject underwent two surgical procedures. The first survival surgery introduced the viral vector to the medial septum and provided time for expression of the optogenetic channel. Rats were anesthetized with 1.5-4% inhaled isoflurane, and a craniectomy was made 0.40 mm anterior and 2.00 mm lateral to bregma on the right side of the skull. A pulled-glass pipette attached to a stereotactically mounted injector (Nanoject; Drummond Scientific Co., Broomall, PA, USA) was used to inject 1.8 µL of 10^{12} particles/mL AAV2-CaMKIIα-hChR2(H134R)-EYFP (courtesy of Dr. Michael Kaplitt) or AAV2-CaMKIIα-eNpHR3.0-EYFP (UNC Vector Core Services, Chapel Hill, NC, USA). This promoter has been described as selectively expressing in the glutamatergic neurons of the MSDB (Kaifosh et al. 2013). The injection was made at a 20° angle to the dorsal-ventral axis (0.40 mm anterior, 2.12 mm lateral at the 20° angle,

5.80 mm ventral to pia along the rotated axis) in order to target the medial septum without damaging the medially-located central sinus. After 5 minutes for equilibration, the injection was made over 7 minutes with the pipette remaining in place an additional 10 minutes post-injection to prevent reflux. Once withdrawn, the scalp was stapled closed, ketofen was administered as an analgesic (3-5 mg/kg), and the rats were quarantined for 72 hours before returning to normal housing.

The second survival surgery was performed two weeks later. A second craniectomy was made over the right dorsal hippocampus centered at 3.50 mm posterior and 2.80 mm lateral to bregma. The dura was incised with a sterile curved scalpel blade. In order to record from the dorsal hippocampus 16-channel microwire multielectrode arrays (Tucker Davis Technologies (TDT), Alachua, FL., USA; MEA) were constructed from sixteen 33 µm diameter tungsten electrodes with polyimide insulation (Figure 4I). The electrodes were arranged in two rows of eight electrodes with 1 mm between rows and 175 µm of space between the electrodes within a row. Ground and reference wires were separated on the array and routed through two stainless steel wires, which were affixed to separate skull screws during the implantation surgery. The two rows were cut to different lengths, 4.0 mm and 3.0 mm, to target and record simultaneously from the hippocampal CA3 and CA1 regions, respectively, enabling multiunit and local field potential recording from the hippocampus distantly from the optical stimulation site in the medial septum. The array was positioned at a 50° angle to midline, with the posterior end swung laterally, to match the positioning of the hippocampal pyramidal cell layers pyramidal cell layers (Rolston et al. 2010). The MEA was lowered while simultaneously recording single unit and local field potential (LFP) activity to attain the ideal positioning

(Rolston et al. 2009). When the electrophysiologic recordings stabilized and the CA1 and CA3 layers were identified, the original injection craniectomy was reopened, and a calibrated optical fiber ferrule (Figure 4E, H) was implanted at a 20° angle to the dorsal-ventral axis (0.40 mm anterior, 2.12 mm lateral in the rotated axis). Stimulation was performed as the ferrule was implanted, with the resulting recordings immediately analyzed spectrographically. Descent was halted when a strong stimulus-response signal was observed in the spectrogram, or when the optical ferrule reached a maximum depth of 5.50 mm from pia along the rotated axis.

Once the electrodes and ferrules were in place, the craniectomy was sealed with dental acrylic (OrthoJet; Lang Dental; Wheeling IL), securing the array and ferrule in place in their respective targets. The rats were administered ketofen (3-5 mg/kg) to minimize pain and returned to normal housing to recover for 3-5 days before optical stimulation and recording experiments were performed.

5.2.2 Optical stimulation and electrophysiologic recordings

Using our adapted NeuroRighter system (CHAPTER III), electrophysiologic recordings were sampled at 25 kHz with a 1-9,000 Hz bandwidth. LFPs were isolated online with a 1-500 Hz 1-pole Butterworth band-pass filter and downsampled to 2000 Hz. Action potentials were isolated online (Newman et al. 2013) and sorted using spike-sorting Wave_clus scripts and superparamagnetic clustering (Quiroga et al. 2004).

To stimulate awake and behaving animals, calibrated ferrules were connected via armored patch fiber cables (200 μm diameter, 0.67 NA, Plexon) to the NeuroRighter platform. ChR2 animals were stimulated with a 465 nm blue LED module. Square-wave stimulation pulses varied between 10, 30, and 50 mW/mm^2; 7, 11 (theta), 17, 23, 35

(beta), and 42 (gamma) Hz; and 2, 5, and 10 ms pulse widths. eNpHR3.0 animals were inhibited with a 620 nm orange LED module. Square-wave stimulation pulses varied between 10, 30, 50, 70, and 90 mW/mm^2; 7, 11 (theta), 17, 23, 35 (beta), and 42 (gamma) Hz; and 2, 5, and 10, 20, and 50 ms pulse widths. Continuous stimulation at 50, 70, and 90 mW/mm^2 was also performed. The experimental protocol consisted of repeated one minute recordings of 20 seconds of pre-stimulation background, 20 seconds of stimulation, and a subsequent 20 seconds of additional post-stimulation background. Stimulation protocols were performed in random order and repeated several times over multiple recording sessions. This setup was able to stimulate and record LFP and single-unit responses from awake and behaving animals uninterrupted for several hours and over several days. Subjects were introduced into an open-field environment for the duration of the experiments. Data were recorded intraoperatively and for up to four weeks postoperatively.

5.2.3 Data analysis

We isolated recording days where we simultaneously recorded CA1 and CA3 single units, and selected those contacts with the highest amplitude and best-looking single units for further analysis. Power spectra, spectrograms, coherence, and coherograms were computed from the LFP on these channels using the Chronux suite of analysis tools and multitaper analysis (Bokil et al. 2010). For spectrum and coherence calculations, T=1, W=5 with 9 Slepian tapers. A Jackknife approach was used to calculate 95% confidence intervals. For spectrogram and coherogram analysis a moving window size of 4s was stepped in 0.5s increments, T=1, W=4 and 7 Slepian tapers. Note that these parameters sacrifice temporal specificity to gain greater resolution in frequency. As a result, edge

transitions in spectrograms and coherograms will be blurred into the pre and post-stimulation epochs. Mean autocorrelation and cross-correlation between CA1 and CA3 were performed to assess alterations in theta phase during the stimulation and non-stimulation epochs, with 95% confidence intervals calculated and presented alongside the mean.

5.2.4 Histology and Immunohistochemistry

Histology was performed after experimentation to verify microelectrode recording locations and light-sensitive ion channel expression. Rats were deeply anesthetized with an overdose of Euthasol (5ml/kg, Virbac, Fort Worth, TX, U.S.A.) injected intraperitoneally. They were then transcardially perfused with 0.9% saline followed by 4% paraformaldehyde in 0.1M phosphate buffer at pH 7.2. The heads, still containing the electrodes and ferrules, were then separated and post-fixed at 4°C overnight. The next day the brains were dissected out, removed, and cryoprotected with 30% sucrose at 4°C. Frozen transverse (horizontal) sections were made of 50 μm thickness on a sliding microtome and collected in 0.1M PBS.

To identify the neurochemical identity of the transfected neurons, we performed immunofluorescence labelling for vesicular glutamate transporter 1 (vGLUT1), choline acetyltransferase (ChAT), and glutamic acid decarboxylase 67 (GAD67). Free-floating sections were rinsed in PBS, blocked in either 4% normal donkey serum (NDS, for ChAT) or 4% normal goat serum (NGS, for GAD/vGLUT1), and 0.1% Triton-X100 for 30 min and rinsed in PBS. After PBS rinses, sections were incubated overnight at 4°C in either goat anti-ChAT (1:100, Millipore) in PBS containing 1% NDS, mouse anti-GAD (1:1000, Millipore) in PBS containing 1% NGS, or mouse anti-vGLUT1 (1:1000,

Millipore) in PBS containing 1% NGS. Sections were rinsed in PBS and incubated in Alexa 488-conjugated donkey anti-goat (1:1000, Life Technologies) for ChAT or Alexa 488-conjugated goat anti-mouse (1:1000, Life Technologies) for GAD and vGLUT1 in 1% NDS (ChAT) or 1% NGS (GAD, vGLUT1) for 1 hour. All sections were additionally counterstained by incubation with 4'6-diamidino-2-phenylindole (DAPI) which labelled cell nuclei. Sections were rinsed in PBS and mounted on glass slides with Fluoromount-G mounting medium (Southern Biotech) for fluorescence microscopy. Sections were imaged in the NIS-Elements software (Nikon Instruments, Inc., Melville, NY, USA) using a Nikon DS-Fil color digital camera on a Nikon E400 microscope equipped with TRITC, FITC, and DAPI fluorescence cubes.

5.3. RESULTS

5.3.1 Histologic verification of channel expression

Injection of AAV2-CaMKIIα based viral vectors produced robust expression in the medial septum (Figure 23), with expression limited to the medial septal nucleus (Figure 23A). Horizontal sections revealed the axonal projections leaving the medial septum (Figure 23B). AAV2-CaMKIIα-eNPHR3.0 expression is not shown because those animals have yet to be sacrificed and processed histologically.
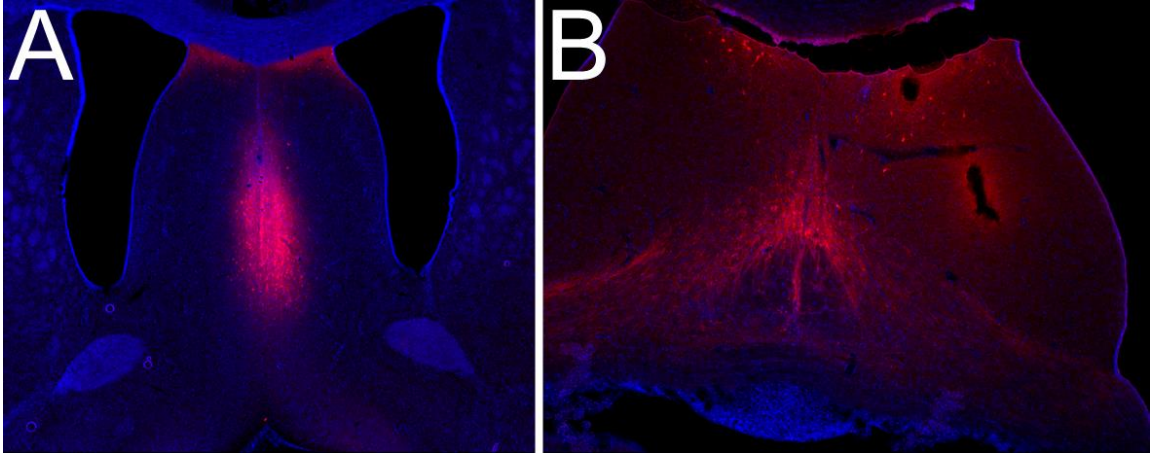
Figure 23: Robust expression of ChR2-mCherrry in the medial septum.
AAV2-CaMKIIα-ChR2-mCherry injection produced robust ChR2-EYFP expression into the medial septum **(red)**. Coronal slices **(A)** demonstrate the localization to the medial septum, while individual neurons and projections to the hippocampus were seen in horizontal slices **(B)**. Blue is DAPI nuclei stain.

To confirm selective expression of the glutamatergic neurons of the medial septum, we performed immunofluorescence labeling for choline acetyltransferase (ChAT, Figure 24A), vesicular glutamate transporter 1 (vGLUT1, Figure 24B), and glutamic acid decarboxylase 67 (GAD67, Figure 24C). Coexpression of CaMKIIα-ChR2-mcherry puncta with identified cholinergic and GABAergic neurons was not observed. vGlut1 glutamatergic neurons, however, did colocalize with CaMKIIα-ChR2-mCherry puncta in expressing neurons.
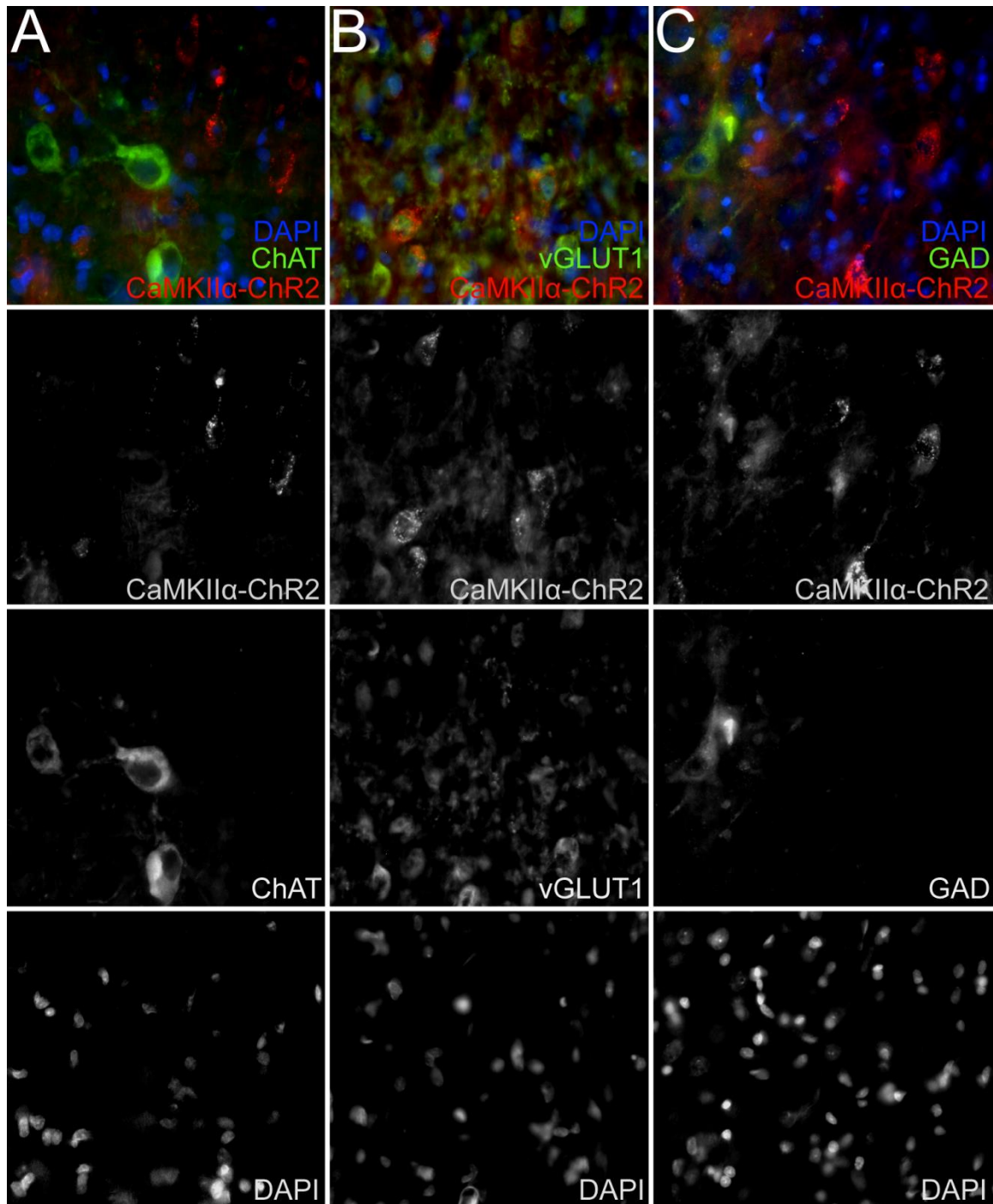
Figure 24: CaMKIIα-ChR2 selectively expressed in glutamatergic neurons of the medial septum.
CaMKIIα-ChR2 expressing neurons **(red puncta)** failed to colocalize with immunolabelled ChAT **(A, green)** or GAD **(C, green)** neurons. However, substantial colocalization was seen with the immunolabelled vGLUT1 neurons **(B, green)**, suggesting ChR2 was selectively expressed in the glutamatergic cell population in the medial septum. DAPI nuclei stain in blue.

5.3.2 Rhythmic excitation of glutamatergic MSDB neurons

5.3.2.1 Evoked LFP response waveforms

To address the hypothesis that glutamatergic MSDB neurons can modulate hippocampal oscillatory activity, we selectively excited this population with hChR2(H134R) in pulse trains of varying width, amplitude, and frequency and examined the resulting hippocampal LFP response. Stimulation generated evoked potentials in both the CA1 and CA3 layers. Unlike GABAergic stimulation (Figure 14: CA3 LFP response as a function of stimulus intensity, frequency, and pulse width.Figure 14), these evoked potentials were not readily visible in the local field potential (Figure 25A). Averaging the response from each pulse across all parameters (peristimulus average) indicated that the evoked potential waveform was highly dependent upon stimulation parameters (Figure 25B). Light intensity was the most important influence, as low intensity stimulation failed to produce a recognizable response, and the amplitude of the response was reduced compared to the GABAergic response (Figure 14). At high intensities, stimulation produced isolated evoked potential waveforms at up to 35 Hz that also increased in amplitude with pulse width. At low gamma frequencies (42 Hz), however, the evoked potentials were sinusoid.
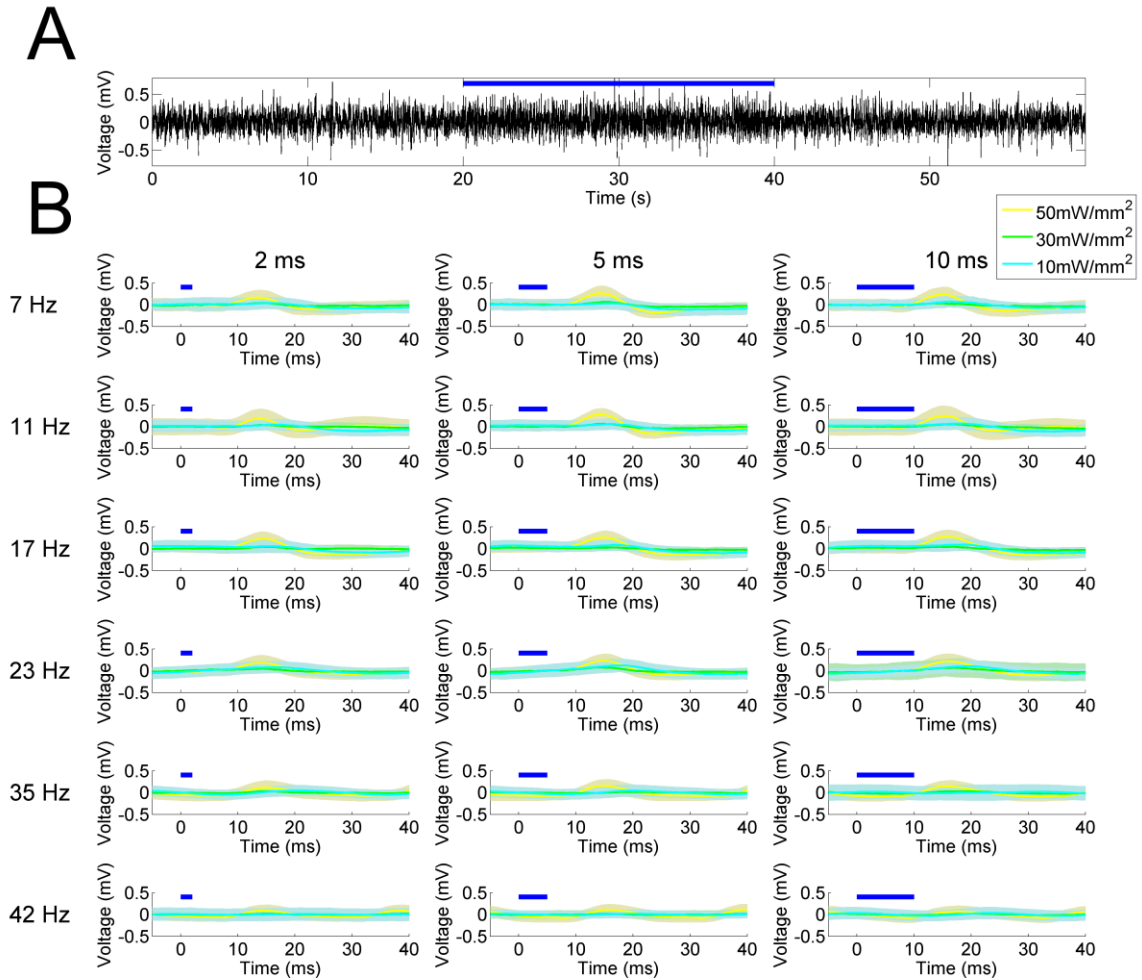
Figure 25: CA3 LFP response as a function of stimulus intensity, frequency, and pulse width.
Stimulation of the glutamatergic neurons of the medial septum generated evoked potentials in the hippocampal LFP. (**A**) An example CA3 LFP recording during 50 mW/mm^2, 7 Hz, 10ms excitation (blue bar). (**B**) Calculating the peristimulus average (thick line is mean, shaded area is standard deviation) response in CA3 across each of the stimulation protocols demonstrated that the evoked potential waveform was highly dependent on the stimulation parameters. Intensity was most important, with low-intensity stimulation barely influencing LFP. Low-frequency stimulation (7-35 Hz) produced defined waveform peaks, particularly at long pulse-widths. At higher frequencies (42 Hz), however, the response was largely sinusoidal at sufficiently high intensity.

5.3.2.2 Frequency-specific responses to excitation in both layers

Spectral analysis was performed to evaluate the impact of stimulation on hippocampal oscillatory activity. We observed a statistically significant stimulus-frequency specific increase in power during the stimulation epoch relative to the pre-stimulation epoch, as well as harmonics of that stimulation frequency, in both of the CA1 and CA3 hippocampal layers (Figure 26). We also noted significant ($p<0.05$) reduction in theta power at frequencies other than the stimulation frequency. CA1-CA3 coherence demonstrated increased coherence at stimulation harmonics as well, but not at the stimulation frequency, similarly to that seen with MSDB GABAergic stimulation (Figure 15). This may also be a result of cross-subject grouping.

Stimulating the glutamatergic neurons at other frequencies also produced a significant ($p<0.05$) stimulus-frequency specific response in the hippocampal LFP (Figure 27), directly transmitting the stimulation pattern to both layers of the hippocampus. With 35 Hz stimulation a slight decrease in power within theta frequencies was also noted, alongside increased CA1-CA3 coherence.
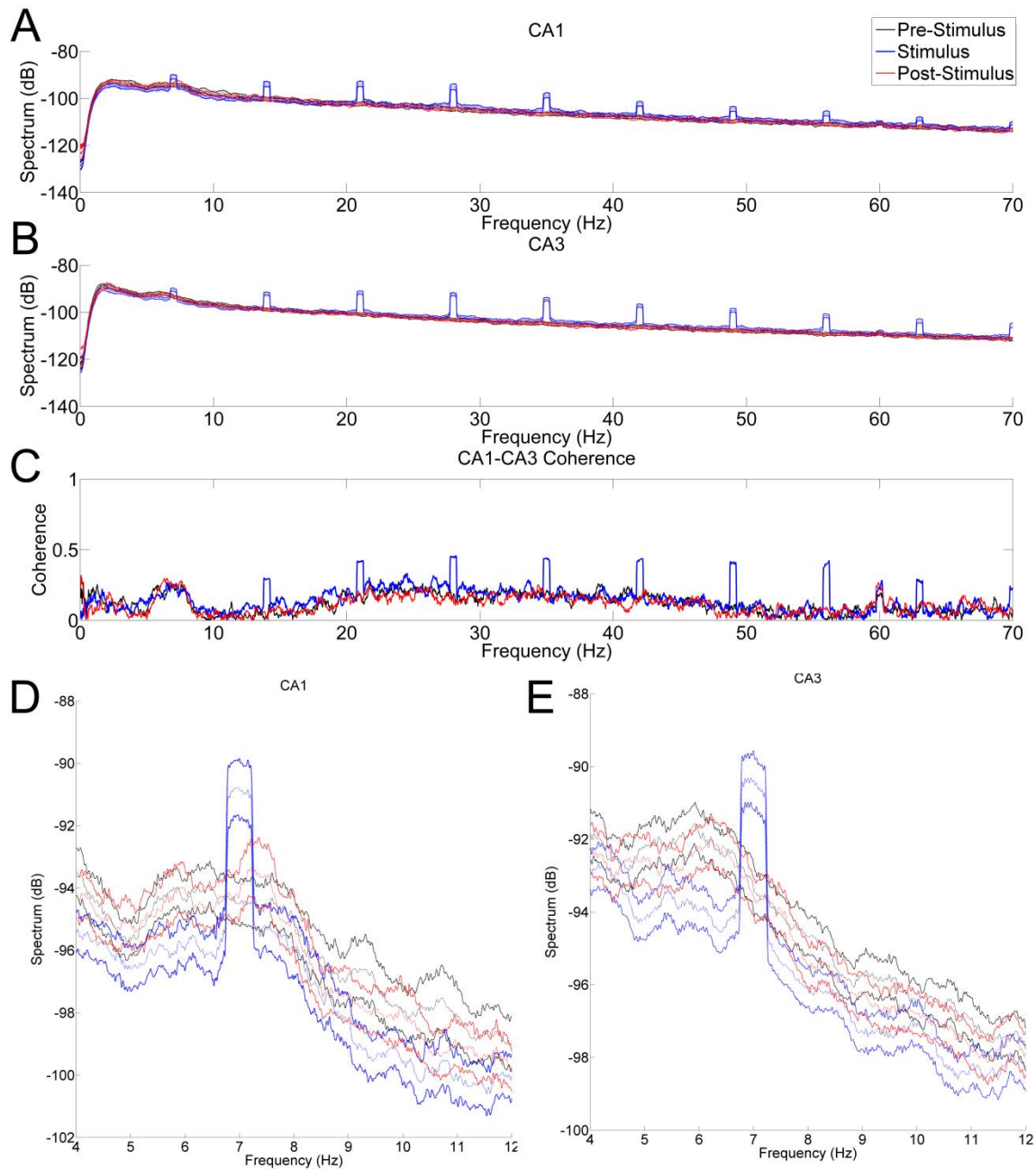
Figure 26: CA1 and CA3 demonstrate stimulation theta frequency-specific increases in power with theta stimulation.

Stimulation was performed at 50 mW/mm^2, 7 Hz, and 10 ms, and the pre-stimulus **(black)**, post-stimulus **(red)** and stimulus **(blue)** epochs across all trials were separated and spectrally examined for changes in power. 95% confidence intervals were calculated for each epoch using a Jackknife approach (dashed lines). Statistically significant (p<0.05) increases in power at the stimulus frequency were demonstrated in both the CA1 **(A)** and CA3 **(B)** layers, alongside stimulation harmonics. Theta power at frequencies other than 7 Hz was slightly, yet significantly, reduced during stimulation **(D,E)**. No significant difference in power was noted between the pre- and post-stimulation epochs. CA1-CA3 coherence at the stimulation frequency **(C)** demonstrated increased coherence at stimulation harmonics.
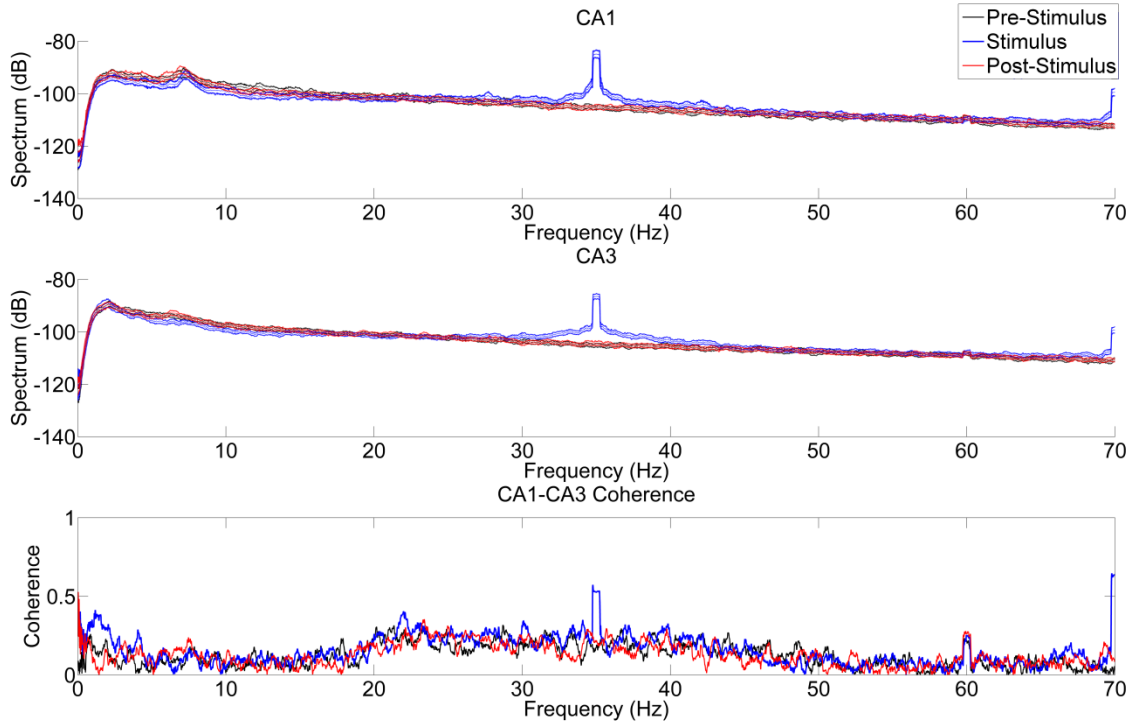
Figure 27: Stimulus-frequency specific increases in spectral power with 35 Hz stimulation. Stimulating with 50 mW/mm^2, 35 Hz, 10 ms pulses also significantly (p<0.05) increased power at the stimulus frequency, as well as significantly reduced hippocampal theta power in both layers, although it affected CA3 to a greater extent than CA1. Unlike 7 Hz glutamatergic stimulation **(Figure 25)**, 35 Hz resulted in a large increase in CA1-CA3 coherence, and also increased coherence at delta frequencies.

Spectrograms were calculated to examine the temporal specificity and consistency of the response to stimulation (Figure 28, Figure 29). Responses were temporally locked to stimulation onset and offset (blue bar) and were consistently represented at the stimulation frequency. Reductions in theta power were noted in both cases, with CA1 theta more influenced by 7 Hz stimulation (Figure 28 A) and CA3 by 35 Hz stimulation (Figure 29 B). A statistically significant (p<0.05) increase in CA1-CA3 coherence, along with a consistent phase relationship, was noted with 35 Hz stimulation (Figure 29 C, D) but not 7 Hz stimulation (Figure 28 C, D).
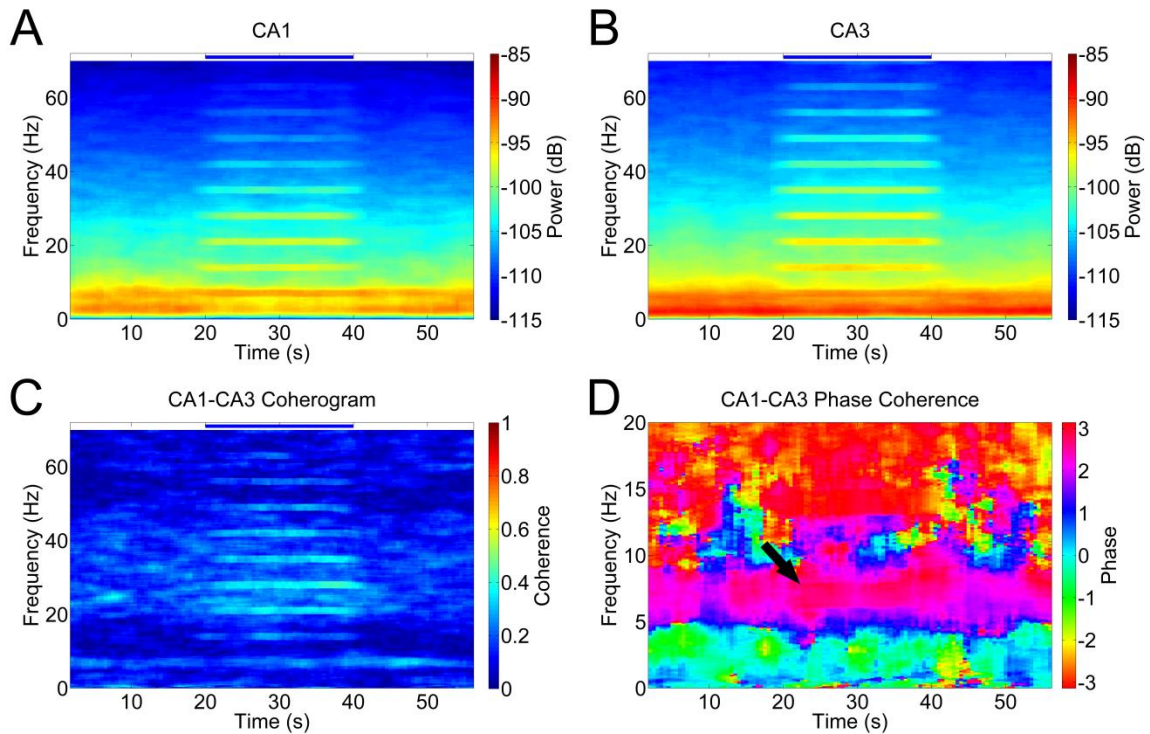
Figure 28: Temporal specificity of the spectrographic and coherence response to 7 Hz stimulation.

Stimulation of MSDB glutamatergic neurons with 50 mW/mm^2, 7 Hz, 10 ms pulses **(blue bar)** consistently increased hippocampal power at the stimulus frequency in both CA1 **(A)** and CA3 **(B)**, alongside decreased power <7 Hz in CA1. While there was a non-significant ($p>0.05$) increase in coherence amplitude **(C)** at the stimulation frequency, examination of the angle of the coherence **(D, black arrow at stimulus frequency)** suggests that the responses in CA1 and CA3 may have maintained a particular phase relationship during stimulation. Note no lasting effects from stimulation into the post-stimulation epoch. Blurring of the edges is due to the wide moving window used in spectral analysis (4s), necessary to properly resolve the frequency bandwidth (1 Hz).
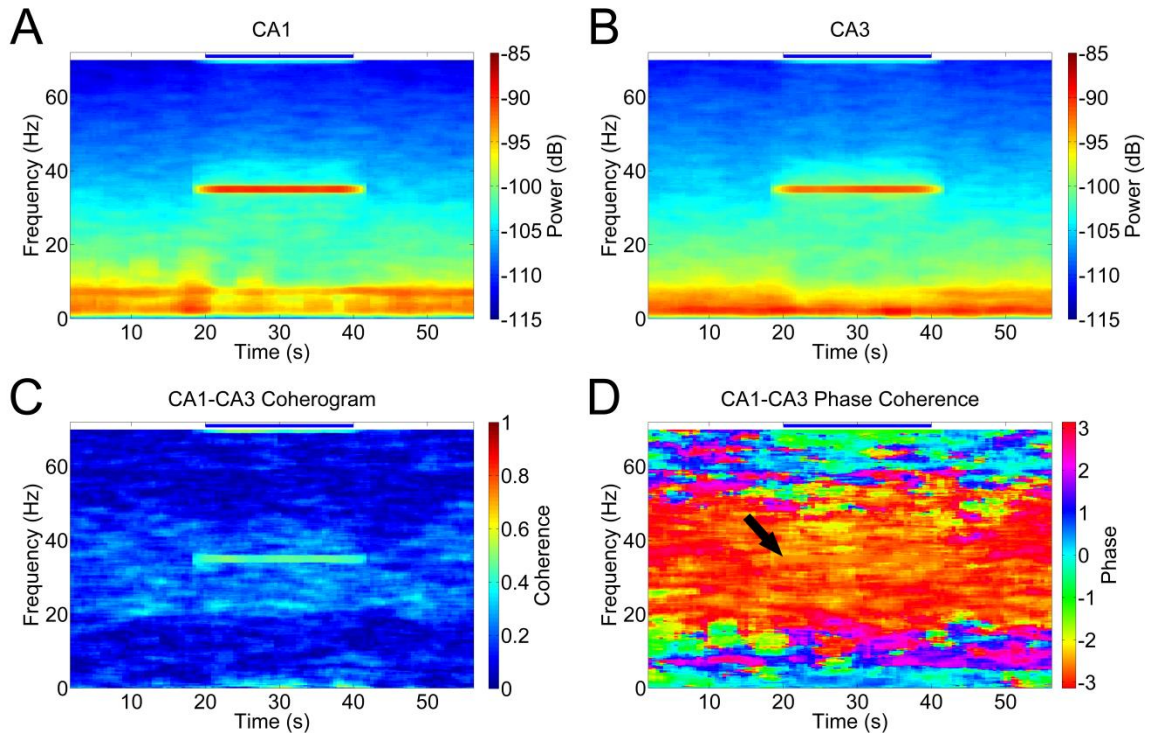
Figure 29: Temporal specificity of the spectrographic and coherence response to 35 Hz stimulation.
Stimulation of MSDB glutamatergic neurons with 50 mW/mm^2, 35 Hz, 10 ms pulses **(blue bar)** also consistently and robustly increased hippocampal power at the stimulus frequency in both CA1 **(A)** and CA3 **(B)**, as well as decreased theta power. Notice that this was more pronounced in CA3 in higher frequency theta. In contrast to 7 Hz stimulation **(Figure 27)**, there was a significant ($p<0.05$) increase in coherence amplitude **(C)** at the stimulation frequency. This was accompanied by a consistent phase relationship **(D, black arrow)**.

5.3.2.3 Phase-locking to the theta stimulus pattern
To explore the phase relationship within the hippocampal layers, as well as between them, we evaluated the autocorrelation of the CA1 and CA3 signals, respectively, in response to theta (7 Hz) stimulation, as well as the cross-correlation between the layers (Figure 30). If the induced oscillations were locked in phase and amplitude throughout the stimulation epoch (Figure 30, blue), then we would observe peaks in the correlation at stimulation lag times. Both CA1 and CA3 signals demonstrated significantly ($p<0.05$) correlated peaks at lags corresponding to the stimulus frequency (Figure 30). These peaks

were consistent well into the lags, indicating that the hippocampal oscillation remained in phase as a result of the stimulus. The CA1-CA3 correlation was not significant from pre-stimulus, but did suggest a negative correlation between CA1 and CA3 (out of phase) with each stimulus. This is in contrast to what was observed with GABAergic stimulation (Figure 19Figure 22), where there was a slight phase difference suggesting CA1 lagged CA3.
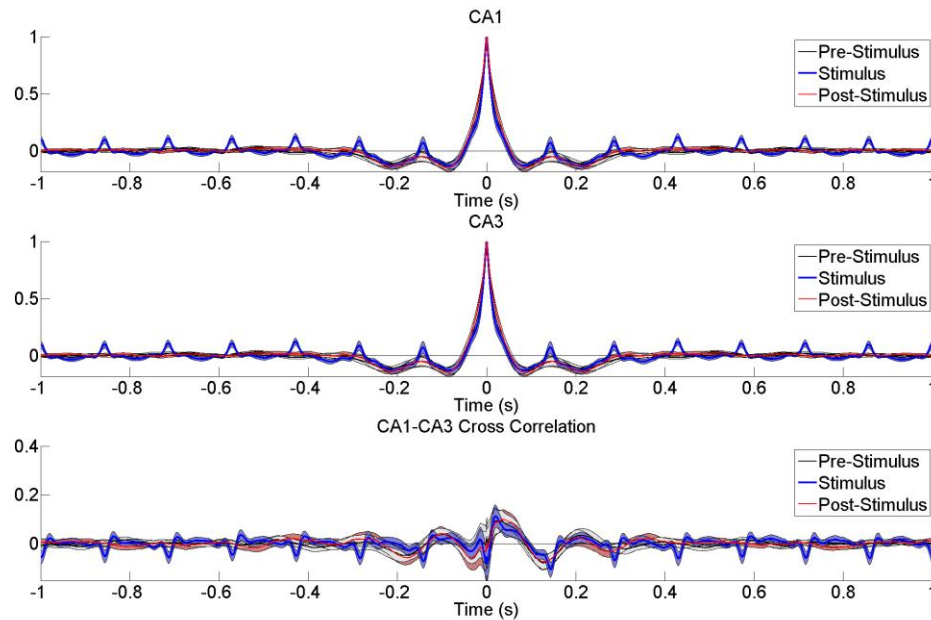
Figure 30: Auto and cross-correlation properties indicate phase-locking to stimulus pulses. Autocorrelation of the CA1 and CA3 LFP-signal demonstrated a consistently significant ($p<0.05$) increase in correlation at the stimulus frequency – as compared to the pre and post-stimulus epochs, suggesting that the LFP response was phase-locked to the stimulus pattern. Cross-correlation between CA1 and CA3 was not significant ($p>0.05$), but suggested CA1 and CA3 were anticorrelated and out of phase with each stimulus. Dark line is the mean. Shaded area is 95% confidence interval.

5.3.3 Inhibition of MSDB glutamatergic neurons

Whereas the preceding experiments explored the *capability* of the MSDB glutamatergic neurons to modulate and drive hippocampal oscillatory activity, the following work utilizes optogenetic inhibition to demonstrate the *necessity* of MSDB glutamatergic neurons for hippocampal theta oscillations.

5.3.3.1 Rhythmic 35 Hz inhibition of MSDB glutamatergic neurons did not alter hippocampal LFP

Rhythmic 90 mW/mm^2, 35 Hz, 10 ms inhibition of MSDB glutamatergic neurons failed to generate statistically meaningful responses in either the CA1 or CA3 hippocampal layers (Figure 31), and did not affect coherence between the two layers.
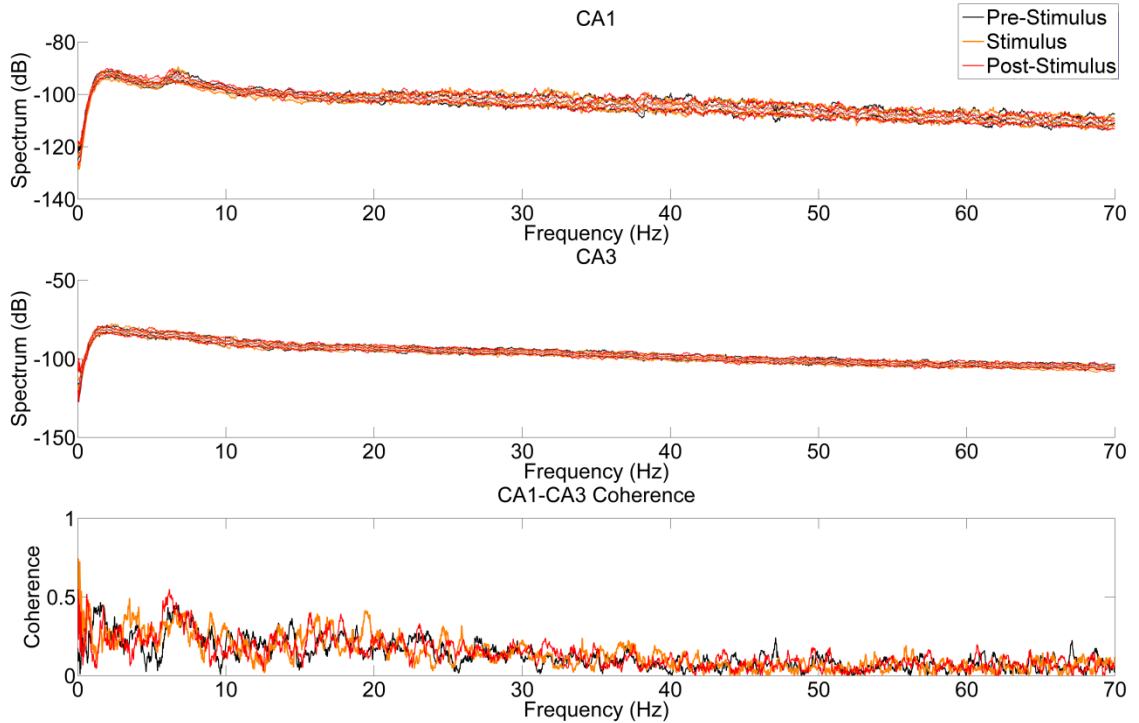
Figure 31: Rhythmic inhibition at 35 Hz does not alter hippocampal spectral power.
Inhibitory stimulation was performed at 90 mW/mm^2, 35 Hz, and 10 ms, and the pre-stimulus **(black)**, post-stimulus **(red)** and inhibitory stimulus **(orange)** epochs across all trials were separated and spectrally examined for changes in spectral power. 95% confidence intervals were calculated for each epoch using a Jackknife approach **(dashed lines)**. No statistically significant changes in power or coherence were noted at any observed frequency.

5.3.3.2 Constant 90 mW/mm^2 inhibition of MSDB glutamatergic neurons does not alter hippocampal LFP power, but may impact theta-phase maintenance.

To examine the necessity of MSDB glutamatergic neurons for awake hippocampal theta power, we performed constant 90 mW/mm^2 inhibition for 20 seconds. Inhibition in this fashion did not alter hippocampal spectral power at any frequency (Figure 32A, B), nor coherence between CA1 and CA3 (Figure 32C, D).
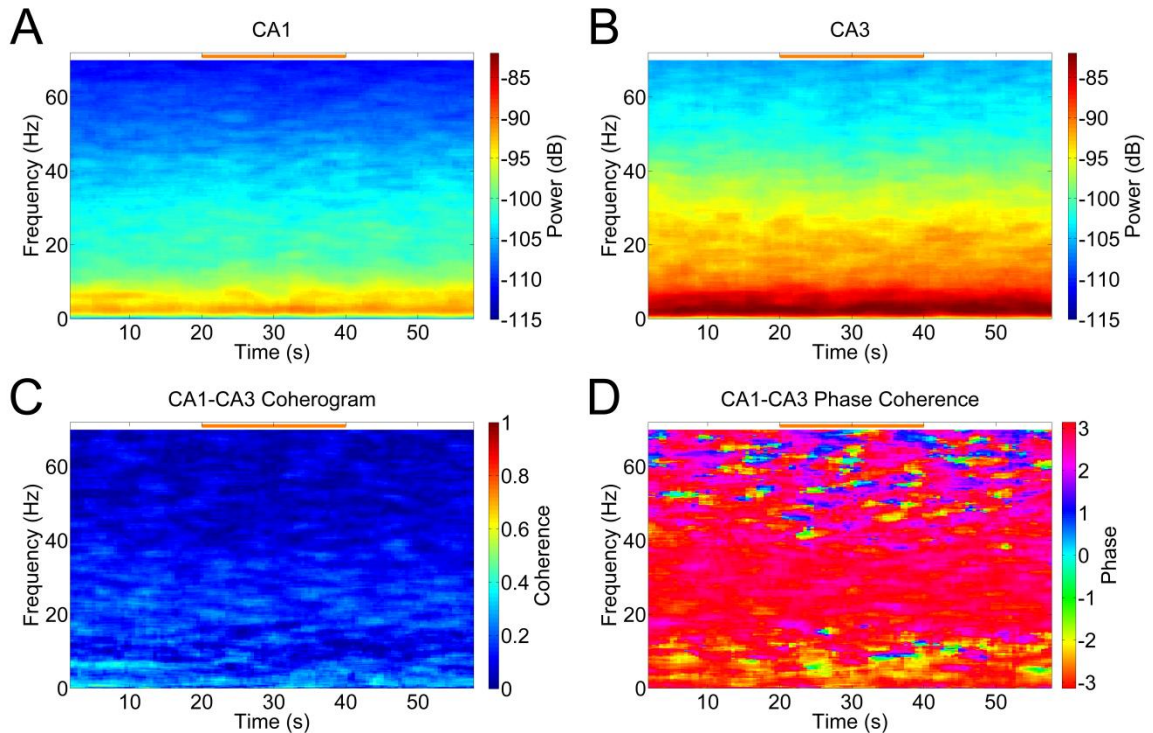
Figure 32: Constant inhibition of MSDB glutamatergic neurons does not alter hippocampal oscillatory power.
Constant inhibition of the MSDB GABAergic neurons for 20 seconds at 90 mW/mm^2 (**orange bar**) failed to significantly alter hippocampal power at any frequency in either CA1 (**A**) and CA3 (**B**) from the pre-stimulus epoch. Similarly, no alterations between the pre-stimulus and post-stimulus epochs were seen in the coherogram (**C**) or the phase coherence (**D**).

Intriguingly, however, constant 90 mW/mm^2 inhibition of the MSDB glutamatergic neurons did impact theta phase relationships as assessed by auto and cross-correlation (Figure 33). Constant inhibition significantly ($p<0.05$) reduced the maintenance of a consistent phase within CA1 and CA3, and between the layers. The initial lag (Figure 33, blue arrow), which corresponds to the most proximal cycle, only trended towards significance ($p>0.05$), but successive oscillatory cycles (Figure 33, green arrow) demonstrated a more pronounced and statistically significant difference between the pre-stimulus and stimulus epochs. This indicates that during inhibition theta was not

maintaining the same phase relationship with successive cycles as it had during the pre-stimulus epoch. During constant inhibition of the glutamatergic neurons of the medial septum, theta oscillatory phase was not maintained, in contrast to GABAergic (Figure 22) and cholinergic (Figure 44) inhibition. This effect continued into the post-stimulus epoch as well (red). While it is unclear why this particular effect persisted beyond the stimulus epoch, it may be a result of a more profound disturbance in network synchronicity. The MSDB and hippocampal network, in response to glutamatergic inhibition, may require more time to reestablish the theta phase relationship.
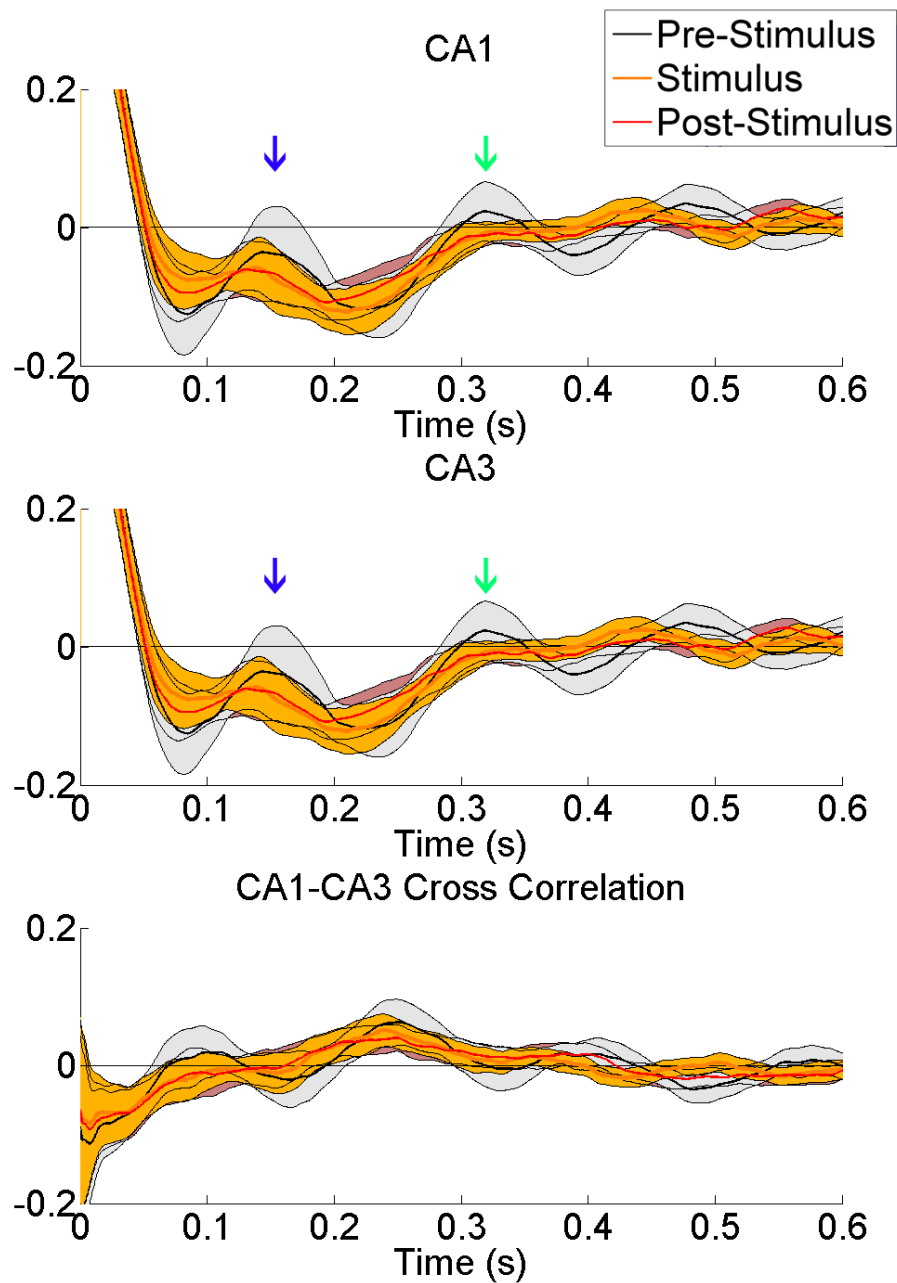
Figure 33: Constant inhibition may alter consistency of hippocampal phase and phase synchrony between CA1 and CA3.
A non-significant trend (p>0.05) towards a less-correlated signal at the first theta lag (**blue arrow**) was noted in the autocorrelation. The differences became significant (p<0.05) at successive lags **(green arrow)**, however, indicating that hippocampal theta phase was not maintained as during the pre-stimulus epoch **(black trace)**. CA1-CA3 correlation, and phase maintenance, was similarly altered.

5.4. DISCUSSION

Rhythmic optogenetic stimulation of glutamatergic MSDB neurons directly transmitted the stimulus frequency pattern to both the CA1 and CA3 hippocampal layers, supporting anatomical evidence that this population directly innervates both layers (Colom et al. 2005). It should be noted that this response could have been routed through the MSDB GABAergic population (CHAPTER IV) via local circuitry, which in turn would drive the hippocampus. However, the pulse-response times between GABAergic and glutamatergic stimulation – despite the difference in amplitude – possessed nearly identical delays. Were the path truly bisynaptic – as opposed to the monosynaptic GABAergic disinhibitory circuit – one would expect a greater delay in transmission, as well as greater variability in response time. In addition, cross-correlation analysis between CA1 and CA3 in both cases indicated GABAergic stimulation produced a lead-lag response in the layers, whereas glutamatergic stimulation produced an anticorrelated (opposing phase) relationship. This suggests that the results observed are acting, at least in part, through direct projections to the hippocampus. However we cannot rule out local MSDB circuitry effects without proper blockade of glutamatergic synaptic input.

Our results also suggest that while glutamatergic MSDB neurons were not necessary for theta power – which was unaffected by inhibition – they do appear to be play a role in maintenance of theta phase. During the stimulus epoch, autocorrelation analysis indicated that theta phase was not as consistent on successive cycles, as compared to the pre-stimulus epoch, which maintained the same theta phase dynamics seen in other interventions (Figure 22).

This finding supports the hypothesis that glutamatergic MSDB neurons are pacing hippocampal theta activity, in that they are coordinating theta so that consistent phase

relationships are maintained. The glutamatergic neurons are well positioned to do so, synapsing onto the local GABAergic and cholinergic neurons of the medial septum (Manseau et al. 2005), as well as in the hippocampus (Colom et al. 2005). More rigorous experimentation and analysis is necessary, however, to confirm this effect, as well as to explore why this particular effect continued into the post-stimulus epoch. Specific examination of this effect during particular behavioral paradigms (locomotion, Morris water maze) will provide greater insight into the functional consequences of manipulating this neural population.

These results also lends support to the growing evidence that MSDB theta is a combinatorial effect (Yoder and Pang 2005). Local and projecting glutamatergic input in the septohippocampal axis may modulate and synchronize extant theta oscillations generated through the MSDB, entorhinal, or intrinsic hippocampal circuits – and may be just one of several methods by which this can be accomplished.

5.5. CONCLUSIONS

Medial septal glutamatergic neurons, when synchronously activated optogenetically, produce stimulation-frequency specific activity in both CA1 and CA3 local field potential, supporting anatomic evidence that these neurons innervate both layers of the hippocampus. Glutamatergic neurons were capable of modulating theta oscillations – as well as other frequencies. Intriguingly, inhibition of this population resulted in a failure of the hippocampus to maintain a consistent theta phase as compared to the pre-stimulus epoch. This effect maintained during the post-stimulus epoch, and is potentially a result of temporary network desynchronization. This lends support to the hypothesis that

glutamatergic neurons of the medial septum serve to coordinate and pace hippocampal theta oscillations.

CHAPTER VI

OPTOGENETIC MODULATION OF MEDIAL SEPTAL CHOLINERGIC NEURONS AND THE IMPACT ON HIPPOCAMPAL ACTIVITY IN AWAKE AND BEHAVING RATS

6.1. INTRODUCTION

Substantial evidence implicates the medial septum-diagonal band complex (MSDB) in the generation and maintenance of the theta rhythm in the hippocampus (Stewart and Fox 1990; Tóth et al. 1997; Buzsáki 2002; Huh et al. 2010). Three genetically-distinct neuron subpopulations have been identified within the MSDB – GABAergic, glutamatergic, and cholinergic neurons – all of which project to the hippocampus and may play a role in modulating hippocampal activity and theta oscillations (Freund and Antal 1988; Sotty et al. 2003; Yoder and Pang 2005; Huh et al. 2010; Bell et al. 2013). Cholinergic MSDB neurons have long been recognized as an important input to the hippocampus (Lewis et al. 1967; Frotscher and Léránth 1985), and implicated as a mediator of theta oscillations (Konopacki et al. 1987).

Cholinergic afferents from the medial septum contact both pyramidal and inhibitory neurons of the hippocampus (Lewis et al. 1967; Frotscher and Léránth 1985), and early hypotheses reasoned that they were providing excitatory cholinergic input to

hippocampal interneurons in order to pace the theta rhythm (Stewart and Fox 1990). However, this hypothesis soon lost favor, as evidence for the GABAergic population emerged (Tóth et al. 1997) and excitatory input from the septum was not observed (Stewart and Fox 1990). Yet the presence of induced theta activity in hippocampal slices via muscarinic agonists suggested that cholinergic inputs still played an important role in this oscillatory rhythm (Konopacki et al. 1987). It has been argued that the theta oscillations generated in these reduced preparations did not reflect naturally occurring theta (Stewart and Fox 1990; Williams and Kauer 1997). But muscarinic agonists delivered to the medial septum in awake animals are able to induce the theta rhythm, alongside behaviors associated with theta (Monmaur and Breton 1991).

Whereas cholinergic lesions in urethane anesthetized rats abolished theta power, lesions in behaving unanesthetized animals of the cholinergic neurons only attenuated it (Yoder and Pang 2005). Yoder et al. suggested that the medial septum was consequently only important for atropine-sensitive theta (theta II), a component of theta in the awake and locomoting animal. Further experiments demonstrated that nicotine recruited the newly-discovered MSDB glutamatergic neurons to excite MSDB GABAergic neurons (Wu et al. 2003). Cholinergic input might then serve as a sort of gain control – providing the necessary background for theta to occur in the septohippocampal axis, but not directly pacing its activity. This was also in agreement with electrophysiologic investigations in anesthetized and unanesthetized rats of the cholinergic neurons of the medial septum, which tended to fire too slowly (~0.3-0.5 Hz) to drive theta oscillations directly (Simon et al. 2006), although other work in slice preparations suggested that they may fire in the appropriate range (Sotty et al. 2003).

Recently, an elegant series of experiments performed by Karen and Andrew Bell et al. used optogenetic methods to control medial septal acetylcholine release in brain slices and dissect the muscarinic and nicotinic inputs to the hippocampal CA1 inhibitory interneurons (Bell et al. 2011; Bell et al. 2013). They demonstrated that nicotinic input to these interneurons produced EPSPs mediated by the activation of α4β2* nicotinic receptors (Bell et al. 2011). These EPSPs had slow kinetics of hundreds of milliseconds in duration, and were mostly subthreshold for activation, making them favorable for integration with other synaptic inputs.

Muscarinic inputs to CA1 interneurons, however, produced a more heterogeneous response – depolarizing, hyperpolarizing, and biphasic (Bell et al. 2013). The authors determined that hyperpolarization was mediated by M_4 receptors, and required less cholinergic presynaptic input as compared to depolarization. Depolarizing responses – correlated with higher levels of induced presynaptic activity – were not mediated by M_1, M_4, or M_5 receptors, and the role of M_2 and M_3 receptors was unclear as the necessary highly selective drugs are unavailable. Interestingly, while stimulation alone failed to produce action potentials in this population, stimulation during synaptically-induced depolarization was able to do so. Biphasic interneurons could furthermore be entrained to fire bursts of action potentials with rhythmic flashes of light. This extensive work suggests that cholinergic input from the medial septum to the hippocampus can place the inhibitory interneurons in a primed state of subthreshold activation. As cholinergic input also activates the glutamatergic population of the medial septum, which in turn activates the GABAergic disinhibitory network (Wu et al. 2003), cholinergic activity in the MSDB may not only prime the hippocampus for rhythmic input, but may also activate the

pacemaking and driving functions of the medial septum. Thus cholinergic activity would generate excited and inhibited states, with low activity hyperpolarizing hippocampal inhibitory interneurons (Bell et al. 2013) thus preventing theta oscillations, and high activity supporting it.

In order to test the hypothesis that MSDB cholinergic neurons modulate hippocampal theta activity, we used optogenetics to selectively excite and inhibit this population in awake and behaving animals. Optogenetic tools provide a powerful methods for genetically and temporally precise manipulation of complex heterogeneous nervous system circuitry (Aravanis et al. 2007; Carter et al. 2009; Gradinaru et al. 2009; Kravitz et al. 2010; Yizhar et al. 2011; Packer et al. 2012; Wykes et al. 2012; Paz et al. 2013). When combined with electrophysiological recordings, optogenetic control can provide unprecedented insight into neural connectivity and function (Bell et al. 2013), particularly in awake and behaving animals (Gradinaru et al. 2009).

6.2. METHODS

6.2.1 Surgeries

2-3 month old (250-300g) adult male ChAT-CRE Long-Evans rats (Witten et al. 2011) were bred from our transgenic rat colony (founder male courtesy of Dr. Karl Deisseroth). Six rats were used in the excitation group, and three rats were used in the inhibition group. No differences were seen between the animals, and so the recordings were grouped for all analyses. All animals were maintained within a 12/12 light/dark cycle vivarium with unlimited access to food and water. This work was conducted in accordance with Emory University's Institute for Animal Care and Use Committee.

Each subject underwent two surgical procedures. The first survival surgery introduced the viral vector to the medial septum and provided time for expression of the optogenetic channel. Rats were anesthetized with 1.5-4% inhaled isoflurane, and a craniectomy was made 0.40 mm anterior and 2.00 mm lateral to bregma on the right side of the skull. A pulled-glass pipette attached to a stereotactically mounted injector (Nanoject; Drummond Scientific Co., Broomall, PA, USA) was used to inject 1.8 µL of 10^{12} particles/mL double-floxed inverted opsin AAV5-EF1a-DIO-hChR2(H134R)-mCherry or AAV5-EF1a-DIO-eNpHR3.0-EYFP (UNC Vector Core Services, Chapel Hill, NC, USA.). This Cre-lox system has demonstrated effectiveness in selectively expressing in the cholinergic neurons of the medial septum (Witten et al. 2011). The injection was made at a 20° angle to the dorsal-ventral axis (0.40 mm anterior, 2.12 mm lateral at the 20° angle, 5.80 mm ventral to pia along the rotated axis) in order to target the medial septum without damaging the medially-located central sinus. After 5 minutes for equilibration, the injection was made over 7 minutes with the pipette remaining in place an additional 10 minutes post-injection to prevent reflux. Once withdrawn, the scalp was stapled closed, ketofen was administered as an analgesic (3-5 mg/kg), and the rats were quarantined for 72 hours before returning to normal housing.

The second survival surgery was performed two weeks later. A second craniectomy was made over the right dorsal hippocampus centered at 3.50 mm posterior and 2.80 mm lateral to bregma. The dura was incised with a sterile curved scalpel blade. In order to record from the dorsal hippocampus 16-channel microwire multielectrode arrays (Tucker Davis Technologies (TDT), Alachua, FL., USA; MEA) were constructed from sixteen 33 µm diameter tungsten electrodes with polyimide insulation (Figure 4I).

The electrodes were arranged in two rows of eight electrodes with 1 mm between rows and 175 μm of space between the electrodes within a row. Ground and reference wires were separated on the array and routed through two stainless steel wires, which were affixed to separate skull screws during the implantation surgery. The two rows were cut to different lengths, 4.0 mm and 3.0 mm, to target and record simultaneously from the hippocampal CA3 and CA1 regions, respectively, enabling multiunit and local field potential recording from the hippocampus distantly from the optical stimulation site in the medial septum. The array was positioned at a 50° angle to midline, with the posterior end swung laterally, to match the positioning of the hippocampal pyramidal cell layers pyramidal cell layers (Rolston et al. 2010). The MEA was lowered while simultaneously recording single unit and local field potential (LFP) activity to attain the ideal positioning (Rolston et al. 2009). When the electrophysiologic recordings stabilized and the CA1 and CA3 layers were identified, the original injection craniectomy was reopened, and a calibrated optical fiber ferrule (Figure 4E, H) was implanted at a 20° angle to the dorsal-ventral axis (0.40 mm anterior, 2.12 mm lateral in the rotated axis). Stimulation was performed as the ferrule was implanted, with the resulting recordings immediately analyzed spectrographically. Descent was halted when a strong stimulus-response signal was observed in the spectrogram, or when the optical ferrule reached a maximum depth of 5.50 mm from pia along the rotated axis.

Once the electrodes and ferrules were in place, the craniectomy was sealed with dental acrylic (OrthoJet; Lang Dental; Wheeling IL), securing the array and ferrule in place in their respective targets. The rats were administered ketofen (3-5 mg/kg) to

minimize pain and returned to normal housing to recover for 3-5 days before optical stimulation and recording experiments were performed.

6.2.2 Optical stimulation and electrophysiologic recordings

Using our adapted NeuroRighter system (CHAPTER III), electrophysiologic recordings were sampled at 25 kHz with a 1-9,000 Hz bandwidth. LFPs were isolated online with a 1-500 Hz 1-pole Butterworth band-pass filter and downsampled to 2000 Hz. Action potentials were isolated online (Newman et al. 2013) and sorted using spike-sorting Wave_clus scripts and superparamagnetic clustering (Quiroga et al. 2004).

To stimulate awake and behaving animals, calibrated ferrules were connected via armored patch fiber cables (200 µm diameter, 0.67 NA, Plexon) to the NeuroRighter platform. ChR2 animals were stimulated with a 465 nm blue LED module. Square-wave stimulation pulses varied between 10, 30, and 50 mW/mm^2; 7, 11 (theta), 17, 23, 35 (beta), and 42 (gamma) Hz; and 2, 5, and 10 ms pulse widths. eNpHR3.0 animals were inhibited with a 620 nm orange LED module. Square-wave stimulation pulses varied between 10, 30, 50, 70, and 90 mW/mm^2; 7, 11 (theta), 17, 23, 35 (beta), and 42 (gamma) Hz; and 2, 5, and 10, 20, and 50 ms pulse widths. Continuous stimulation at 50, 70, and 90 mW/mm^2 was also performed. The experimental protocol consisted of repeated one minute recordings of 20 seconds of pre-stimulation background, 20 seconds of stimulation, and a subsequent 20 seconds of additional post-stimulation background. Stimulation protocols were performed in random order and repeated several times over multiple recording sessions. This setup was able to stimulate and record LFP and single-unit responses from awake and behaving animals uninterrupted for several hours and over several days. Subjects were introduced into an open-field environment for the duration of

the experiments. Data were recorded intraoperatively and for up to four weeks postoperatively.

6.2.3 Data analysis

We isolated recording days where we simultaneously recorded CA1 and CA3 single units, and selected those contacts with the highest amplitude and best-looking single units for further analysis. Power spectra, spectrograms, coherence, and coherograms were computed from the LFP on these channels using the Chronux suite of analysis tools and multitaper analysis (Bokil et al. 2010). For spectrum and coherence calculations, T=1, W=5 with 9 Slepian tapers. A Jackknife approach was used to calculate 95% confidence intervals. For spectrogram and coherogram analysis a moving window size of 4s was stepped in 0.5s increments, T=1, W=4 and 7 Slepian tapers. Note that these parameters sacrifice temporal specificity to gain greater resolution in frequency. As a result, edge transitions in spectrograms and coherograms will be blurred into the pre and post-stimulation epochs. Mean autocorrelation and cross-correlation between CA1 and CA3 were performed to assess alterations in theta phase during the stimulation and non-stimulation epochs, with 95% confidence intervals calculated and presented alongside the mean.Single-unit firing rates were assessed using the Chronux locfit density command (Bokil et al. 2010). We used a rate density-estimation type family, and smoother with a nearest neighbor parameter of 0.2 (20% of the nearest data points were used). In the case of single recordings, histograms of the number of spikes detected in 1 second bins were used to provide an estimate of the firing rate.

6.2.4 Histology and immunohistochemistry

Histology was performed after experimentation to verify microelectrode recording locations and light-sensitive ion channel expression. Rats were deeply anesthetized with an overdose of Euthasol (5ml/kg, Virbac, Fort Worth, TX, U.S.A.) injected intraperitoneally. They were then transcardially perfused with 0.9% saline followed by 4% paraformaldehyde in 0.1M phosphate buffer at pH 7.2. The heads, still containing the electrodes and ferrules, were then separated and post-fixed at 4°C overnight. The next day the brains were dissected out, removed, and cryoprotected with 30% sucrose at 4°C. Frozen transverse (horizontal) sections were made of 50 µm thickness on a sliding microtome and collected in 0.1M PBS.

To identify the neurochemical identity of the transfected neurons, we performed immunofluorescence labelling choline acetyltransferase (ChAT. Free-floating sections were rinsed in PBS, blocked in either 4% normal donkey serum (NDS, for ChAT) and 0.1% Triton-X100 for 30 min and rinsed in PBS. After PBS rinses, sections were incubated overnight at 4ºC in goat anti-ChAT (1:100, Millipore) in PBS containing 1% NDS. Sections were rinsed in PBS and incubated in Alexa 488-conjugated donkey anti-goat (1:1000, Life Technologies) in 1% NDS (ChAT) for 1 hour. All sections were additionally counterstained by incubation with 4'6-diamidino-2-phenylindole (DAPI) which labelled cell nuclei. Sections were rinsed in PBS and mounted on glass slides with Fluoromount-G mounting medium (Southern Biotech) for fluorescence microscopy. Sections were imaged in the NIS-Elements software (Nikon Instruments, Inc., Melville, NY, USA) using a Nikon DS-Fil color digital camera on a Nikon E400 microscope equipped with TRITC, FITC, and DAPI fluorescence cubes.

6.3. RESULTS

6.3.1 Histologic verification of channel expression

Injection of AAV5-EF1a-DIO viruses into positively genotyped ChAT-CRE transgenic rats produced robust expression in cholinergic neurons of the medial septum (Figure 34). Both AAV5-EF1a-DIO-ChR2-mCherry (Figure 34A) and AAV5-EF1a-DIO-eNPHR3.0-EYFP (Figure 34B) were found to express in the region. ChR2-mCherry expression colocalized with cholinergic neurons of the medial septum, supporting cell-type specificity in these experiments.
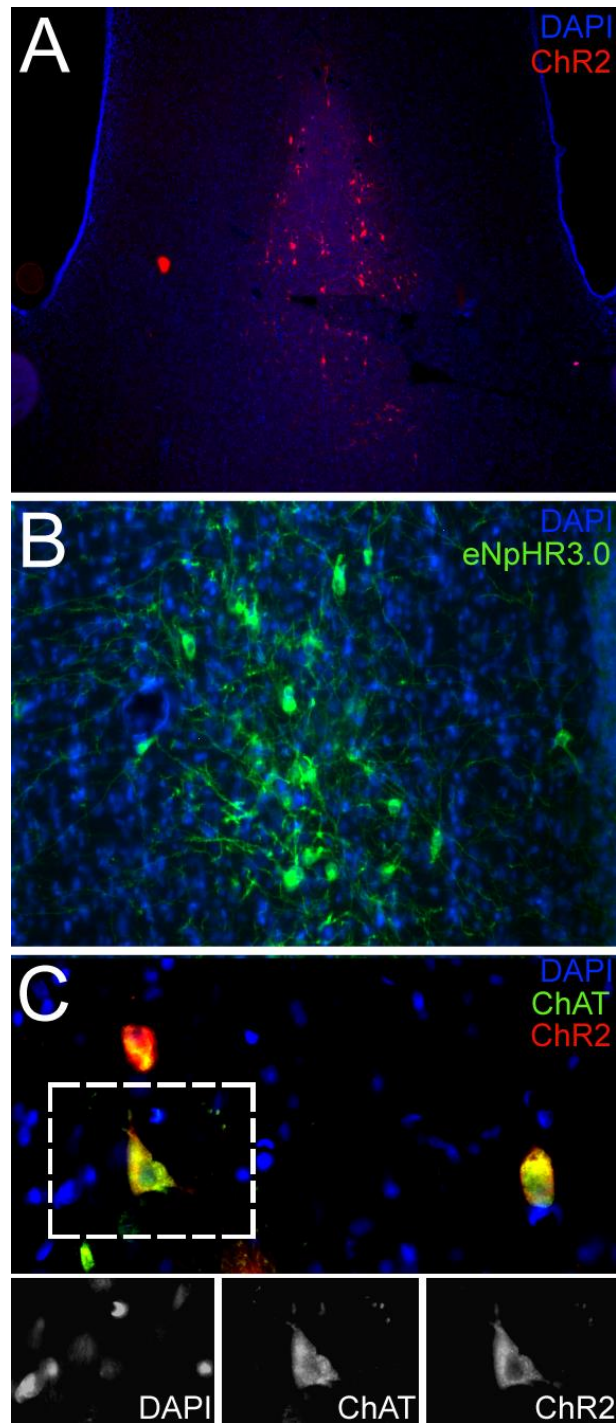
Figure 34: Robust and selective expression of ChR2-mCherry in transgenic Chat-CRE medial septal cholinergic neurons.

Expression in the medial septum of AAV5-EF1a-DIO viruses in ChAT-CRE transgenic rats was readily observed **(A)** ChR2-mCherry expressing neurons **(red)** were observed in the medial septum. **(B)** eNpHR3.0-EYFP **(green)** expression was also observed post-injection. **(C)** MSDB ChR2 expressing neurons **(red)** colocalized with immunofluorescently labelled cholinergic neurons **(ChAT, green).** DAPI nuclei stain in blue.

6.3.2 Rhythmic excitation of cholinergic MSDB neurons

6.3.2.1 Rhythmic cholinergic MSDB stimulation fails to alter hippocampal LFP dynamics at any stimulation frequency

To assess the hypothesis that MSDB cholinergic activity modulates hippocampal theta activity, we selectively excited the cholinergic MSDB neurons with hChR2(H134R) in pulse trains of varying width, amplitude, and frequency, and examined the resultant hippocampal LFP response. Unlike GABAergic (Figure 14) and glutamatergic (Figure 25) stimulation, however, no visible response in the local field potential to any stimulation pattern was observed in either layer of the hippocampus. Peristimulus averages also failed to demonstrate a noticeable LFP response to stimulus.
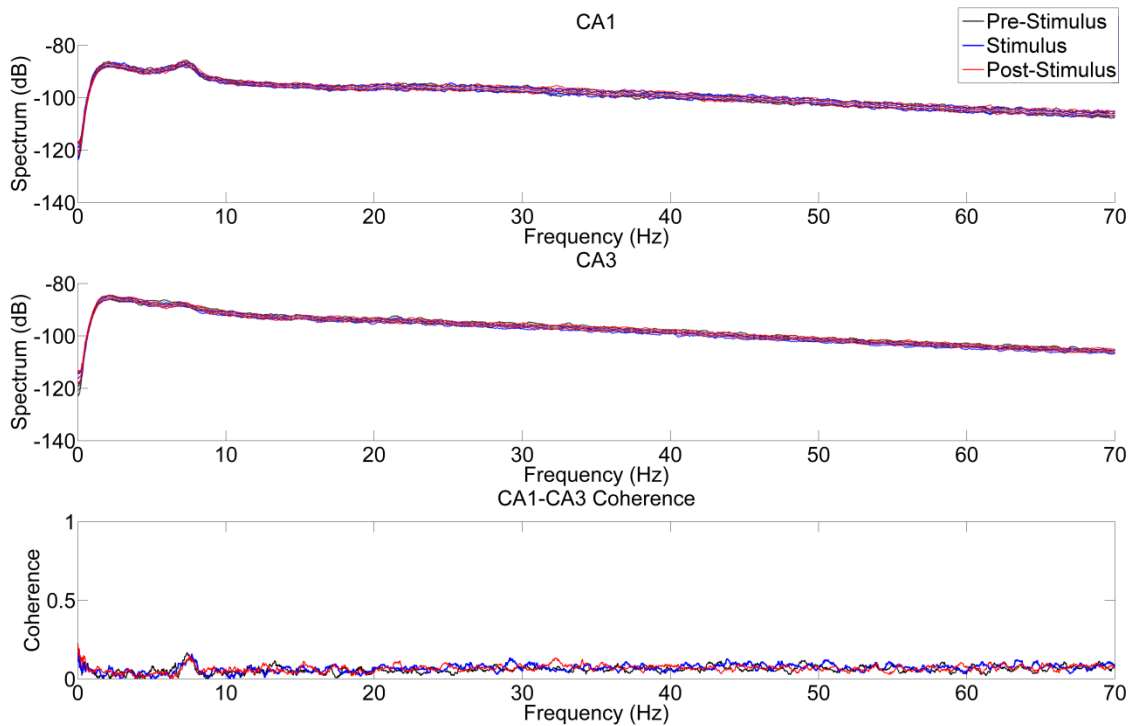
Figure 35: Rhythmic 7 Hz cholinergic stimulation fails to alter hippocampal LFP power
Stimulating with 50 mW/mm^2, 7 Hz, 10 ms pulses failed to alter hippocampal power in either layer. Coherence was similarly unaffected.
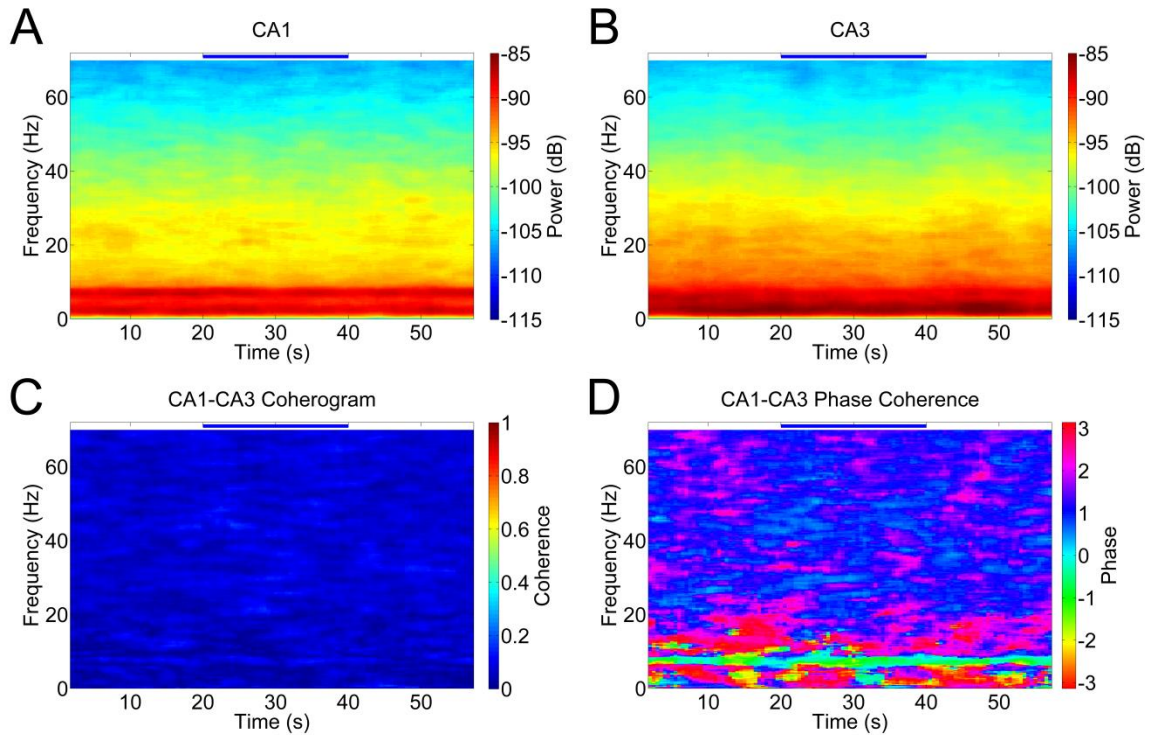
Figure 36: Rhythmic 7 Hz cholinergic stimulation fails to alter hippocampal LFP power and coherence

Stimulation of MSDB cholinergic neurons with 50 mW/mm^2, 7 Hz, 10 ms pulses (**blue bar**) did not alter power at any frequency in either CA1 (**A**) or CA3 (**B**), nor did it alter coherence amplitude (**C**) or phase (**D**).

As cholinergic neurons are thought to be slow firing, we explored whether stimulus frequency had an impact on hippocampal LFP. Spectral and coherence analysis of 7 Hz (Figure 35, Figure 36) and 35 Hz (Figure 37, Figure 38) stimulation also did not reveal any significant differences between the pre-stimulation and stimulation epochs across either layer.
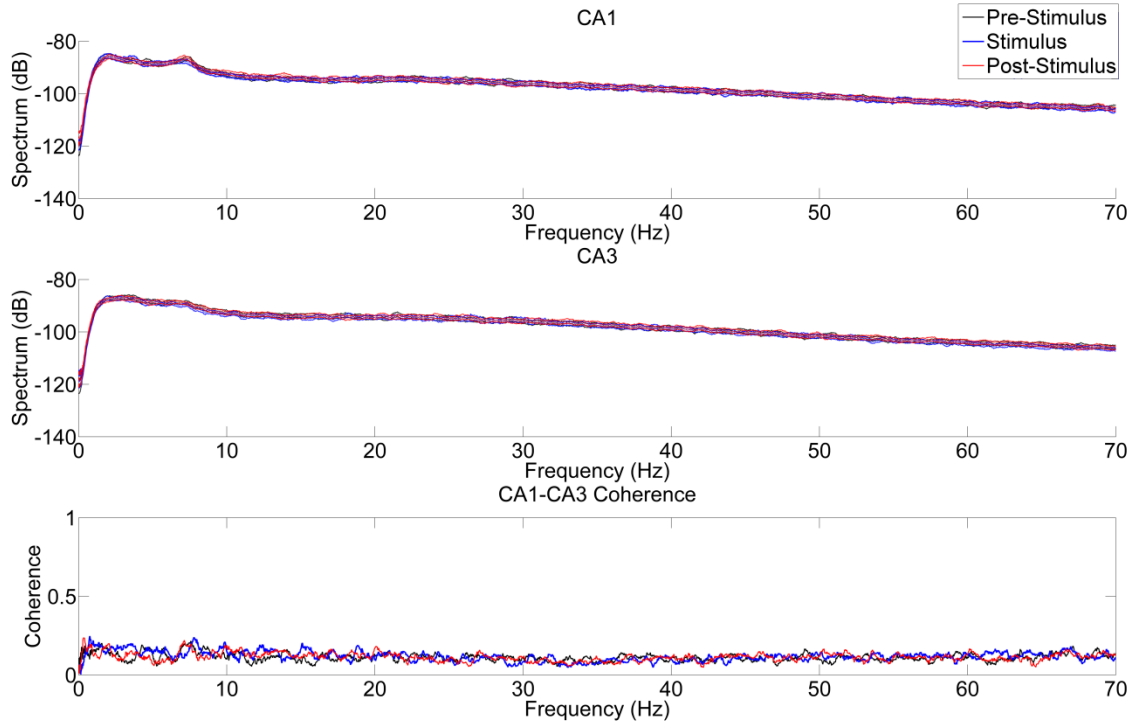
Figure 37: Rhythmic 35 Hz cholinergic stimulation fails to alter hippocampal LFP power
Stimulating with 50 mW/mm^2, 35 Hz, 10 ms pulse trains failed to alter hippocampal power in either layer, or coherence between the layers, from the prestimlus epoch.
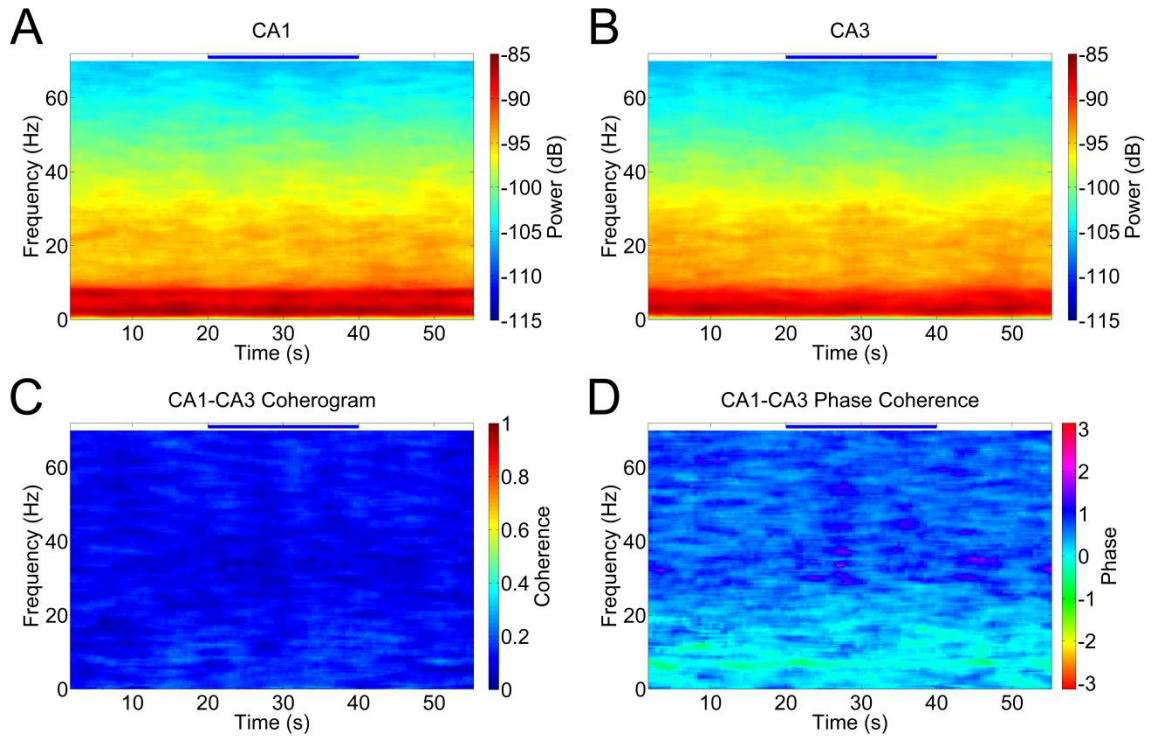
Figure 38: 35 Hz stimulation of MSDB cholinergic neurons fails to alter hippocampal power or coherence

Stimulation of MSDB cholinergic neurons with 50 mW/mm^2, 35 Hz, 10 ms pulses **(blue bar)** did not alter power at any frequency in either CA1 **(A)** or CA3 **(B)**, nor did it alter coherence amplitude **(C)** or phase **(D).**

Similarly, theta phase as assessed by autocorrelation analysis was not altered by stimulation (Figure 39).
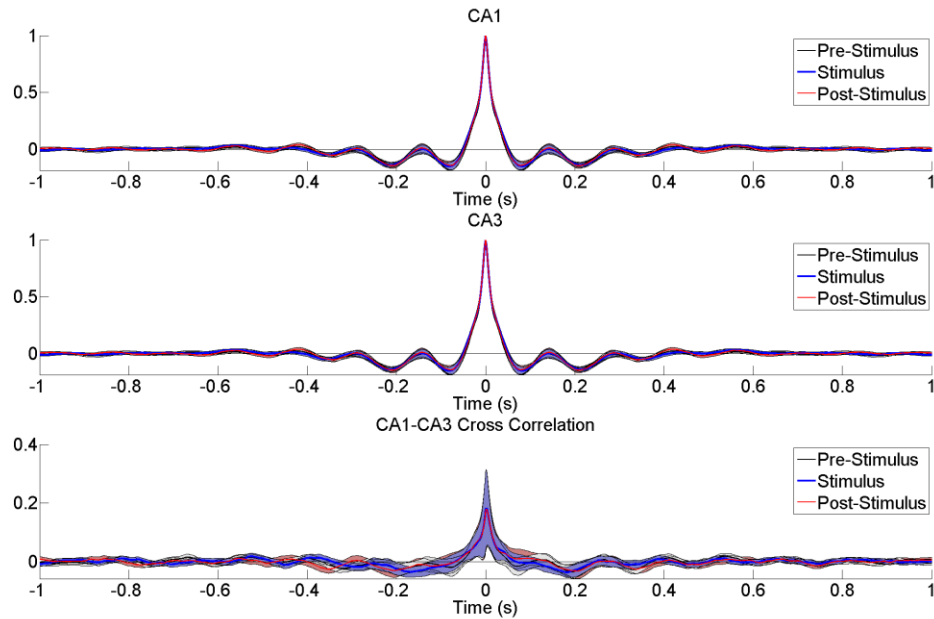
Figure 39: 7 Hz stimulation does not alter theta phase in CA1 or CA3
No significant changes in the auto-correlation signal were between the pre-stimulus (black) and stimulus (blue) epochs was seen during 50 mW/mm^2, 7 Hz, 10ms stimulation.

6.3.2.2 CA3 Single-unit firing rate changes observed during implantation under anesthesia

During implantation of two animals, we observed single-unit firing rate changes in the CA3 layer in response to 50 mW/mm^2, 35 Hz, 10 ms stimulation of MSDB cholinergic neurons in two animals. These firing rate changes were profound and coincided with stimulation onset (Figure 40). Some units decreased their firing rate (Figure 40A) whereas others increased (Figure 40B). This could occur in the same stimulation session. In one case (Figure 40B), firing rate increase was associated with a decrease in power >40 Hz in the LFP. This was not seen for decreased firing rates, nor in the awake animal. These results suggest that our targeting and stimulation parameters were effective, but hippocampal LFP was simply non-responsive to cholinergic activity.
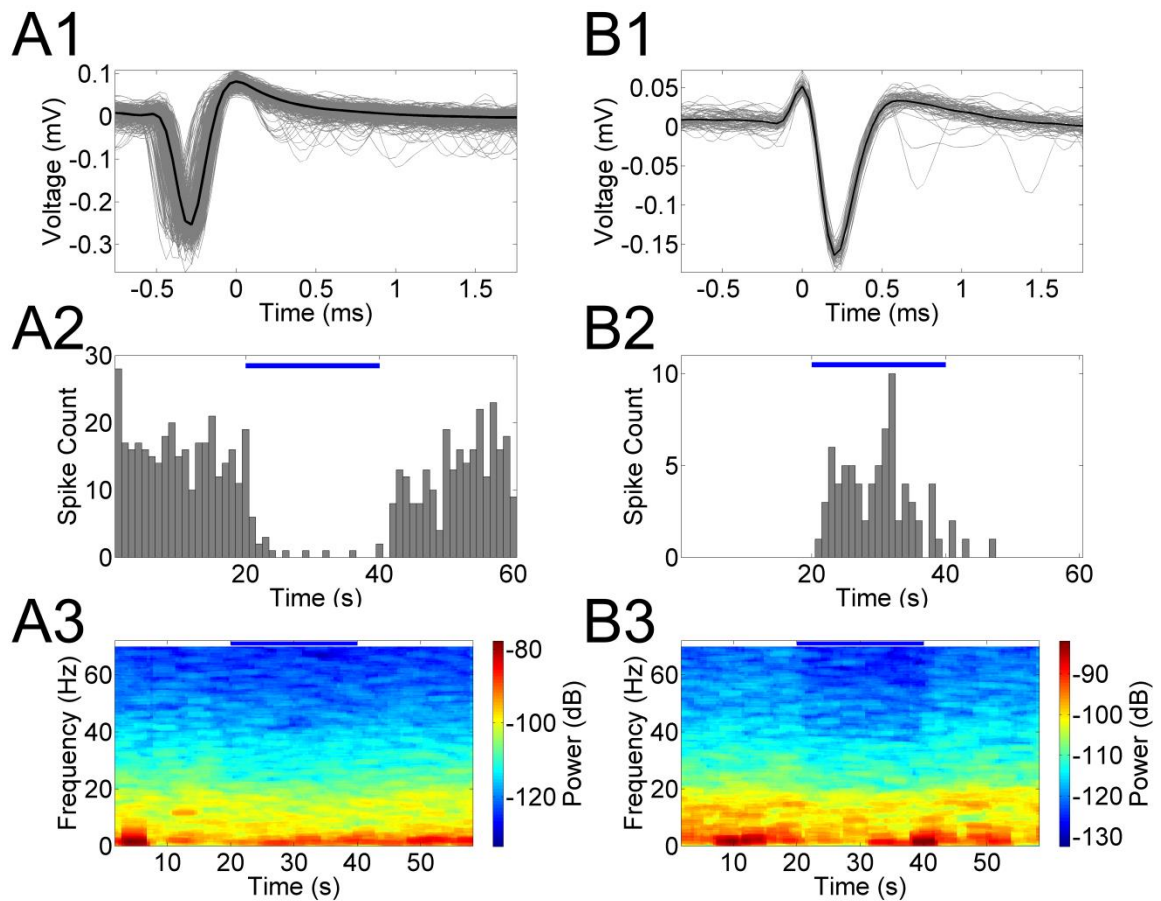
Figure 40: Single-unit response to stimulation during surgical implantation
In two animals we noted profound single-unit firing rate changes at the target site during surgery and under isoflurane anesthesia. Two example units from the same animal and the same stimulation/recording session are illustrated here **(A,B).** Unit **A** had a marked decrease in firing rate with 50 mW/mm^2, 35 Hz, 10ms onset **(A2)** that was unaccompanied by any noticeable changes in hippocampal LFP **(A3)**. Unit **B**, on the other hand, increased its firing rate in response to stimulation **(B2)**. Note that there was a decrease in LFP power >40 Hz accompanying this firing rate increase.

6.3.2.3 Three isolated CA3 and CA1 single units reduced their firing rate in response to 50 mW/mm^2, 35 Hz, 10 ms stimulation of cholinergic neurons of the medial septum

Based on the single-unit results under anesthesia, we examined single-unit firing rate

changes during stimulation in 50 mW/mm^2, 35 Hz, 10 ms cholinergic stimulation

recordings. We isolated 77 putative neurons, most of which did not possess demonstrable

changes in firing rate during excitation. However, we identified three neurons – one from CA3 and two from CA1 – whose firing rates consistently decreased in response to ChR2 stimulation in multiple trials (Figure 41), as evidenced by the rate estimation functions calculated for each neuron.
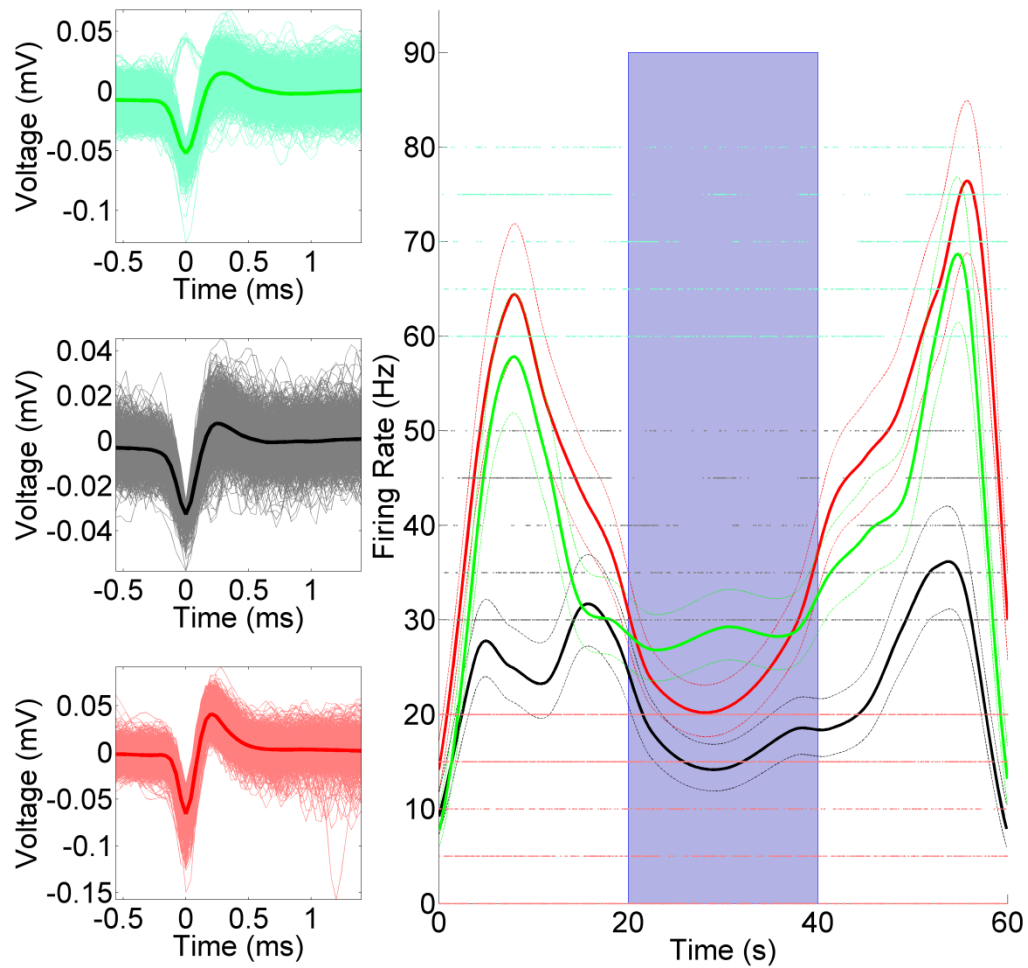
Figure 41: Three CA1 and CA3 single units reduced their firing rate in response to 50 mW/mm^2, 35 Hz, 10 ms stimulation of cholinergic MSDB neurons

Three neurons – two from CA1 **(black, red)**, one from CA3 **(green)** responded to stimulation of MSDB cholinergic neurons with 50mW/mm^2, 35 Hz, 10 ms stimulation **(blue area)** with a reduction in firing rate. Dashed lines are 95% confidence intervals, while solid lines are the estimated smoothed firing rate. Lighter traces in the same color reflect the single unit waveforms and their raster spike times.

6.3.3 Inhibition of MSDB cholinergic neurons

It's possible that the lack of response to cholinergic stimulation was due to maximal

activation of cholinergic activity, wherein additional cholinergic stimulation may not

significantly alter theta power or hippocampal activity. Thus, we sought to test whether

optogenetic inhibition of cholinergic MSDB neurons would alter hippocampal theta

activity, addressing the *necessity* of this subpopulation for theta in the awake animal.
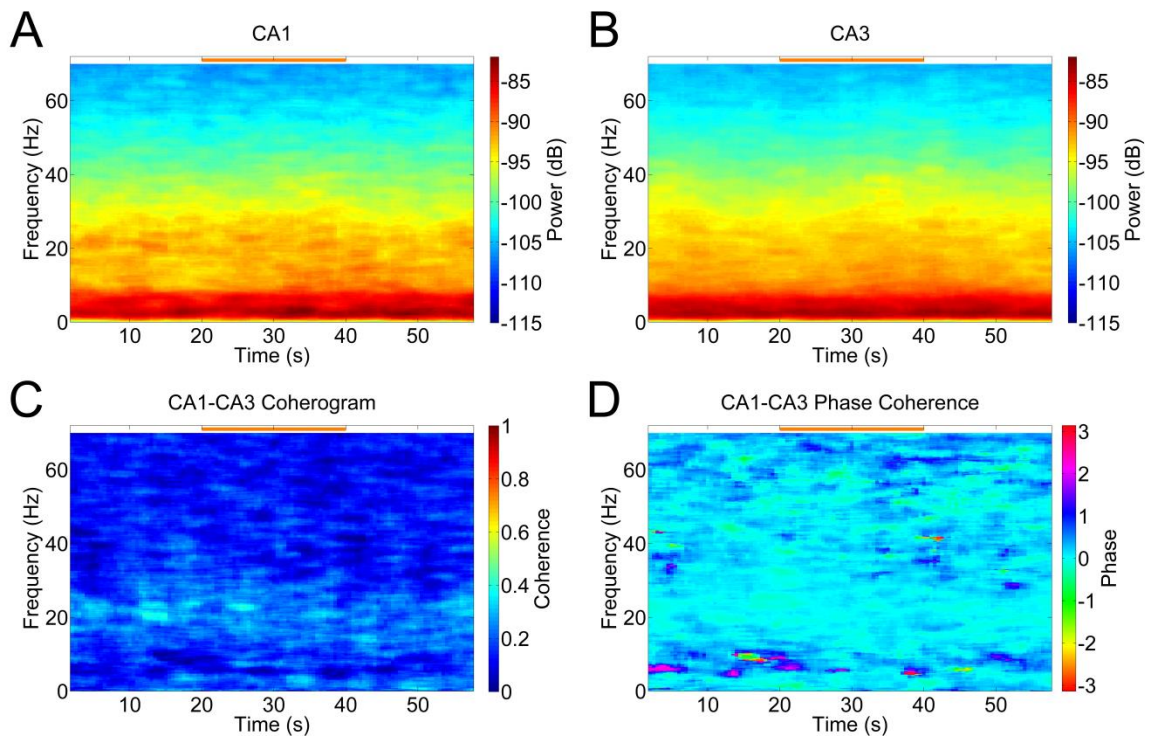
Figure 42: Rhythmic inhibition at 35 Hz does not alter hippocampal spectral power.
Rhythmic inhibition of the MSDB cholinergic neurons for with 90 mW/mm^2 **(orange bar)** failed
to significantly alter hippocampal power at any frequency in either CA1 **(A)** and CA3 **(B)** from
the pre-stimulus epoch. No significant differences were noted between the pre-stimulus and post-
stimulus epochs in the coherogram **(C)** or the phase coherence **(D).**

6.3.3.1 Rhythmic 35 Hz inhibition of MSDB cholinergic neurons did not alter hippocampal LFP power or coherence

We first examined whether rhythmic inhibition could alter hippocampal LFP power or coherence. However, rhythmic inhibition at 90 mW/mm^2, 35 Hz, 10 ms failed to demonstrate any alteration to hippocampal spectral power or coherence (Figure 42).

We then examined constant inhibition of the cholinergic neurons using 90mW/mm^2 inhibition. Similarly, however, no alterations were observed in hippocampal LFP activity as assessed spectrographically (Figure 43).
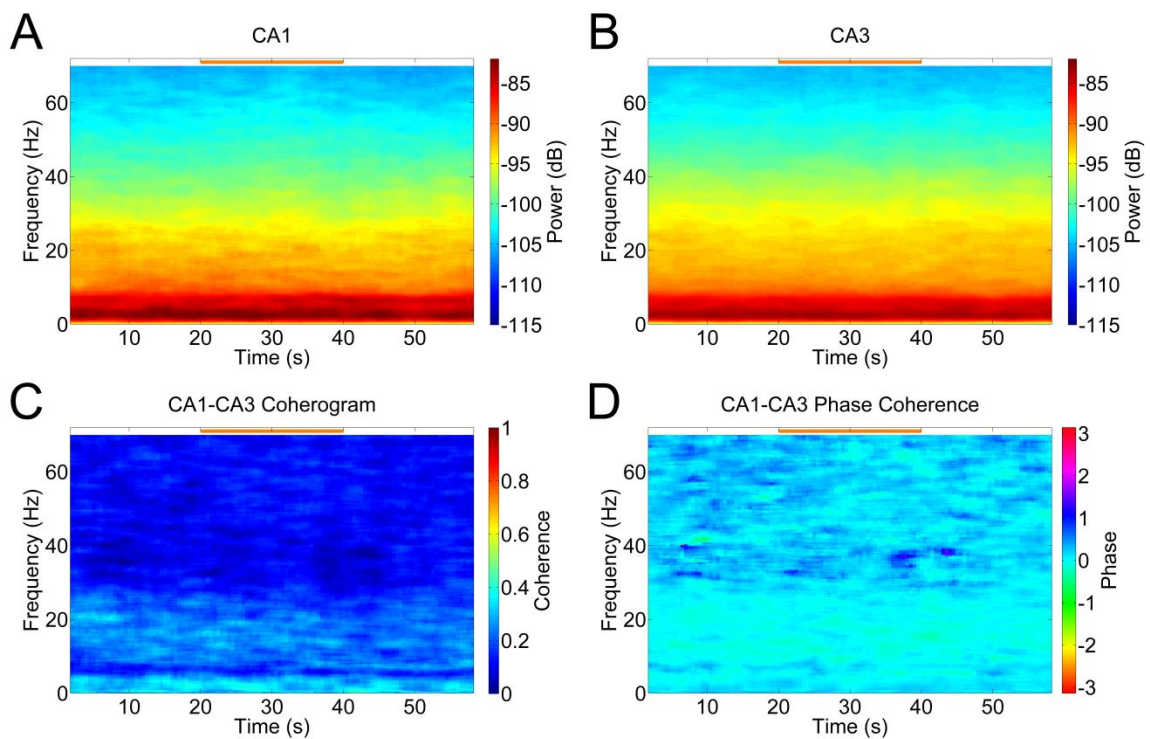
Figure 43: Constant inhibition of MSDB cholinergic neurons does not alter hippocampal oscillatory power
Constant inhibition of the MSDB cholinergic neurons for 20 seconds at 90 mW/mm^2 (**orange bar**) failed to significantly alter hippocampal power at any frequency in either CA1 (**A**) and CA3 (**B**) from the pre-stimulus epoch. No significant differences were observed between the pre-stimulus and post-stimulus epochs in the coherogram (**C**) or the phase coherence (**D**).

Unlike inhibition of the glutamatergic population (Figure 33), no significant changes in theta phase were observed with constant inhibition of the cholinergic MSDB neurons (Figure 44).
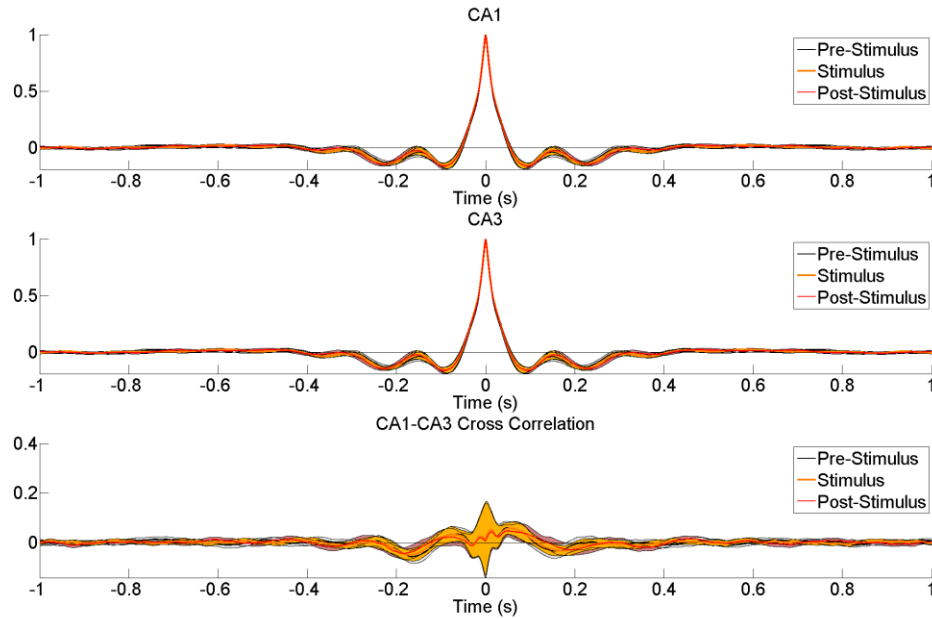
Figure 44: Constant inhibition does not alter theta phase in or between CA1 and CA3
No significant changes in the auto-correlation signal were between the pre-stimulus (black) and stimulus (orange) epochs was seen during 90 mW/mm^2, 20s inhibition.

6.3.3.2 No hippocampal single units altered their firing rate in response to optogenetic inhibition
Rhythmic and constant inhibition of the MSDB cholinergic neurons failed to demonstrate significant changes in single unit firing rate in detected and isolated CA1 or CA3 hippocampal neurons.

6.4. DISCUSSION

We hypothesized that the cholinergic neurons of the MSDB were serving as a gain control for theta, locally increasing the firing rate of glutamatergic and GABAergic neurons and priming the hippocampus for input. Stimulating the cholinergic neurons would, in theory, promote an excited state that could increase power at theta frequencies, whereas inhibiting the cholinergic neurons would reduce theta power. Neither of these results was born out in our experiments in awake and behaving transgenic ChAT-CRE transgenic rats.

Neither optogenetic stimulation nor inhibition of the MSDB cholinergic neurons in awake animals altered hippocampal local field potential power at theta or other frequencies. Under anesthesia during the implantation surgery, two animals demonstrated changes in single unit firing rate in response to 50 mW/mm^2, 35 Hz, 10 ms stimulation (Figure 40). We also noted that during the same stimulation protocol in awake animals; three neurons reduced their firing rate during the stimulus epoch (Figure 41). No changes in firing rate were noted during inhibition of the same population.

We cannot rule out the possibility that our inhibitory paradigm failed to arrest neural activity in the cholinergic neurons of the medial septum. While the parameters we chose demonstrated functional effects in hippocampus in response to inhibition of the GABAergic (Figure 20) and glutamatergic (Figure 33) populations, no similar response or effect was noted in the cholinergic. Optogenetic stimulation and inhibition is partially dependent upon the membrane and electrochemical gradient properties of the expressing neurons, and it may be that the cholinergic population is more resistant to inhibition, or requires a greater transmembrane current, to completely silence. As the expression was robust and targeted appropriately (Figure 34), and no significant changes in hardware

implantation technique were made, this response is less likely due to a technical error particular to these subjects. Further investigation within the medial septum, as well as of the single unit recordings from the hippocampus, will be necessary to tease out the effectiveness of MSDB cholinergic inhibition and the interpretation of these results.

If cholinergic input largely impacts single-unit firing rates in inhibitory interneurons, then these results may also reflect poor targeting of our electrode arrays. We targeted our contacts to the pyramidal cell layer of the hippocampus. Yet nicotinic inputs from the medial septum project to inhibitory interneurons of the stratum lacunosum moleculare (Bell et al. 2011), and muscarinic inputs also have pronounced impacts on hippocampal interneurons (Bell et al. 2013). Our electrodes may simply be sampling from poorly responsive neurons, resulting in a poor signal-to-noise ratio. It is also possible that we are not activating a sufficient population of MSDB cholinergic neurons to generate a response. Introducing an electrode into the medial septum alongside the optical ferrule could provide greater insight into the effectiveness of our stimulation and inhibition techniques. These experiments, however suggest that cholinergic neurons do not pace or modulate hippocampal theta oscillations in the awake animal.

Behavioral and network state may be highly important. Cholinergic input to the deafferented hippocampus is capable of generating theta-like oscillations (Konopacki et al. 1987), and perhaps this represents a particular hippocampal state in which cholinergic input is most effective. Urethane anesthesia is another case in which cholinergic inputs produced a demonstrable effect (Yoder and Pang 2005).

Indeed, combinatorial effects may play an important role. Cholinergic input alone may not be sufficient to alter septohippocampal dynamics, but instead may require concurrent GABAergic or glutamatergic activity to modulate the network. Non-specific electrical stimulation – which may be activating all three populations – has been used effectively to treat memory dysfunction due to medial septal lesions (McNaughton et al. 2006), and combinatorial effects of lesioning multiple cell populations have been observed (Yoder and Pang 2005). Future experiments will need to explore these interactions in well-defined behavioral states to better elucidate MSDB cholinergic neuron functionality in the septohippocampal network.

6.5. CONCLUSIONS

Optogenetic excitation and inhibition of the MSDB cholinergic neurons failed to appreciably modulate hippocampal oscillatory power at any frequency, including theta. We did observe modulation of single-unit firing rates in rare cases in both anesthetized and awake animals, but the robustness of this effect is unclear.

CHAPTER VII

CONCLUSIONS

In this thesis, I have described the current state of epilepsy therapy, with particular regard to clinical trials in deep brain stimulation. I have also shown how current deep brain stimulation therapies are largely empirically derived with regard to targets and parameters, and argued that a more mechanistic approach is appropriate. I described our motivation for targeting the medial septum, and the importance of the hippocampal theta rhythm. I described new technologies, software, and adaptations to NeuroRighter to enable concurrent optogenetic neuromodulation and electrophysiology in awake and behaving animals, and demonstrated how these technologies and techniques can be used in several experimental approaches. I then utilized this system to explore medial septal input to the hippocampus. I selectively excited and inhibited each cell population in the medial septum with a variety of stimulation patterns, and analyzed the impact on hippocampal activity.

From these experiments, it appears no medial septal neural population is necessary for the presence of the hippocampal theta power, but that at least two are capable of modulating it. Synchronous GABAergic and glutamatergic inputs from the medial septum to the hippocampus are each capable of pacing and driving hippocampal oscillations (Figure 15Figure 26), with the former impacting the network more robustly than the latter. While inhibiting the GABAergic neurons did not alter theta or

hippocampal activity, inhibiting the glutamatergic neurons impacted the maintenance of phase synchrony and consistency in both hippocampal layers (Figure 33), potentially desynchronizing theta. Cholinergic inputs to the hippocampus could in a few circumstances modulate single unit firing rates, but did not demonstrably affect local field potential.

Together, this suggests a particular model for the septohippocampal axis and theta. Cholinergic neurons of the medial septum serve to prepare or inhibit hippocampal interneurons from firing (Bell et al. 2011; Bell et al. 2013), and act locally within the medial septum to excite glutamatergic neurons (Wu et al. 2003). These excited glutamatergic neurons experience submembrane threshold oscillations sufficient to produce fast and cluster-firing spike trains (Sotty et al. 2003; Huh et al. 2010). Some of this output projects directly to the hippocampus, while others act locally on MSDB GABAergic neurons (Wu et al. 2003). The GABAergic neurons then serve to amplify the synchronized glutamatergic pacemaker signal, and transmit it to the hippocampus, where it modulates extant theta resonance in the hippocampal circuit to maintain a defined and paced phase relationship between neurons within the septohippocampal axis.

7.1. FUTURE EXPERIMENTAL THOUGHTS FOR ELUCIDATING MSDB-HIPPOCAMPAL INTERACTIONS

Testing the veracity of this model will require combinatorial approaches. For example, this model predicts that inhibition of the GABAergic MSDB neurons with concurrent rhythmic excitation of the glutamatergic neurons should reduce the presence of a stimulus-frequency specific oscillation in the hippocampus, whereas the opposite

experiment should be unaffected. Excitation and inhibition of entorhinal inputs to the hippocampus should also prove useful in determining theta's origins and effects.

Coupling these experiments to a memory task will also provide great insight into the functional consequences of excitation and inhibition of these medial septal neuron subpopulations. One major limitation of this work was the lack of electrophysiologic recording performed within the medial septum alongside the hippocampus. This would not only provide greater insight into the effectiveness of excitatory and inhibitory inputs, it would also provide useful information concerning coherence activity across the entire septohippocampal axis, particularly in regards to particular single unit firing patterns. In addition, more extensive instrumentation of the hippocampus with tetrode-based recordings (Manns et al. 2007) would provide greater insight into spike-field interactions and the impact of cholinergic input. Indeed, further assessment of the impact of single unit firing rates, firing times, and coherence with local field potential would provide useful insight into the role these subpopulations play in normal hippocampal function.

7.2. APPLYING OUR FINDINGS TO AN OPTOGENETIC THERAPY FOR EPILEPSY

One goal of this research was to identify a viable target for septohippocampal theta modulation of hippocampal epilepsy. From the evidence generated, it appears that optogenetic stimulation of the GABAergic MSDB neurons is most promising, due to its robust impact on hippocampal oscillatory activity (Figure 15). Indeed, if we can identify epileptic events we may be able to drive the hippocampus such that the seizure is unable to generalize. However, it has been noted that GABAergic neuron population was the most vulnerable to cell death as a result of pilocarpine-induced epileptic activity (Garrido Sanabria et al. 2006). While I have preliminary evidence that GABAergic stimulation of

the medial septum in the tetanus toxin model can successfully modulate hippocampal activity, it may not be sufficient in the epileptic animal.

However, Colom et al. successfully reduced epileptic activity with three disparate methods of theta induction – spontaneous, pharmacologic, and sensory (Colom et al. 2006). Consequently, they hypothesized that it was not the method of theta generation that was antiepileptic but instead simply the oscillatory state itself. As the glutamatergic population of the medial septum appears to be spared in pilocarpine-induced epileptic animals (Garrido Sanabria et al. 2006), modulating the glutamatergic activity (perhaps in synergy with the GABAergic) could bypass the injured circuit and restore normal function. We are currently preparing the necessary experiments for long-term epileptic experiments using these hypotheses as a basis.

REFERENCES

Al-Otaibi, F. A., C. Hamani and A. M. Lozano (2011). "Neuromodulation in Epilepsy." Neurosurgery **69**(4): 957-979.

Amar, A. P. M. D., M. L. J. M. D. Apuzzo and C. Y. M. D. P. D. Liu (2004). "Vagus Nerve Stimulation Therapy after Failed Cranial Surgery for Intractable Epilepsy: Results from the Vagus Nerve Stimulation Therapy Patient Outcome Registry." Neurosurgery **55**(5): 1086-1093.

Andrade, D. M. M. D. M., D. M. Zumsteg, C. M. Hamani, M. M. D. M. F. Hodaie, S. P. Sarkissian, A. M. M. D. P. F. Lozano and R. A. M. D. M. F. Wennberg (2006). "Long-term follow-up of patients with thalamic deep brain stimulation for epilepsy." Neurology **66**(10): 1571-1573.

Arabadzisz, D., K. Antal, F. Parpan, Z. Emri and J.-M. Fritschy (2005). "Epileptogenesis and chronic seizures in a mouse model of temporal lobe epilepsy are associated with distinct EEG patterns and selective neurochemical alterations in the contralateral hippocampus." Experimental Neurology **194**(1): 76-90.

Aravanis, A. M., L.-P. Wang, F. Zhang, L. A. Meltzer, M. Z. Mogri, M. B. Schneider and K. Deisseroth (2007). "An optical neural interface: in vivo control of rodent motor cortex with integrated fiberoptic and optogenetic technology." Journal of Neural Engineering **4**(3): S143-S156.

Ayling, O. G. S., T. C. Harrison, J. D. Boyd, A. Goroshkov and T. H. Murphy (2009). "Automated light-based mapping of motor cortex by photoactivation of channelrhodopsin-2 transgenic mice." Nat Meth **6**(3): 219-224.

Bari, B. A., D. R. Ollerenshaw, D. C. Millard, Q. Wang and G. B. Stanley (2013). "Behavioral and Electrophysiological Effects of Cortical Microstimulation Parameters." PLoS ONE **8**(12): e82170.

Beleza, P. (2009). "Refractory Epilepsy: A Clinically Oriented Review." European Neurology **62**(2): 65-71.

Bell, K. A., H. Shim, C.-K. Chen and A. R. McQuiston (2011). "Nicotinic excitatory postsynaptic potentials in hippocampal CA1 interneurons are predominantly mediated by nicotinic receptors that contain α4 and β2 subunits." Neuropharmacology **61**(8): 1379-1388.

Bell, L. A., K. A. Bell and A. R. McQuiston (2013). "Synaptic muscarinic response types in hippocampal CA1 interneurons depend on different levels of presynaptic activity and different muscarinic receptor subtypes." Neuropharmacology **73**(0): 160-173.

Benabid, A. L., A. Benazzous and P. Pollak (2002). "Mechanisms of deep brain stimulation." <u>Movement Disorders</u> **17**(S3): S73-S74.

Benabid, A. L. M. D. P. D., L. M. D. Minotti, A. M. D. Koudsie, A. M. D. de Saint Martin and E. M. D. Hirsch (2002). "Antiepileptic Effect of High-frequency Stimulation of the Subthalamic Nucleus (Corpus Luysi) in a Case of Medically Intractable Epilepsy Caused by Focal Dysplasia: A 30-month Follow-up: Technical Case Report." <u>Neurosurgery</u> **50**(6): 1385-1392.

Berndt, A., M. Prigge, D. Gradmann and P. Hegemann (2010). "Two Open States with Progressive Proton Selectivities in the Branched Channelrhodopsin-2 Photocycle." <u>Biophysical Journal</u> **98**(5): 753-761.

Bland, B. H. and L. V. Colom (1993). "Extrinsic and intrinsic properties underlying oscillation and synchrony in limbic cortex." <u>Progress in Neurobiology</u> **41**(2): 157-208.

Blits, B., S. Derks, J. Twisk, E. Ehlert, J. Prins and J. Verhaagen (2010). "Adeno-associated viral vector (AAV)-mediated gene transfer in the red nucleus of the adult rat brain: Comparative analysis of the transduction properties of seven AAV serotypes and lentiviral vectors." <u>Journal of Neuroscience Methods</u> **185**(2): 257-263.

Blomstedt, P., R. L. Sjöberg, M. Hansson, O. Bodlund and M. I. Hariz (2013). "Deep Brain Stimulation in the Treatment of Obsessive-Compulsive Disorder." <u>World Neurosurgery</u> **80**(6): e245-e253.

Boëx, C., M. Seeck, S. Vulliémoz, A. O. Rossetti, C. Staedler, L. Spinelli, A. J. Pegna, E. Pralong, J.-G. Villemure, G. Foletti and C. Pollo (2011). "Chronic deep brain stimulation in mesial temporal lobe epilepsy." <u>Seizure</u> **20**(6): 485-490.

Bokil, H., P. Andrews, J. E. Kulkarni, S. Mehta and P. P. Mitra (2010). "Chronux: A platform for analyzing neural signals." <u>Journal of Neuroscience Methods</u> **192**(1): 146-151.

Bondallaz, P., C. Boëx, A. O. Rossetti, G. Foletti, L. Spinelli, S. Vulliemoz, M. Seeck and C. Pollo (2013). "Electrode location and clinical outcome in hippocampal electrical stimulation for mesial temporal lobe epilepsy." <u>Seizure</u> **22**(5): 390-395.

Boon, P., R. Raedt, V. de Herdt, T. Wyckhuys and K. Vonck (2009). "Electrical Stimulation for the Treatment of Epilepsy." <u>Neurotherapeutics</u> **6**(2): 218-227.

Boon, P., K. Vonck, V. De Herdt, A. Van Dycke, M. Goethals, L. Goossens, M. Van Zandijcke, T. De Smedt, I. Dewaele, R. Achten, W. Wadman, F. Dewaele, J. Caemaert and D. Van Roost (2007). "Deep Brain Stimulation in Patients with Refractory Temporal Lobe Epilepsy." <u>Epilepsia</u> **48**(8): 1551-1560.

Borhegyi, Z., V. Varga, N. Szilágyi, D. Fabo and T. F. Freund (2004). "Phase Segregation of Medial Septal GABAergic Neurons during Hippocampal Theta Activity." The Journal of Neuroscience **24**(39): 8470-8479.

Boyden, E. S., F. Zhang, E. Bamberg, G. Nagel and K. Deisseroth (2005). "Millisecond-timescale, genetically targeted optical control of neural activity." Nat Neurosci **8**(9): 1263-1268.

Brocker, D. T., B. D. Swan, D. A. Turner, R. E. Gross, S. B. Tatter, M. Miller Koop, H. Bronte-Stewart and W. M. Grill (2013). "Improved efficacy of temporally non-regular deep brain stimulation in Parkinson's disease." Experimental Neurology **239**(0): 60-67.

Burger, C., O. S. Gorbatyuk, M. J. Velardo, C. S. Peden, P. Williams, S. Zolotukhin, P. J. Reier, R. J. Mandel and N. Muzyczka (2004). "Recombinant AAV Viral Vectors Pseudotyped with Viral Capsids from Serotypes 1, 2, and 5 Display Differential Efficiency and Cell Tropism after Delivery to Different Regions of the Central Nervous System." Mol Ther **10**(2): 302-317.

Butson, C. R., S. E. Cooper, J. M. Henderson and C. C. McIntyre (2007). "Patient-specific analysis of the volume of tissue activated during deep brain stimulation." Neuroimage **34**(2): 661-670.

Buzsáki, G. (2002). "Theta Oscillations in the Hippocampus." Neuron **33**(3): 325-340.

Buzsáki, G., C. A. Anastassiou and C. Koch (2012). "The origin of extracellular fields and currents — EEG, ECoG, LFP and spikes." Nat Rev Neurosci **13**(6): 407-420.

Buzsaki, G. and E. I. Moser (2013). "Memory, navigation and theta rhythm in the hippocampal-entorhinal system." Nat Neurosci **16**(2): 130-138.

Calgary, U. o., C. University of Western Ontario, U. o. Toronto, D. University and U. o. Alberta. "A Multicenter Study of Hippocampal Electrical Stimulation (HS, in Mesial Temporal Lobe Epilepsy (METTLE)." In: ClinicalTrials.gov Retrieved January 17, 2013.

Capecci, M., R. A. Ricciuti, A. Ortenzi, A. Paggi, V. Durazzi, F. Rychlicki, L. Provinciali, M. Scerrati and M. G. Ceravolo (2012). "Chronic bilateral subthalamic stimulation after anterior callosotomy in drug-resistant epilepsy: Long-term clinical and functional outcome of two cases." Epilepsy Research **98**(2–3): 135-139.

Cardin, J. A. (2012). "Dissecting local circuits in vivo: Integrated optogenetic and electrophysiology approaches for exploring inhibitory regulation of cortical activity." Journal of Physiology-Paris **106**(3–4): 104-111.

Cardin, J. A., M. Carlen, K. Meletis, U. Knoblich, F. Zhang, K. Deisseroth, L.-H. Tsai and C. I. Moore (2010). "Targeted optogenetic stimulation and recording of neurons in vivo using cell-type-specific expression of Channelrhodopsin-2." Nat. Protocols **5**(2): 247-254.

Carter, M. E., A. Adamantidis, H. Ohtsu, K. Deisseroth and L. de Lecea (2009). "Sleep Homeostasis Modulates Hypocretin-Mediated Sleep-to-Wake Transitions." J. Neurosci. **29**(35): 10939-10949.

Chabardès, S., P. Kahane, L. Minotti, A. Koudsie, E. Hirsch and A.-L. Benabid (2002). "Deep brain stimulation in epilepsy with particular reference to the subthalamic nucleus." Epileptic Disorders **4**(Supplement 3): S83-93.

Chaturvedi, A., T. J. Foutz and C. C. McIntyre (2012). "Current steering to activate targeted neural pathways during deep brain stimulation of the subthalamic region." Brain Stimulation **5**(3): 369-377.

Cheney, P. D., D. M. Giffin and G. M. Van Acker (2012). "Neural Hijacking: Action of High-Frequency Electrical Stimulation on Cortical Circuits." The Neuroscientist.

Chkhenkeli, S. A. and I. S. Chkhenkeli (1997). "Effects of therapeutic stimulation of nucleus caudatus on epileptic electrical activity of brain in patients with intractable epilepsy." Stereotact Funct Neurosurg **69**(1-4 Pt 2): 221-224.

Chkhenkeli, S. A., M. Šramka, G. S. Lortkipanidze, T. N. Rakviashvili, E. S. Bregvadze, G. E. Magalashvili, T. S. Gagoshidze and I. S. Chkhenkeli (2004). "Electrophysiological effects and clinical results of direct brain stimulation for intractable epilepsy." Clinical Neurology and Neurosurgery **106**(4): 318-329.

Chow, B. Y., X. Han, A. S. Dobry, X. Qian, A. S. Chuong, M. Li, M. A. Henninger, G. M. Belfort, Y. Lin, P. E. Monahan and E. S. Boyden (2010). "High-performance genetically targetable optical neural silencing by light-driven proton pumps." Nature **463**(7277): 98-102.

Cockrell, A. S. and T. Kafri (2007). "Gene delivery by lentivirus vectors." Molecular Biotechnology **36**(3): 184-204.

Colom, L. V. (2006). "Septal networks: relevance to theta rhythm, epilepsy and Alzheimer's disease." Journal of Neurochemistry **96**(3): 609-623.

Colom, L. V., M. T. Castaneda, T. Reyna, S. Hernandez and E. Garrido-sanabria (2005). "Characterization of medial septal glutamatergic neurons and their projection to the hippocampus." Synapse **58**(3): 151-164.

Colom, L. V., A. Garcia-Hernandez, M. T. Castaneda, M. G. Perez-Cordova and E. R. Garrido-Sanabria (2006). "Septo-Hippocampal Networks in Chronically Epileptic Rats: Potential Antiepileptic Effects of Theta Rhythm Generation." J Neurophysiol **95**(6): 3645-3653.

Colom, L. V. and E. Garrido-Sanabria (2007). "Modulation of normal and altered hippocampal excitability states by septal networks." Journal of Neuroscience Research **85**(13): 2839-2843.

Cooke, P. M. and R. S. Snider (1955). "Some Cerebellar Influences on Electrically-Induced Cerebral Seizures*." Epilepsia **C4**(1): 19-28.

Cooper, I., A. Upton and I. Amin (1980). "Reversibility of chronic neurologic deficits. Some effects of electrical stimulation of the thalamus and internal capsule in man." Appl. Neurophysiol. **43**(3-5): 244-258.

Cooper Is, A. I. R. M. W. J. M. P. T. (1976). "Chronic cerebellar stimulation in epilepsy: Clinical and anatomical studies." Archives of Neurology **33**(8): 559-570.

Cooper, I. S., I. Amin and S. Gilman (1973). "The effect of chronic cerebellar stimulation upon epilepsy in man." Trans Am Neurol Assoc **98**: 192-196.

Cukiert, A., C. M. Cukiert, M. Argentoni-Baldochi, C. Baise, C. R. Forster, V. A. Mello, J. A. Burattini and A. M. Lima (2011). "Intraoperative neurophysiological responses in epileptic patients submitted to hippocampal and thalamic deep brain stimulation." Seizure **20**(10): 748-753.

Davidson, B. L. and X. O. Breakefield (2003). "Viral vectors for gene delivery to the nervous system." Nat Rev Neurosci **4**(5): 353-364.

Detre, J. A., D. C. Alsop, G. K. Aguirre and M. R. Sperling (1996). "Coupling of Cortical and Thalamic Ictal Activity in Human Partial Epilepsy: Demonstration by Functional Magnetic Resonance Imaging." Epilepsia **37**(7): 657-661.

Diester, I., M. T. Kaufman, M. Mogri, R. Pashaie, W. Goo, O. Yizhar, C. Ramakrishnan, K. Deisseroth and K. V. Shenoy (2011). "An optogenetic toolbox designed for primates." Nat Neurosci **14**(3): 387-397.

Dinner, D. S., S. Neme, D. Nair, E. B. Montgomery Jr, K. B. Baker, A. Rezai and H. O. Lüders (2002). "EEG and evoked potential recording from the subthalamic nucleus for deep brain stimulation of intractable epilepsy." Clinical Neurophysiology **113**(9): 1391-1402.

Dugladze, T., I. Vida, A. B. Tort, A. Gross, J. Otahal, U. Heinemann, N. J. Kopell and T. Gloveli (2007). "Impaired Hippocampal Rhythmogenesis in a Mouse Model of

Mesial Temporal Lobe Epilepsy." Proceedings of the National Academy of Sciences of the United States of America **104**(44): 17530-17535.

Duprez, T. P., B. A. Serieh and C. Raftopoulos (2005). "Absence of Memory Dysfunction after Bilateral Mammillary Body and Mammillothalamic Tract Electrode Implantation: Preliminary Experience in Three Patients." American Journal of Neuroradiology **26**(1): 195-198.

Ellis, T. L. and A. Stevens (2008). "Deep brain stimulation for medically refractory epilepsy." Neurosurgical Focus **25**(3): E11.

Engel, J., Jr. (2013). "Why is there still doubt to cut it out?" Epilepsy Curr **13**(5): 198-204.

Engel, J., M. P. McDermott, S. Wiebe and et al. (2012). "Early surgical therapy for drug-resistant temporal lobe epilepsy: A randomized trial." JAMA **307**(9): 922-930.

Engel, J., P. C. Van Ness, T. B. Rasmussen and L. M. Ojemann (1993). Outcome with respect to epileptic seizures. Surgical Treatment of the Epilepsies. J. Jerome Engel. New York, Raven Press**:** 609-621.

Fan, W., S. Eran, I. Maesoon, C. Il-Joo, Y. Eui-Sung, B. György, D. W. Kensall and Y. Euisik (2013). "An implantable neural probe with monolithically integrated dielectric waveguide and recording electrodes for optogenetics applications." Journal of Neural Engineering **10**(5): 056012.

Fisher, R., V. Salanova, T. Witt, R. Worth, T. Henry, R. Gross, K. Oommen, I. Osorio, J. Nazzaro, D. Labar, M. Kaplitt, M. Sperling, E. Sandok, J. Neal, A. Handforth, J. Stern, A. DeSalles, S. Chung, A. Shetter, D. Bergen, R. Bakay, J. Henderson, J. French, G. Baltuch, W. Rosenfeld, A. Youkilis, W. Marks, P. Garcia, N. Barbaro, N. Fountain, C. Bazil, R. Goodman, G. McKhann, K. B. Krishnamurthy, S. Papavassiliou, C. Epstein, J. Pollard, L. Tonder, J. Grebin, R. Coffey and N. Graves (2010). "Electrical stimulation of the anterior nucleus of thalamus for treatment of refractory epilepsy." Epilepsia **51**(5): 899-908.

Fisher, R. S., S. Uematsu, G. L. Krauss, B. J. Cysyk, R. McPherson, R. P. Lesser, B. Gordon, P. Schwerdt and M. Rise (1992). "Placebo-Controlled Pilot Study of Centromedian Thalamic Stimulation in Treatment of Intractable Seizures." Epilepsia **33**(5): 841-851.

Fountas, K. N., E. Kapsalaki and G. Hadjigeorgiou (2010). "Cerebellar stimulation in the management of medically intractable epilepsy: a systematic and critical review." Neurosurgical Focus **29**(2): E8.

Franzini, A., G. Messina, C. Marras, F. Villani, R. Cordella and G. Broggi (2008). "Deep Brain Stimulation of Two Unconventional Targets in Refractory Non-Resectable Epilepsy." Stereotactic and Functional Neurosurgery **86**(6): 373-381.

Freund, T. F. and M. Antal (1988). "GABA-containing neurons in the septum control inhibitory interneurons in the hippocampus." Nature **336**(6195): 170-173.

Freund, T. F. and G. Buzsáki (1996). "Interneurons of the hippocampus." Hippocampus **6**(4): 347-470.

Frotscher, M. and C. Léránth (1985). "Cholinergic innervation of the rat hippocampus as revealed by choline acetyltransferase immunocytochemistry: A combined light and electron microscopic study." The Journal of Comparative Neurology **239**(2): 237-246.

Gale, K. (1992). "Subcortical structures and pathways involved in convulsive seizure generation." J Clin Neurophysiol **9**(2): 264-277.

Garant, D. S. and K. Gale (1983). "Lesions of substantia nigra protect against experimentally induced seizures." Brain Research **273**(1): 156-161.

García-Hernández, A., B. H. Bland, J. C. Facelli and L. V. Colom (2010). "Septo-hippocampal networks in chronic epilepsy." Experimental Neurology **222**(1): 86-92.

Garrido Sanabria, E. R., M. T. Castañeda, C. Banuelos, M. G. Perez-Cordova, S. Hernandez and L. V. Colom (2006). "Septal GABAergic neurons are selectively vulnerable to pilocarpine-induced status epilepticus and chronic spontaneous seizures." Neuroscience **142**(3): 871-883.

Gloveli, T., T. Dugladze, S. Saha, H. Monyer, U. Heinemann, R. D. Traub, M. A. Whittington and E. H. Buhl (2005). "Differential involvement of oriens/pyramidale interneurones in hippocampal network oscillations <i>in vitro</i>." The Journal of Physiology **562**(1): 131-147.

Gradinaru, V., M. Mogri, K. R. Thompson, J. M. Henderson and K. Deisseroth (2009). "Optical Deconstruction of Parkinsonian Neural Circuitry." Science **324**(5925): 354-359.

Gradinaru, V., F. Zhang, C. Ramakrishnan, J. Mattis, R. Prakash, I. Diester, I. Goshen, K. R. Thompson and K. Deisseroth (2010). "Molecular and Cellular Approaches for Diversifying and Extending Optogenetics." Cell **141**(1): 154-165.

Gross, R. and M. McDougal (2013). "Technological Advances in the Surgical Treatment of Movement Disorders." Current Neurology and Neuroscience Reports **13**(8): 1-12.

Gross, R. E. (2008). "Activation of Subthalamic Nucleus Outflow by High-Frequency Stimulation Is Consistent with the Nigral Control of Epilepsy Model." Stereotactic and Functional Neurosurgery **86**(4): 216-218.

Gunaydin, L. A., O. Yizhar, A. Berndt, V. S. Sohal, K. Deisseroth and P. Hegemann (2010). "Ultrafast optogenetic control." Nat Neurosci **13**(3): 387-392.

Guye, M., J. Régis, M. Tamura, F. Wendling, A. M. Gonigal, P. Chauvel and F. Bartolomei (2006). "The role of corticothalamic coupling in human temporal lobe epilepsy." Brain **129**(7): 1917-1928.

Hammond, E. J., B. M. Uthman, B. J. Wilder, E. Ben-Menachem, A. Hamberger, T. Hedner and R. Ekman (1992). "Neurochemical effects of vagus nerve stimulation in humans." Brain Research **583**(1–2): 300-303.

Han, X., X. Qian, J. G. Bernstein, H.-h. Zhou, G. T. Franzesi, P. Stern, R. T. Bronson, A. M. Graybiel, R. Desimone and E. S. Boyden (2009). "Millisecond-Timescale Optical Control of Neural Dynamics in the Nonhuman Primate Brain." Neuron **62**(2): 191-198.

Handforth, A., A. A. F. DeSalles and S. E. Krahl (2006). "Deep Brain Stimulation of the Subthalamic Nucleus as Adjunct Treatment for Refractory Epilepsy." Epilepsia **47**(7): 1239-1241.

Haneef, Z., A. Lenartowicz, H. J. Yeh, H. S. Levin, J. Engel and J. M. Stern (2013). "Functional connectivity of hippocampal networks in temporal lobe epilepsy." Epilepsia: n/a-n/a.

Hariz, M. I., P. Blomstedt and L. Zrinzo (2010). "Deep brain stimulation between 1947 and 1987: the untold story." Neurosurgical Focus **29**(2): E1.

Hauptmann, C., J. C. Roulet, J. J. Niederhauser, W. Döll, M. E. Kirlangic, B. Lysyansky, V. Krachkovskyi, M. A. Bhatti, U. B. Barnikol, L. Sasse, C. P. Bührle, E. J. Speckmann, M. Götz, V. Sturm, H. J. Freund, U. Schnell and P. A. Tass (2009). "External trial deep brain stimulation device for the application of desynchronizing stimulation techniques." Journal of Neural Engineering **6**(6): 066003.

Helmstaedter, C., S. Richter, S. Röske, F. Oltmanns, J. Schramm and T.-N. Lehmann (2008). "Differential effects of temporal pole resection with amygdalohippocampectomy versus selective amygdalohippocampectomy on material-specific memory in patients with mesial temporal lobe epilepsy." Epilepsia **49**(1): 88-97.

Helmstaedter, C., S. Roeske, S. Kaaden, C. E. Elger and J. Schramm (2011). "Hippocampal resection length and memory outcome in selective epilepsy surgery." Journal of Neurology, Neurosurgery & Psychiatry **82**(12): 1375-1381.

Henderson, J. M. M. D., T. P. D. Federici and N. M. D. Boulis (2009). "OPTOGENETIC NEUROMODULATION." Neurosurgery **64**(5): 796-804.

Histed, M. H., V. Bonin and R. C. Reid (2009). "Direct Activation of Sparse, Distributed Populations of Cortical Neurons by Electrical Microstimulation." Neuron **63**(4): 508-522.

Hodaie, M., Richard A. Wennberg, Jonathan O. Dostrovsky and Andres M. Lozano (2002). "Chronic Anterior Thalamus Stimulation for Intractable Epilepsy." Epilepsia **43**(6): 603-608.

Holtzheimer, P. E., M. E. Kelley, R. E. Gross, M. M. Filkowski, S. J. Garlow, A. Barrocas, D. Wint, M. C. Craighead, J. Kozarsky, R. Chismar, J. L. Moreines, K. Mewes, P. R. Posse, D. A. Gutman and H. S. Mayberg "Subcallosal Cingulate Deep Brain Stimulation for Treatment-Resistant Unipolar and Bipolar Depression." Arch Gen Psychiatry **69**(2): 150-158.

Howard, D. B., K. Powers, Y. Wang and B. K. Harvey (2008). "Tropism and toxicity of adeno-associated viral vector serotypes 1, 2, 5, 6, 7, 8, and 9 in rat neurons and glia in vitro." Virology **372**(1): 24-34.

Huh, C. Y. L., R. Goutagny and S. Williams (2010). "Glutamatergic Neurons of the Mouse Medial Septum and Diagonal Band of Broca Synaptically Drive Hippocampal Pyramidal Cells: Relevance for Hippocampal Theta Rhythm." The Journal of Neuroscience **30**(47): 15951-15961.

Hunka, K., O. Suchowersky, S. Wood, L. Derwent and Z. H. T. Kiss (2005). "Nursing Time to Program and Assess Deep Brain Stimulators in Movement Disorder Patients." Journal of Neuroscience Nursing **37**(4): 204-210.

Iadarola, M. J. and K. Gale (1982). "Substantia Nigra: Site of Anticonvulsant Activity Mediated by γ -aminobutyric Acid." Science **218**(4578): 1237-1240.

Iwata, K. and R. S. Snider (1959). "Cerebello-hippocampal influences on the electroencephalogram." Electroencephalography and Clinical Neurophysiology **11**(3): 439-446.

Jahanshahi, A., J. Mirnajafi-Zadeh, M. Javan, M. Mohammad-Zadeh and R. Rohani (2009). "The antiepileptogenic effect of electrical stimulation at different low frequencies is accompanied with change in adenosine receptors gene expression in rats." Epilepsia **50**(7): 1768-1779.

Jensen, O. and L. L. Colgin (2007). "Cross-frequency coupling between neuronal oscillations." <u>Trends in Cognitive Sciences</u> **11**(7): 267-269.

Kaifosh, P., M. Lovett-Barron, G. F. Turi, T. R. Reardon and A. Losonczy (2013). "Septo-hippocampal GABAergic signaling across multiple modalities in awake mice." <u>Nat Neurosci</u> **16**(9): 1182-1184.

Kerrigan, J. F., B. Litt, R. S. Fisher, S. Cranstoun, J. A. French, D. E. Blum, M. Dichter, A. Shetter, G. Baltuch, J. Jaggi, S. Krone, M. Brodie, M. Rise and N. Graves (2004). "Electrical Stimulation of the Anterior Nucleus of the Thalamus for the Treatment of Intractable Epilepsy." <u>Epilepsia</u> **45**(4): 346-354.

Khurram, A. and J. P. Seymour (2013). <u>Investigation of the photoelectrochemical effect in optoelectrodes and potential uses for implantable electrode characterization*</u>. Engineering in Medicine and Biology Society (EMBC), 2013 35th Annual International Conference of the IEEE.

Kim, W. and N. Pouratian (2014). "Deep Brain Stimulation for Tourette Syndrome." <u>Neurosurgery clinics of North America</u> **25**(1): 117-135.

King, D., R. A. Bronen, D. D. Spencer and S. S. Spencer (1997). "Topographic distribution of seizure onset and hippocampal atrophy: Relationship between MRI and depth EEG." <u>Electroencephalography and Clinical Neurophysiology</u> **103**(6): 692-697.

Kitchigina, V., I. Popova, V. Sinelnikova, A. Malkov, E. Astasheva, L. Shubina and R. Aliev (2013). "Disturbances of septohippocampal theta oscillations in the epileptic brain: Reasons and consequences." <u>Experimental Neurology</u> **247**(0): 314-327.

Kitchigina, V. F. and M. V. Butuzova (2009). "Theta activity of septal neurons during different epileptic phases: The same frequency but different significance?" <u>Experimental Neurology</u> **216**(2): 449-458.

Klausberger, T., P. J. Magill, L. F. Marton, J. D. B. Roberts, P. M. Cobden, G. Buzsaki and P. Somogyi (2003). "Brain-state- and cell-type-specific firing of hippocampal interneurons in vivo." <u>Nature</u> **421**(6925): 844-848.

Klein, R. L., E. M. Meyer, A. L. Peel, S. Zolotukhin, C. Meyers, N. Muzyczka and M. A. King (1998). "Neuron-Specific Transduction in the Rat Septohippocampal or Nigrostriatal Pathway by Recombinant Adeno-associated Virus Vectors." <u>Experimental Neurology</u> **150**(2): 183-194.

Konopacki, J., M. B. Maciver, B. H. Bland and S. H. Roth (1987). "Theta in hippocampal slices: Relation to synaptic responses of dentate neurons." <u>Brain Research Bulletin</u> **18**(1): 25-27.

Krack, P., V. Fraix, A. Mendes, A.-L. Benabid and P. Pollak (2002). "Postoperative management of subthalamic nucleus stimulation for Parkinson's disease." Movement Disorders **17**(S3): S188-S197.

Krauss, G. L. and M. Z. Koubeissi (2007). "Cerebellar and thalamic stimulation treatment for epilepsy." Acta Neurochir Suppl **97**(Pt 2): 347-356.

Kravitz, A. V., B. S. Freeze, P. R. L. Parker, K. Kay, M. T. Thwin, K. Deisseroth and A. C. Kreitzer (2010). "Regulation of parkinsonian motor behaviours by optogenetic control of basal ganglia circuitry." Nature **advance online publication**.

Krook-Magnuson, E., C. Armstrong, M. Oijala and I. Soltesz (2013). "On-demand optogenetic control of spontaneous seizures in temporal lobe epilepsy." Nat Commun **4**: 1376.

Kusske, J. A., G. A. Ojemann and A. A. Ward Jr (1972). "Effects of lesions in ventral anterior thalamus on experimental focal epilepsy." Experimental Neurology **34**(2): 279-290.

Kwan, P., S. C. Schachter and M. J. Brodie (2011). "Drug-Resistant Epilepsy." New England Journal of Medicine **365**(10): 919-926.

Kwan, P. and M. R. Sperling (2009). "Refractory seizures: Try additional antiepileptic drugs (after two have failed) or go directly to early surgery evaluation?" Epilepsia **50**: 57-62.

Lee, K. J., K. S. Jang and Y. M. Shon (2006). Chronic deep brain stimulation of subthalamic and anterior thalamic nuclei for controlling refractory partial epilepsy. Advances in Functional and Reparative Neurosurgery. J. Chang, Y. Katayama and T. Yamamoto, Springer Vienna. **99:** 87-91.

Lega, B. C., C. H. Halpern, J. L. Jaggi and G. H. Baltuch (2010). "Deep brain stimulation in the treatment of refractory epilepsy: Update on current data and future directions." Neurobiology of Disease **38**(3): 354-360.

Levy, L. F. and W. C. Auchterlonie (1979). "Chronic Cerebellar Stimulation in the Treatment of Epilepsy." Epilepsia **20**(3): 235-245.

Lewis, P. R., C. C. D. Shute and A. Silver (1967). "Confirmation from choline acetylase analyses of a massive cholinergic innervation to the rat hippocampus." The Journal of Physiology **191**(1): 215-224.

Lian, J., M. Bikson, C. Sciortino, W. C. Stacey and D. M. Durand (2003). "Local Suppression of Epileptiform Activity by Electrical Stimulation in Rat Hippocampus In Vitro." The Journal of Physiology **547**(2): 427-434.

Lim, S.-N., S.-T. Lee, Y.-T. Tsai, I. A. Chen, P.-H. Tu, J.-L. Chen, H.-W. Chang, Y.-C. Su and T. Wu (2007). "Electrical Stimulation of the Anterior Nucleus of the Thalamus for Intractable Epilepsy: A Long-term Follow-up Study." Epilepsia **48**(2): 342-347.

Lin, J. Y., P. M. Knutsen, A. Muller, D. Kleinfeld and R. Y. Tsien (2013). "ReaChR: a red-shifted variant of channelrhodopsin enables deep transcranial optogenetic excitation." Nat Neurosci **16**(10): 1499-1508.

Lin, W., K. McKinney, L. Liu, S. Lakhlani and L. Jennes (2003). "Distribution of Vesicular Glutamate Transporter-2 Messenger Ribonucleic Acid and Protein in the Septum-Hypothalamus of the Rat." Endocrinology **144**(2): 662-670.

Lipponen, A., B. T. Woldemichael, K. Gurevicius and H. Tanila (2012). "Artificial Theta Stimulation Impairs Encoding of Contextual Fear Memory." PLoS ONE **7**(11): e48506.

Liu, X., S. Ramirez, P. T. Pang, C. B. Puryear, A. Govindarajan, K. Deisseroth and S. Tonegawa (2012). "Optogenetic stimulation of a hippocampal engram activates fear memory recall." Nature **484**(7394): 381-385.

Loddenkemper, T., A. Pan, S. Neme, K. B. Baker, A. R. Rezai, D. S. Dinner, E. B. J. Montgomery and H. O. Luders (2001). "Deep Brain Stimulation in Epilepsy." Journal of Clinical Neurophysiology **18**(6): 514-532.

Lüttjohann, A. and G. van Luijtelaar (2012). "The dynamics of cortico-thalamo-cortical interactions at the transition from pre-ictal to ictal LFPs in absence epilepsy." Neurobiology of Disease **47**(1): 49-60.

Madisen, L., T. Mao, H. Koch, J.-m. Zhuo, A. Berenyi, S. Fujisawa, Y.-W. A. Hsu, A. J. Garcia, X. Gu, S. Zanella, J. Kidney, H. Gu, Y. Mao, B. M. Hooks, E. S. Boyden, G. Buzsaki, J. M. Ramirez, A. R. Jones, K. Svoboda, X. Han, E. E. Turner and H. Zeng (2012). "A toolbox of Cre-dependent optogenetic transgenic mice for light-induced activation and silencing." Nat Neurosci **15**(5): 793-802.

Maks, C. B., C. R. Butson, B. L. Walter, J. L. Vitek and C. C. McIntyre (2009). "Deep brain stimulation activation volumes and their association with neurophysiological mapping and therapeutic outcomes." Journal of Neurology, Neurosurgery & Psychiatry **80**(6): 659-666.

Manns, I. D., L. Mainville and B. E. Jones (2001). "Evidence for glutamate, in addition to acetylcholine and GABA, neurotransmitter synthesis in basal forebrain neurons projecting to the entorhinal cortex." Neuroscience **107**(2): 249-263.

Manns, J. R., E. A. Zilli, K. C. Ong, M. E. Hasselmo and H. Eichenbaum (2007). "Hippocampal CA1 spiking during encoding and retrieval: Relation to theta phase." Neurobiology of Learning and Memory **87**(1): 9-20.

Manseau, F., M. Danik and S. Williams (2005). "A functional glutamatergic neurone network in the medial septum and diagonal band area." The Journal of Physiology **566**(3): 865-884.

McIntyre, C. C., C. R. Butson, C. B. Maks and A. M. Noecker (2006). Optimizing Deep Brain Stimulation Parameter Selection with Detailed Models of the Electrode-Tissue Interface. Engineering in Medicine and Biology Society, 2006. EMBS '06. 28th Annual International Conference of the IEEE.

McIntyre, C. C. and W. M. Grill (2002). "Extracellular Stimulation of Central Neurons: Influence of Stimulus Waveform and Frequency on Neuronal Output." Journal of Neurophysiology **88**(4): 1592-1604.

McIntyre, C. C., M. Savasta, L. Kerkerian-Le Goff and J. L. Vitek (2004). "Uncovering the mechanism(s) of action of deep brain stimulation: activation, inhibition, or both." Clinical Neurophysiology **115**(6): 1239-1248.

McLachlan, R. S., S. Pigott, J. F. Tellez-Zenteno, S. Wiebe and A. Parrent (2010). "Bilateral hippocampal stimulation for intractable temporal lobe epilepsy: Impact on seizures and memory." Epilepsia **51**(2): 304-307.

McNaughton, N., M. Ruan and M.-A. Woodnorth (2006). "Restoring theta-like rhythmicity in rats restores initial learning in the Morris water maze." Hippocampus **16**(12): 1102-1110.

Miatton, M., D. Van Roost, E. Thiery, E. Carrette, A. Van Dycke, K. Vonck, A. Meurs, G. Vingerhoets and P. Boon (2011). "The cognitive effects of amygdalohippocampal deep brain stimulation in patients with temporal lobe epilepsy." Epilepsy & Behavior **22**(4): 759-764.

Miller, J. W., G. M. Turner and B. C. Gray (1994). "Anticonvulsant effects of the experimental induction of hippocampal theta activity." Epilepsy Research **18**(3): 195-204.

Miller, R. (1996). "Cortico-thalamic interplay and the security of operation of neural assemblies and temporal chains in the cerebral cortex." Biological Cybernetics **75**(3): 263.

Mondragon, S. and M. Lamarche (1990). "Suppression of motor seizures after specific thalamotomy in chronic epileptic monkeys." Epilepsy Research **5**(2): 137-145.

Monmaur, P. and P. Breton (1991). "Elicitation of hippocampal theta by intraseptal carbachol injection in freely moving rats." Brain Research **544**(1): 150-155.

Montoya, C. P. and R. S. Sainsbury (1985). "The effects of entorhinal cortex lesions on type 1 and type 2 theta." Physiology & Behavior **35**(1): 121-126.

Montplaisir, J., M. Laverdière, J. Saint-Hilaire and I. Rouleau (1987). "Nocturnal sleep recording in partial epilepsy: a study with depth electrodes." Journal of Clinical Neurophysiology **4**(4): 383-388.

Morrell, M. J. (2011). "Responsive cortical stimulation for the treatment of medically intractable partial epilepsy." Neurology **77**(13): 129501394.

Moruzzi, G. (1950). "Effects at different frequencies of cerebellar stimulation upon postural tonus and myotatic reflexes." Electroencephalography and Clinical Neurophysiology **2**(1–4): 463-469.

Mueller, S. G., K. D. Laxer, J. Barakos, I. Cheong, D. Finlay, P. Garcia, V. Cardenas-Nicolson and M. W. Weiner (2010). "Involvement of the thalamocortical network in TLE with and without mesiotemporal sclerosis." Epilepsia **51**(8): 1436-1445.

Mullan Ss, V. G. G. K. J. J. M. M. M. (1967). "Thalamic lesions for the control of epilepsy: A study of nine cases." Archives of Neurology **16**(3): 277-285.

Nathanson, J. L., R. Jappelli, E. D. Scheeff, G. Manning, K. Obata, S. Brenner and E. M. Callaway (2009). "Short promoters in viral vectors drive selective expression in mammalian inhibitory neurons, but do not restrict activity to specific inhibitory cell-types." Frontiers in Neural Circuits **3**.

Newman, J. P. (2013). Optogenetic Feedback Control of Neural Activity. Doctor of Philosophy, Georgia Institute of Technology.

Newman, J. P., R. Zeller-Townson, M.-f. Fong, S. Arcot Desai, R. E. Gross and S. M. Potter (2013). "Closed-loop, multichannel experimentation using the open-source NeuroRighter electrophysiology platform." Frontiers in Neural Circuits **6**.

Oikawa, H., M. Sasaki, Y. Tamakawa and A. Kamei (2001). "The circuit of Papez in mesial temporal sclerosis: MRI." Neuroradiology **43**(3): 205-210.

Okun, M. S., B. V. Gallo, G. Mandybur, J. Jagid, K. D. Foote, F. J. Revilla, R. Alterman, J. Jankovic, R. Simpson, F. Junn, L. Verhagen, J. E. Arle, B. Ford, R. R. Goodman, R. M. Stewart, S. Horn, G. H. Baltuch, B. H. Kopell, F. Marshall, D. Peichel, R. Pahwa, K. E. Lyons, A. I. Tröster, J. L. Vitek and M. Tagliati (2012). "Subthalamic deep brain stimulation with a constant-current device in Parkinson's disease: an open-label randomised controlled trial." The Lancet Neurology **11**(2): 140-149.

Osorio, I., J. Overman, J. Giftakis and S. B. Wilkinson (2007). "High Frequency Thalamic Stimulation for Inoperable Mesial Temporal Epilepsy." Epilepsia **48**(8): 1561-1571.

Packer, A. M., D. S. Peterka, J. J. Hirtz, R. Prakash, K. Deisseroth and R. Yuste (2012). "Two-photon optogenetics of dendritic spines and neural circuits." Nat Meth **9**(12): 1202-1205.

Papez, J. W. (1937). "A proposed mechanism of emotion." Archives of Neurology & Psychiatry **38**(4): 725-743.

Patel, J., S. Fujisawa, A. Berényi, S. Royer and G. Buzsáki (2012). "Traveling Theta Waves along the Entire Septotemporal Axis of the Hippocampus." Neuron **75**(3): 410-417.

Paterna, J. C., T. Moccetti, A. Mura, J. Feldon and H. Bueler (2000). "Influence of promoter and WHV post-transcriptional regulatory element on AAV-mediated transgene expression in the rat brain." Gene Ther **7**(15): 1304-1311.

Paz, J. T., T. J. Davidson, E. S. Frechette, B. Delord, I. Parada, K. Peng, K. Deisseroth and J. R. Huguenard (2012). "Closed-loop optogenetic control of thalamus as a tool for interrupting seizures after cortical injury." Nat Neurosci **advance online publication**.

Paz, J. T., T. J. Davidson, E. S. Frechette, B. Delord, I. Parada, K. Peng, K. Deisseroth and J. R. Huguenard (2013). "Closed-loop optogenetic control of thalamus as a tool for interrupting seizures after cortical injury." Nat Neurosci **16**(1): 64-70.

Quiroga, R. Q., Z. Nadasdy and Y. Ben-Shaul (2004). "Unsupervised Spike Detection and Sorting with Wavelets and Superparamagnetic Clustering." Neural Computation **16**(8): 1661-1687.

Ranck, J. J. B. (1975). "Which elements are excited in electrical stimulation of mammalian central nervous system: A review." Brain Research **98**(3): 417-440.

Rolston, J. D., S. A. Desai, N. G. Laxpati and R. E. Gross (2011). "Electrical Stimulation for Epilepsy: Experimental Approaches." Neurosurgery clinics of North America **22**(4): 425-442.

Rolston, J. D., R. E. Gross and S. M. Potter (2009). Common median referencing for improved action potential detection with multielectrode arrays. Engineering in Medicine and Biology Society, 2009. EMBC 2009. Annual International Conference of the IEEE.

Rolston, J. D., R. E. Gross and S. M. Potter (2009). "A low-cost multielectrode system for data acquisition enabling real-time closed-loop processing with rapid recovery from stimulation artifacts." Frontiers in Neuroengineering **2**.

Rolston, J. D., R. E. Gross and S. M. Potter (2009). NeuroRighter: Closed-loop multielectrode stimulation and recording for freely moving animals and cell cultures. Engineering in Medicine and Biology Society, 2009. EMBC 2009. Annual International Conference of the IEEE.

Rolston, J. D., R. E. Gross and S. M. Potter (2010). "Closed-loop, open-source electrophysiology." Frontiers in Neuroscience **4**.

Rolston, J. D., N. G. Laxpati, C. A. Gutekunst, S. M. Potter and R. E. Gross (2010). "Spontaneous and evoked high-frequency oscillations in the tetanus toxin model of epilepsy." Epilepsia.

Sander, J. W. (2003). "The epidemiology of epilepsy revisited." Current Opinion in Neurology **16**(2): 165-170.

Simon, A. P., F. Poindessous-Jazat, P. Dutar, J. Epelbaum and M.-H. Bassant (2006). "Firing Properties of Anatomically Identified Neurons in the Medial Septum of Anesthetized and Unanesthetized Restrained Rats." The Journal of Neuroscience **26**(35): 9038-9046.

Sironi, V. a. (2011). "Origin and evolution of deep brain stimulation." Frontiers in integrative neuroscience **5**(August): 42-42.

Smith, Y., A. Galvan, T. J. Ellender, N. Doig, R. M. Villalba, I. H. Ocampo, T. Wichman and P. Bolam (2014). "The Thalamostriatal System in Normal and Diseased States." Frontiers in Systems Neuroscience **8**.

Sotty, F., M. Danik, F. Manseau, F. Laplante, R. Quirion and S. Williams (2003). "Distinct electrophysiological properties of glutamatergic, cholinergic and GABAergic rat septohippocampal neurons: novel implications for hippocampal rhythmicity." The Journal of Physiology **551**(3): 927-943.

Sparta, D. R., A. M. Stamatakis, J. L. Phillips, N. Hovelso, R. van Zessen and G. D. Stuber (2012). "Construction of implantable optical fibers for long-term optogenetic manipulation of neural circuits." Nat. Protocols **7**(1): 12-23.

Sramka, M. and S. A. Chkhenkeli (1990). "Clinical experience in intraoperational determination of brain inhibitory structures and application of implanted neurostimulators in epilepsy." Stereotact Funct Neurosurg **55**: 56-59.

Stanley, G. B. (2013). "Reading and writing the neural code." Nat Neurosci **16**(3): 259-263.

Stewart, M. and S. E. Fox (1990). "Do septal neurons pace the hippocampal theta rhythm?" Trends in Neurosciences **13**(5): 163-169.

Stypulkowski, P. H., J. E. Giftakis and T. M. Billstrom (2011). "Development of a Large Animal Model for Investigation of Deep Brain Stimulation for Epilepsy." Stereotactic and Functional Neurosurgery **89**(2): 111-122.

Stypulkowski, P. H., S. R. Stanslaski, T. J. Denison and J. E. Giftakis (2013). "Chronic Evaluation of a Clinical System for Deep Brain Stimulation and Recording of Neural Network Activity." Stereotactic and Functional Neurosurgery **91**(4): 220-232.

Suthana, N., Z. Haneef, J. Stern, R. Mukamel, E. Behnke, B. Knowlton and I. Fried (2012). "Memory Enhancement and Deep-Brain Stimulation of the Entorhinal Area." New England Journal of Medicine **366**(6): 502-510.

Tchumatchenko, T., J. P. Newman, M.-f. Fong and S. M. Potter (2013). "Delivery of continuously-varying stimuli using ChR2." Frontiers in Neural Circuits **7**.

Tellez-Zenteno, J. F. M. D. P., R. S. M. McLachlan, A. M. Parrent, C. S. P. Kubu and S. M. Wiebe (2006). "Hippocampal electrical stimulation in mesial temporal lobe epilepsy." Neurology **66**(10): 1490-1494.

Tenenbaum, L., A. Chtarto, E. Lehtonen, T. Velu, J. Brotchi and M. Levivier (2004). "Recombinant AAV-mediated gene delivery to the central nervous system." The Journal of Gene Medicine **6**(S1): S212-S222.

Tønnesen, J., A. T. Sørensen, K. Deisseroth, C. Lundberg and M. Kokaia (2009). "Optogenetic control of epileptiform activity." Proceedings of the National Academy of Sciences **106**(29): 12162-12167.

Tóth, K., T. F. Freund and R. Miles (1997). "Disinhibition of rat hippocampal pyramidal cells by GABAergic afferents from the septum." The Journal of Physiology **500**(Pt 2): 463-474.

Tyrand, R., M. Seeck, L. Spinelli, E. Pralong, S. Vulliémoz, G. Foletti, A. O. Rossetti, G. Allali, G. Lantz, C. Pollo and C. Boëx (2012). "Effects of amygdala–hippocampal stimulation on interictal epileptic discharges." Epilepsy Research **99**(1–2): 87-93.

University Hospital, G. and Medtronic. "Controlled Randomized Stimulation Versus Resection (CoRaStiR)." In: ClinicalTrials.gov Retrieved January 17, 2013.

Urrestarazu, E., J. Iriarte, M. Alegre, J. Guridi, M. C. Rodríguez-Oroz, J. Obeso, C. Viteri and J. Artieda (2009). "Subthalamic role on the generation of spikes in temporal epilepsy." Epilepsy Research **83**(2–3): 257-260.

Valentín, A., E. García Navarrete, R. Chelvarajah, C. Torres, M. Navas, L. Vico, N. Torres, J. Pastor, R. Selway, R. G. Sola and G. Alarcon (2013). "Deep brain stimulation of the centromedian thalamic nucleus for the treatment of generalized and frontal epilepsies." Epilepsia **54**(10): 1823-1833.

Van Buren, J. M., J. H. Wood, J. Oakley and F. Hambrecht (1978). "Preliminary evaluation of cerebellar stimulation by double-blind stimulation and biological criteria in the treatment of epilepsy." Journal of Neurosurgery **48**(3): 407-416.

Van Rijckevorsel, K., B. Abu Serieh, M. De Tourtchaninoff and C. Raftopoulos (2005). "Deep EEG Recordings of the Mammillary Body in Epilepsy Patients." Epilepsia **46**(5): 781-785.

Vanderwolf, C. H. (1975). "Neocortical and hippocampal activation in relation to behavior: Effects of atropine, eserine, phenothiazines, and amphetamine." Journal of Comparative and Physiological Psychology **88**(1): 300-323.

Velasco, A. L., F. Velasco, F. Jiménez, M. Velasco, G. Castro, J. D. Carrillo-Ruiz, G. Fanghänel and B. Boleaga (2006). "Neuromodulation of the Centromedian Thalamic Nuclei in the Treatment of Generalized Seizures and the Improvement of the Quality of Life in Patients with Lennox–Gastaut Syndrome." Epilepsia **47**(7): 1203-1212.

Velasco, A. L., F. Velasco, M. Velasco, D. Trejo, G. Castro and J. D. Carrillo-Ruiz (2007). "Electrical Stimulation of the Hippocampal Epileptic Foci for Seizure Control: A Double-Blind, Long-Term Follow-Up Study." Epilepsia **48**(10): 1895-1903.

Velasco, A. L., M. Velasco, F. Velasco, D. Menes, F. Gordon, L. Rocha, M. Briones and I. Márquez (2000). "Subacute and Chronic Electrical Stimulation of the Hippocampus on Intractable Temporal Lobe Seizures: Preliminary Report." Archives of Medical Research **31**(3): 316-328.

Velasco, F., J. D. Carrillo-Ruiz, F. Brito, M. Velasco, A. L. Velasco, I. Marquez and R. Davis (2005). "Double-blind, Randomized Controlled Pilot Study of Bilateral Cerebellar Stimulation for Treatment of Intractable Motor Seizures." Epilepsia **46**(7): 1071-1081.

Velasco, F., M. Velasco, F. Jimenez, A. L. Velasco, F. Brito, M. Rise and J. D. Carrillo-Ruiz (2000). "Predictors in the Treatment of Difficult-to-control Seizures by Electrical Stimulation of the Centromedian Thalamic Nucleus." Neurosurgery **47**(2): 295-305.

Velasco, F., M. Velasco, C. Ogarrio and G. Fanghanel (1987). "Electrical Stimulation of the Centromedian Thalamic Nucleus in the Treatment of Convulsive Seizures: A Preliminary Report." Epilepsia **28**(4): 421-430.

Velasco, F., M. Velasco, A. L. Velasco and F. Jimenez (1993). "Effect of Chronic Electrical Stimulation of the Centromedian Thalamic Nuclei on Various Intractable Seizure Patterns: I. Clinical Seizures and Paroxysmal EEG Activity." Epilepsia **34**(6): 1052-1064.

Velasco, M., F. Velasco, A. L. Velasco, G. Velasco and F. Jiménez (1993). "Effect of Chronic Electrical Stimulation of the Centromedian Thalamic Nuclei on Various Intractable Seizure Patterns: II. Psychological Performance and Background EEG Activity." Epilepsia **34**(6): 1065-1074.

Vercueil, L., A. Benazzouz, C. Deransart, K. Bressand, C. Marescaux, A. Depaulis and A. L. Benabid (1998). "High-frequency stimulation of the sub-thalamic nucleus suppresses absence seizures in the rat: comparison with neurotoxic lesions." Epilepsy Research **31**(1): 39-46.

Vesper, J., B. Steinhoff, S. Rona, C. Wille, S. Bilic, G. Nikkhah and C. Ostertag (2007). "Chronic High-Frequency Deep Brain Stimulation of the STN/SNr for Progressive Myoclonic Epilepsy." Epilepsia **48**(10): 1984-1989.

Villette, V., F. Poindessous-Jazat, A. Simon, C. Léna, E. Roullot, B. Bellessort, J. Epelbaum, P. Dutar and A. Stéphan (2010). "Decreased Rhythmic GABAergic Septal Activity and Memory-Associated θ Oscillations after Hippocampal Amyloid-β Pathology in the Rat." The Journal of Neuroscience **30**(33): 10991-11003.

Viswanathan, A. and R. D. Freeman (2007). "Neurometabolic coupling in cerebral cortex reflects synaptic more than spiking activity." Nat Neurosci **10**(10): 1308-1312.

Voigts, J., J. H. Siegle, D. L. Pritchett and C. I. Moore (2013). "The flexDrive: An ultra-light implant for optical control and highly parallel chronic recording of neuronal ensembles in freely moving mice." Frontiers in Systems Neuroscience **7**.

Vonck, K., M. Sprengers, E. Carrette, I. Dauwe, M. Miatton, A. Meurs, L. Goossens, D. E. H. V, R. Achten, E. Thiery, R. Raedt, V. A. N. R. D and P. Boon (2013). "A decade of experience with deep brain stimulation for patients with refractory medial temporal lobe epilepsy." Int J Neural Syst **23**(1): 1250034.

Wagenaar, D. and S. Potter (2002). "Real-time multi-channel stimulus artifact suppression by local curve fitting." J Neurosci Methods **120**(2): 113 - 120.

WHO. (October 2012). "Epilepsy." WHO Factsheet Retrieved December 8, 2009.

Wiebe, S., W. T. Blume, J. P. Girvin and M. Eliasziw (2001). "A Randomized, Controlled Trial of Surgery for Temporal-Lobe Epilepsy." New England Journal of Medicine **345**(5): 311-318.

Wille, C., B. J. Steinhoff, D.-M. Altenmüller, A. M. Staack, S. Bilic, G. Nikkhah and J. Vesper (2011). "Chronic high-frequency deep-brain stimulation in progressive myoclonic epilepsy in adulthood—Report of five cases." Epilepsia **52**(3): 489-496.

Williams, J. H. and J. A. Kauer (1997). Properties of Carbachol-Induced Oscillatory Activity in Rat Hippocampus.

Witten, Ilana B., Elizabeth E. Steinberg, Soo Y. Lee, Thomas J. Davidson, Kelly A. Zalocusky, M. Brodsky, O. Yizhar, Saemi L. Cho, S. Gong, C. Ramakrishnan, Garret D. Stuber, Kay M. Tye, Patricia H. Janak and K. Deisseroth (2011). "Recombinase-Driver Rat Lines: Tools, Techniques, and Optogenetic Application to Dopamine-Mediated Reinforcement." Neuron **72**(5): 721-733.

Wright, G. D., D. L. McLellan and J. G. Brice (1984). "A double-blind trial of chronic cerebellar stimulation in twelve patients with severe epilepsy." Journal of Neurology, Neurosurgery & Psychiatry **47**(8): 769-774.

Wu, M., T. Hajszan, C. Leranth and M. Alreja (2003). "Nicotine recruits a local glutamatergic circuit to excite septohippocampal GABAergic neurons." European Journal of Neuroscience **18**(5): 1155-1168.

Wykes, R. C., J. H. Heeroma, L. Mantoan, K. Zheng, D. C. MacDonald, K. Deisseroth, K. S. Hashemi, M. C. Walker, S. Schorge and D. M. Kullmann (2012). "Optogenetic and Potassium Channel Gene Therapy in a Rodent Model of Focal Neocortical Epilepsy." Science Translational Medicine **4**(161): 161ra152.

Yizhar, O., Lief E. Fenno, Thomas J. Davidson, M. Mogri and K. Deisseroth (2011). "Optogenetics in Neural Systems." Neuron **71**(1): 9-34.

Yoder, R. M. and K. C. Pang (2005). "Involvement of GABAergic and cholinergic medial septal neurons in hippocampal theta rhythm." Hippocampus **15**(3): 381-392.

Zhang, B., J. Chu, J. Zhang and Y. Ma (2008). "Change of Extracellular Glutamate and Gamma-Aminobutyric Acid in Substantia Nigra and Globus Pallidus during Electrical Stimulation of Subthalamic Nucleus in Epileptic Rats." Stereotactic and Functional Neurosurgery **86**(4): 208-215.

Zhang, F., A. M. Aravanis, A. Adamantidis, L. de Lecea and K. Deisseroth (2007). "Circuit-breakers: optical technologies for probing neural signals and systems." Nat Rev Neurosci **8**(8): 577-581.

Zhong, K., D.-C. Wu, M.-M. Jin, Z.-H. Xu, Y. Wang, W.-W. Hou, X.-M. Li, S.-H. Zhang and Z. Chen (2012). "Wide therapeutic time-window of low-frequency stimulation at the subiculum for temporal lobe epilepsy treatment in rats." Neurobiology of Disease **48**(1): 20-26.

Ziburkus, J., J. R. Cressman, E. Barreto and S. J. Schiff (2006). "Interneuron and Pyramidal Cell Interplay During In Vitro Seizure-Like Events." J Neurophysiol **95**(6): 3948-3954.